FUNCTIONAL LIPIDOMICS ANALYSIS OF RETROVIRUS ENVELOPES

CHAN LER MIN, ROBIN BARRY

BSC (HON), NUS

A THESIS SUBMITTED FOR THE DEGREE OF DOCTOR OF PHILOSOPHY

DEPARTMENT OF BIOCHEMISTRY

NATIONAL UNIVERSITY OF SINGAPORE

2008

Acknowledgements

The successful completion of this project and thesis was dependent on a number of key people:

1. First and foremost, I would like to thank my supervisor Dr Markus Wenk for the excellent support, encouragement and guidance he has given me throughout my PhD studies.

2. Great appreciation goes out to our collaborators Dr Walther Mothes (Yale University) and Dr David Ott (NCI Fredrick) who worked closely with me to see through this project.

3. In addition, I would like to specially thank Dr Pradeep Uchil (Yale University), Dr Jing Jin (Yale University), Dr Shui Guanghou (NUS), Mr Lukas Tanner (NUS), Ms Cheong Wei Fun (NUS) and Ms Chua Gek Huey (NUS) for helping me with various technical issues related to this project.

4. This initial draft of this thesis was critically read by Mr Lukas Tanner and Ms Lynette Lim of the Wenk Lab. In addition, I would also like to thank my thesis advisory committee Dr Vincent Chow and Dr Paul Macary for their valuable advices on improving the thesis.

5. In addition, I would like to thank all other members of the Wenk lab, for their valuable suggestions and camaraderie during my time spent in the lab.

Last but not least, I am extremely thankful to my wife Charlotte, Mum and Dad, family and friends for the understanding and moral support that they have provided me in abundance over the years.

Table of Contents

Summary

Retrovirus particles are surrounded by a lipid envelope that is acquired from their host cell during budding. While it is clear that lipids play important roles in its replication cycle, many potential functions remain poorly characterized. An important first step towards elucidating these functions would be a detailed biochemical characterization of the lipid inventory of retrovirus envelopes. We hypothesize that the enrichment of particular lipid classes in retrovirus envelopes is an indication that these lipids may play important roles in retrovirus replication (Aloia et al., 1993; Brugger et al., 2006).

The lipidome of highly purified retroviruses human immunodeficiency virus (HIV) and murine leukemia virus (MLV) was analyzed comparatively to their corresponding host membrane lipids. Using primarily electrospray ionization mass spectrometry (ESI-MS) based methods, a wide variety of lipid classes were covered in this analysis, including glycerophospholipids, sphingolipids, glycerolipids and sterols. We report that both HIV and MLV share a similar lipid composition to their host plasma membrane and each other despite being produced from different cell types. Significantly, a few classes of lipids remain enriched in the both retrovirus envelopes over their respective host plasma membrane: 1) phosphoinositides, phosphorylated derivatives of phosphatidylinositol; 2) raft lipids including cholesterol, ceramide and the glycosphingolipid GM3. Microvesicles, which are similar in size to viruses and are also released from the plasma membrane of HIV producing cells, exhibit a similar lipid composition to retroviruses. However, while microvesicles are enriched in raft lipids, they are not enriched in phosphoinositides. These data suggest that while raft lipids may play a general role in vesicle budding, phosphoinositides seem to play a critical role specifically in retrovirus assembly and budding.

Based on the lipid composition analysis, we first decided to investigate the role of phosphoinositides in retrovirus budding. Analysis of virus like particles produced using mutant HIV Gag mapped the enrichment of PIP_2 in HIV envelope to the polybasic matrix domain of HIV Gag. One specific phosphoinositide isomer, $PI(4,5)P_2$, has been implicated in membrane targeting of HIV Gag (Ono et al., 2004; Saad et al., 2006). Consistent with this observation, we showed that enzymatic depletion of $PI(4,5)P_2$ from cells reduced both HIV-1 and MLV production. In the second line of investigation, we studied the effects of using phenyl-2-hexadecanoylamino-3-morpholino-1-propanol (PPMP) to deplete cellular glycosphingolipid levels and its impact on MLV infectivity. We demonstrated that MLV infectivity may be hindered or enhanced by PPMP treatment, depending on whether glycosphingolipids are virus- or cell-associated. Thirdly, we examined the asymmetric distribution of aminophospholipids in purified MLV. Aminophospholipids that was exposed on the outer leaflet of MLV envelopes was modified using trinitrobenzenesulfonic acid (TNBS) and analyzed by ESI-MS. It was found that plasmalogen phosphatidylethanolamine are specifically enriched in the outer leaflet of the MLV membrane.

Overall, the lipidomics experimental approach used in this study enabled the identification of several important lipid molecules that contribute significantly towards retroviral replication. Taking a broader view, this approach should be equally useful in the study of other medically important enveloped viruses.

List of Tables

List of Figures

List of Abbreviations

Lipid classes

Phosphatidylserine	PS
Phosphatidylethanolamine	PE
Plasmalogen phosphatidylethanolamine	pPE
Phosphatidylcholine	PC
Ether phosphatidylcholine	ePC
Phosphatidylinositol	PI
Phosphatidylinositol phosphate	PIP
Phosphatidylinositol bisphosphate	PIP_2
Phosphatidic Acid	PA
Sphingomyelin	SM
Dihydrosphingomyelin	dhSM
Ceramide	Cer
Glucosylceramide	GluCer
Cholesterol	Chol
Cholesterol Ester	CE
Monoacylglycerol	MG
Diacylglycerol	DG
Triacylglycerol	TG

Reagents

Phenyl-2-hexadecanoylamino-3-morphilino-1-propanol	PPMP
Trinitrobenzenesulfonic acid	TNBS

Methods

Electrospray ionization mass pectrometry	ESI-MS
Time of flight	Tof

List of Publications

Chan, R., Uchil, P. D., Jin, J., Shui, G., Ott, D. E., Mothes, W. and Wenk, M. R. 2008. Retroviruses human immunodeficiency virus and murine leukemia virus are enriched in phosphoinositides. J Virol. 82: 11228-38

Yeo, D. S., Chan, R., Brown, G., Ying, L., Sutejo, R., Aitken, J., Tan, B. H., Wenk, M. R. and Sugrue, R. J. 2009. Evidence that selective changes in the lipid composition of raft-membranes occur during respiratory syncytial virus infection. Virology. 386: 168-82

Chapter 1 – Introduction

The Acquired Immune Deficiency Syndrome, commonly known as AIDS, continues to be a major health pandemic. Based on the 2007 AIDS Epidemic Update published jointly by UNAIDS and WHO (UNAIDS and WHO, 2007), it was estimated that 33.2 million people worldwide, of which 2.5 million are children under 15 years old, live with Human Immunodeficiency Virus (HIV), the causative agent of AIDS. The bulk of these patients live in Sub-Saharan Africa (22.5 million) followed by South and South East Asia (4.0 million), Eastern Europe and Central Asia (1.2-2.0 million) and Latin America (1.6 million). The 2007 death toll as a result of AIDS was approximately 2.1 million people worldwide with 76% of these deaths occurring in sub-Saharan Africa (UNAIDS figures), making AIDS the leading cause of death in that region. Because of such blistering figures, it is not surprising to know that HIV is one of the world's most intensively studied human pathogen. As a result, enormous progress has been made in understanding molecular details of HIV replication cycles.

1.1 Basic retrovirus biology

While HIV is one of the most studied member of the Retroviridae family, it belongs to just one of seven genera or subfamilies. These seven include Alpharetrovirus, Betaretrovirus, Gammaretrovirus, Deltaretrovirus, Epsilonretrovirus (all of which used to be classified under the Oncovirus genus), Lentivirus (which includes HIV) and Spumavirus (Table 1). Retroviruses cause a wide variety of diseases besides AIDS, ranging from malignancies and neurological disorders. All retroviruses genomes contain three major structural genes – group-specific-antigen protein (Gag), Gag-polymerase (Pol) and the envelope glycoprotein

(Env). Retroviruses can be further described as simple or complex depending on the presence of additional genes. The genomes of simple retroviruses such as Murine Leukemia Virus (MLV) and Avian Leukosis Virus (ALV) consist only of three structural genes, whereas complex retroviruses such as HIV and Simian Immunodeficiency Virus (SIV) contain additional regulatory and accessory genes such as negative regulatory factor (Nef), viral infectivity factor (Vif), regulator of virion (Rev), transactivator (Tat), viral protein R, and viral protein U or viral protein X, all of which are essential for viral pathogenesis in vivo (Malim and Emerman, 2008).

Genus	**Examples**	**Morphology**
Alpharetrovirus	Avian leukosis virus (ALV) Rous sarcoma virus (RSV)	C-type
Betaretrovirus	Mouse mammary tumor virus (MMTV) Mason-Pfizer monkey virus (MPMV) Jaagsiekte sheep retrovirus (JSRV)	B-, D-type
Gammaretrovirus	Murine leukemia virus (MLV) Feline leukemia virus (FLV) Gibbon ape leukemia virus (GaLV)	C-type
Deltaretrovirus	Human T-lymphotropic virus (HTLV)-1, -2 Bovine leukemia virus (BLV) Simian T-lymphotropic virus (STLV)-1, -2, -3	-
Epsilonretrovirus	Walleye dermal sarcoma virus Walleye epidermal hyperplasia virus 1	-
Lentivirus	Human immunodeficiency virus (HIV)-1, -2 Simian immunodeficiency virus (SIV) Equine infectious anemia virus (EIAV) Caprine arthritis encephalitis virus (CAEV)	Rod/cone core
Spumavirus	Human foamy virus (HFV)	Immature

Table 1. The retrovirus family and their representative species.

The basic structural unit of a retroviral virion is similar to other enveloped viruses (Figure 1A). Each infectious virion carries two identical positive-sense RNA genome contained within a protein cage of matrix (MA), capsid (CA), and nucleocapsid (NC)

subunits that are formed by the proteolysis of a Gag precursor protein during virus maturation. The Pol gene products are packaged into the viral core consisting of reverse transcriptase (RT) responsible for the conversion of viral RNA into DNA, protease (PR) responsible for processing Gag precursor proteins into their mature products, and integrase (IN) that inserts the viral DNA in the host genome. Encapsulating this core is a host derived lipid bilayer that provides a protective membranous envelope to house its fusion glycoprotein Env.

The general replication cycle of retroviruses is illustrated in Figure 1B. In the early phase of its replication cycle, retroviruses gain entry into cells by first binding to specific receptors on the cell surface, followed by the fusion of the virion membrane with the host membrane. This process releases the internal viral core containing the reverse transcription complex (RTC) into the cytoplasm followed by its disassembly. The RTC containing the viral RNA and RT protein performs the reverse transcription of the RNA genome into double stranded cDNA, which is next delivered into the nucleus in the form of a pre-integration complex (PIC). In the nucleus, the PIC becomes uncoated and the cDNA is integrated into the host genome by the IN activity, resulting in a provirus that serves as a template for transcription of viral mRNA by the host RNA polymerase II system. It is this DNA intermediate step that is unique to retroviruses. Comparatively, other RNA viruses utilize their genomes directly as mRNA for the production of viral proteins.

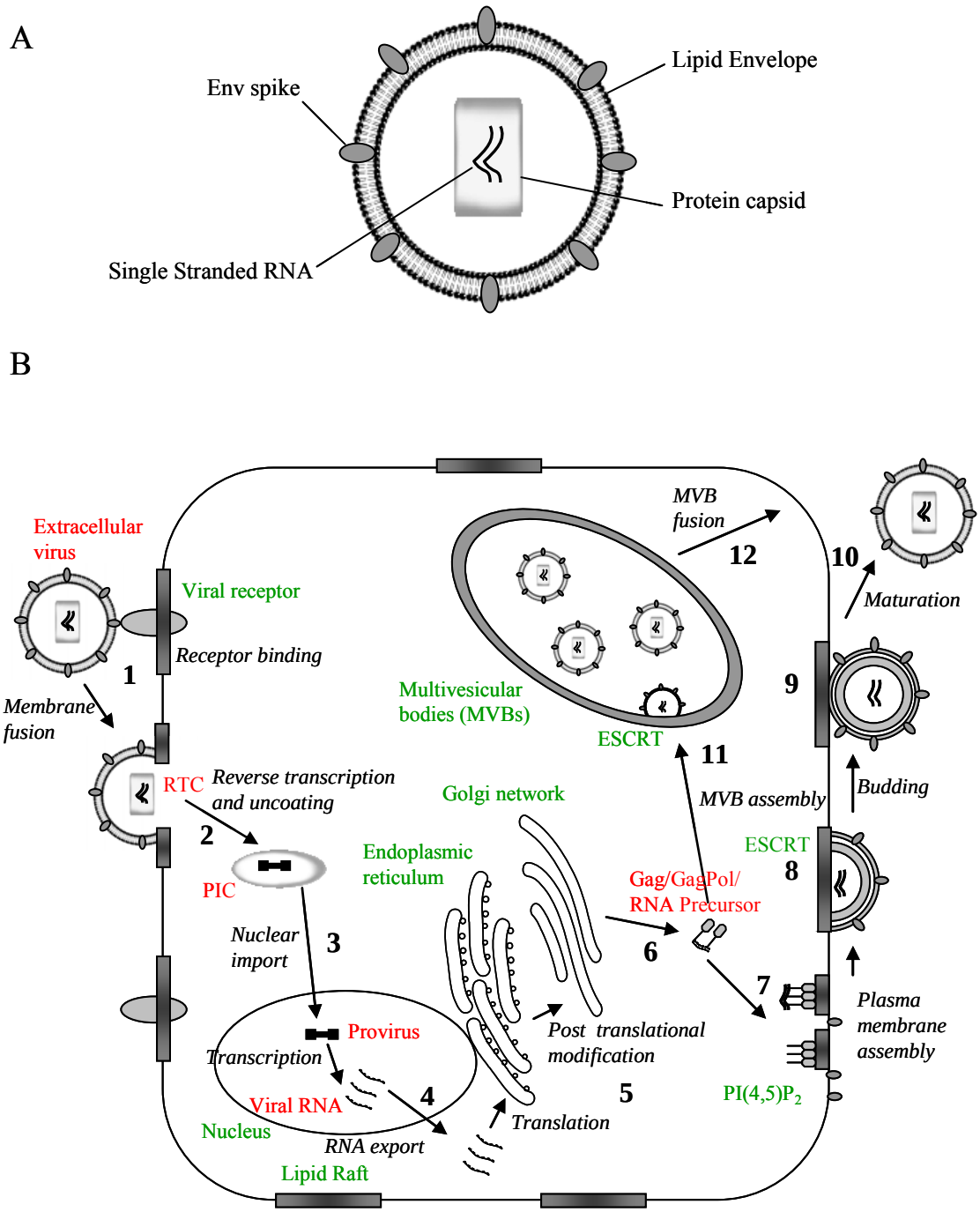

Figure 1. Illustrative cartoon of a retrovirus particle (A). Simplified illustration of the retrovirus lifecycle (B). Retroviruses enter cells through initial contact with its receptors followed by fusion of the virus particle (Step 1). RTC is released into the cell and the RNA genome is reverse transcribed into double stranded cDNA as part of the PIC (Step 2). The cDNA is delivered into the cell nucleus and integrated in the host genome (Step 3). The viral cDNA is transcribed (Step 4) and viral RNA is translated (Step 5) using the host cell machinery to produce Gag and other proteins not shown here (Step 6). In most cell types, Gag/GagPol RNA precursors are targeted to plasma membrane for assembly and budding through acidic membrane lipids such as PI(4,5)P_2 (Step 7). Gag then recruits ESCRT proteins which assist the budding (Step 8) and fission process (Step 9). Infective viruses are produced through viral protease action (Step 10). However, in some cell types, Gag may be targeted to MVBs, budding into its lumen using the ESCRT machinery (Step 11). These viruses are released from the cell when MVBs fuses with the limiting plasma membrane (Step 12). Host structures and virus structures are labeled in green and red respectively. Please see text for additional details and references.

The late phase of the retroviral life cycle begins with the processing and export of viral mRNA out of the nucleus. Following viral protein translation, Gag proteins and viral RNAs are transported to the site of particle assembly. Depending on cell type and virus species, the assembly site can occur at the plasma membrane (Jouvenet et al., 2006; Neil et al., 2006; Ono and Freed, 2004) or at multivesicular bodies (MVBs) via the vesicular trafficking pathway (Mothes et al., 2000b; Nguyen et al., 2003; Ono and Freed, 2004; Pelchen-Matthews et al., 2003). The process of retrovirus budding requires the endosomal sorting complex required for transport (ESCRT) machinery, which is a collection of approximately 20 host proteins that mediate cargo protein sorting into the endosomal pathway under normal cellular function. In retrovirus infected cells, Gag redirects multiple components of the host ESCRT machinery to the budding site at the plasma membrane or MVBs to promote virion budding and release (Strack et al., 2003; von Schwedler et al., 2003). This is followed by viral protease action that produces mature retrovirus particles.

1.2 The role of lipids in retrovirus replication

The replication cycle of retroviruses and other enveloped viruses is a process regulated by the synergistic interaction of viral proteins and host factors. Unlike proteins, the contribution of lipids to this process has been largely neglected thus far. Lipids can be envisioned as multidimensional entities, from larger lipid aggregates such as the lipid rafts within subcellular membranes to structurally diverse single lipid molecules (Figure 2). In addition, lipids are non-randomly distributed in cellular membranes, which serve to compartmentalize their function in specific cellular locations (Figure 3). Like proteins, the structural diversity and topological specificity of lipid molecules translate to a myriad of potential functional roles in general enveloped virus replication (Table 2). The following review will mostly focus on the functions of lipids with respect to retroviruses.

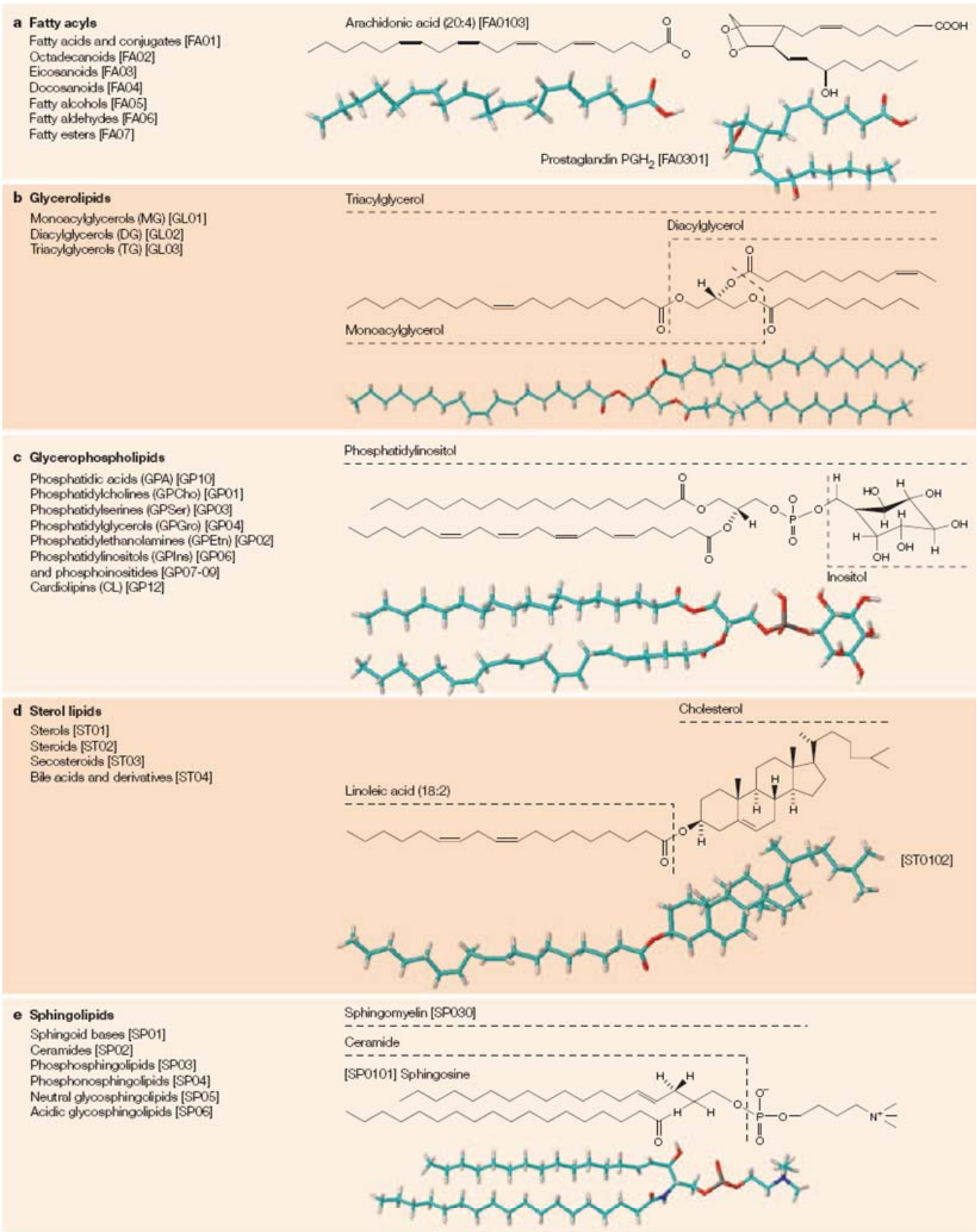

Figure 2. Lipid diversity in nature.
Lipids are grouped in five different classes according to their structural and chemical properties. Prominent representatives of each lipid are illustrated. Figure taken from (Wenk, 2005).

Stage	Involvement of lipids	Selected References
Extracellular	Viral envelopes are enriched in sphingomyelin	(Brugger et al., 2006; van Genderen et al., 1994)
	Envelope cholesterol is critical for structure and infectivity	(Campbell et al., 2002; Graham et al., 2003)
Docking	Phosphatidylserine stimulates entry of enveloped viruses	(Callahan et al., 2003; Coil and Miller, 2005a)
	Vaccinia virus uses phosphatidylserine in apoptotic mimicry to infect cells	(Mercer and Helenius, 2008)
	Cell surface glycosphingolipids act as alternative receptors for viral envelope proteins	(Campanero-Rhodes et al., 2007a; Fantini et al., 1993)
Entry	Signaling via lipid kinases is activated during viral entry	(Pelkmans et al., 2005)
	Sphingolipids and glycolipids regulate CD4-dependent chemokine receptor mediated fusion of HIV	(Ablan et al., 2006; Finnegan et al., 2004; Finnegan et al., 2007; Hug et al., 2000; Puri et al., 1998; Puri et al., 2004; Rawat et al., 2006)
	Cholesterol in both virus- and cell- associated membrane is required for fusion and infection	(Guyader et al., 2002; Liao et al., 2001; Liao et al., 2003)
	Lysolipids are able to inhibit fusion of influenza virus and tick-borne encephalitis virus	(Chernomordik et al., 1993; Stiasny and Heinz, 2004)
Intracellular replication	HIV Nef up-regulates cholesterol biosynthesis to support lipid raft formation	(van 't Wout et al., 2005b; Zheng et al., 2003)
	Cholesterol efflux is impaired in HIV infected cells.	(Mujawar et al., 2006)
	Fatty acyl and cholesterol synthesis are required for Hepatitis C virus RNA replication	(Kapadia and Chisari, 2005; Su et al., 2002)
	Host protein geranylgeranylation is required for Hepatitis C virus RNA replication	(Kapadia and Chisari, 2005; Ye et al., 2003)
	Lysobisphosphatidic acid and PI(3)P regulate release of VSV nucleocapsid into cytoplasm	(Le, I et al., 2005)
	Ethanolamine phospholipids required for Sindbis virus production	(Kuge et al., 1989)
	Semliki Forest virus mRNA capping enzyme requires association with anionic membrane phospholipids for activity	(Ahola et al., 1999; Spuul et al., 2007)
Budding and escape	Vaccinia virus envelope protein p37 has lipase activity required for egress from cell	(Baek et al., 1997)
	HIV Gag protein interaction with the plasma membrane is regulated by myristol switch	(Resh, 2004; Saad et al., 2007; Zhou et al., 1994)
	Viral assembly and budding occur from plasma membrane lipid rafts that are enriched in cholesterol, sphingolipids and glycolipid	(Beer et al., 2005; Nguyen and Hildreth, 2000; Ono et al., 2007; Ono and Freed, 2001; Scheiffele et al., 1999)
	Nef transports cholesterol to site of HIV budding	(Brugger et al., 2007; Zheng et al., 2003)
	HIV particle assembly is modulated by inositol phosphate molecules	(Campbell et al., 2001; Shkriabai et al., 2006)
	HIV Gag is targeted to plasma membrane by specific interaction with $PI(4,5)P_2$	(Chukkapalli et al., 2008; Ono et al., 2004; Saad et al., 2006)
	Unsaturated fatty acids block HIV budding	(Lindwasser and Resh, 2002)

Table 2. Known functions of lipid classes at various steps in enveloped virus replication.
Adapted from (Wenk, 2006)

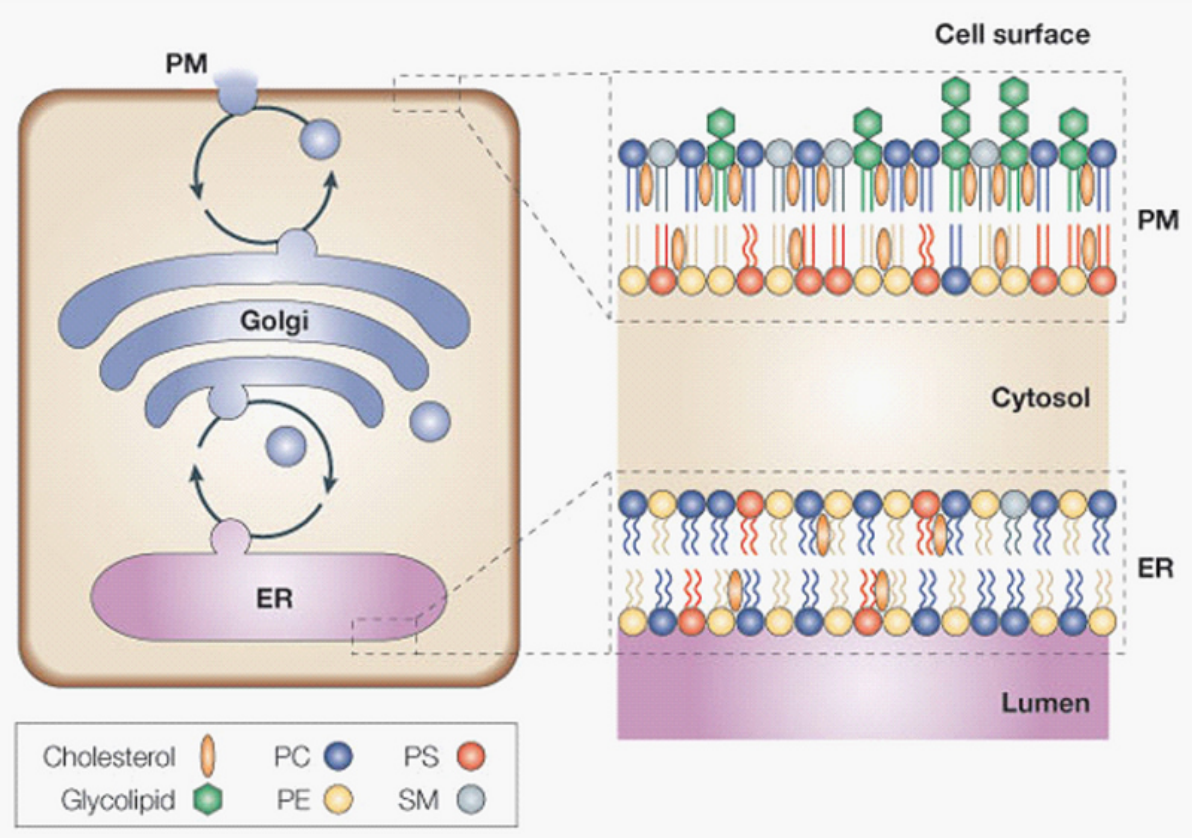

Figure 3. Membrane lipids show non-random distribution between and within organelles that are connected by vesicular pathways.
The plasma membrane (labeled PM in the figure) is rich in sterols, sphingolipids and saturated glycerolipids. Due to their high packing densities, these lipids promote bilayer rigidity and impermeability. In addition, the plasma membrane has an asymmetric lipid arrangements with the aminophospholipids concentrated in the cytosolic leaflet and the sphingolipids concentrated in the exoplasmic leaflet. The membrane topology of cholesterol is not known, but its location is probably determined by its high affinity for sphingolipids and saturated glycerolipids. The endoplasmic reticulum (ER) membrane, on the other hand, shows a symmetric lipid distribution and primarily contains unsaturated glycerolipids that make the membrane flexible, and therefore facilitate the incorporation of newly synthesized proteins. Figure taken from (Holthuis and Levine, 2005).

1.2.1 Extracellular structural integrity and morphology

The most obvious role of the lipid envelope is to provide a protective membrane to the fragile internal contents of an extracellular retrovirus. High levels of lipid ordering and rigidity has been reported not only with HIV (Aloia et al., 1988; Aloia et al., 1993) but a range of other retroviruses as well, including equine infectious anemia virus (EIAV), bovine leukemia virus (BLV), murine leukemia virus (MLV) and avian myelolastosis virus (Slosberg and Montelaro, 1982). This physical characteristic is in turn attributed to the high cholesterol/sphingomyelin to phospholipids ratio present in retroviral envelopes. As a proof

of concept, it has been shown that the removal of virion-associated cholesterol in HIV (Figure 4) and SIV using 2-hydroxy-propyl-β-cyclodextrin (β-cyclodextrin) permeabilizes the viral membrane (Graham et al., 2003). As a result, the retroviruses become inactivated due to a loss in their protein core and genome integrity. This led to the suggestion that removal of raft lipids may provide therapeutic intervention against HIV infection (Nguyen and Taub, 2004) and is currently being investigated in animal models using SIV (Ambrose et al., 2008) .

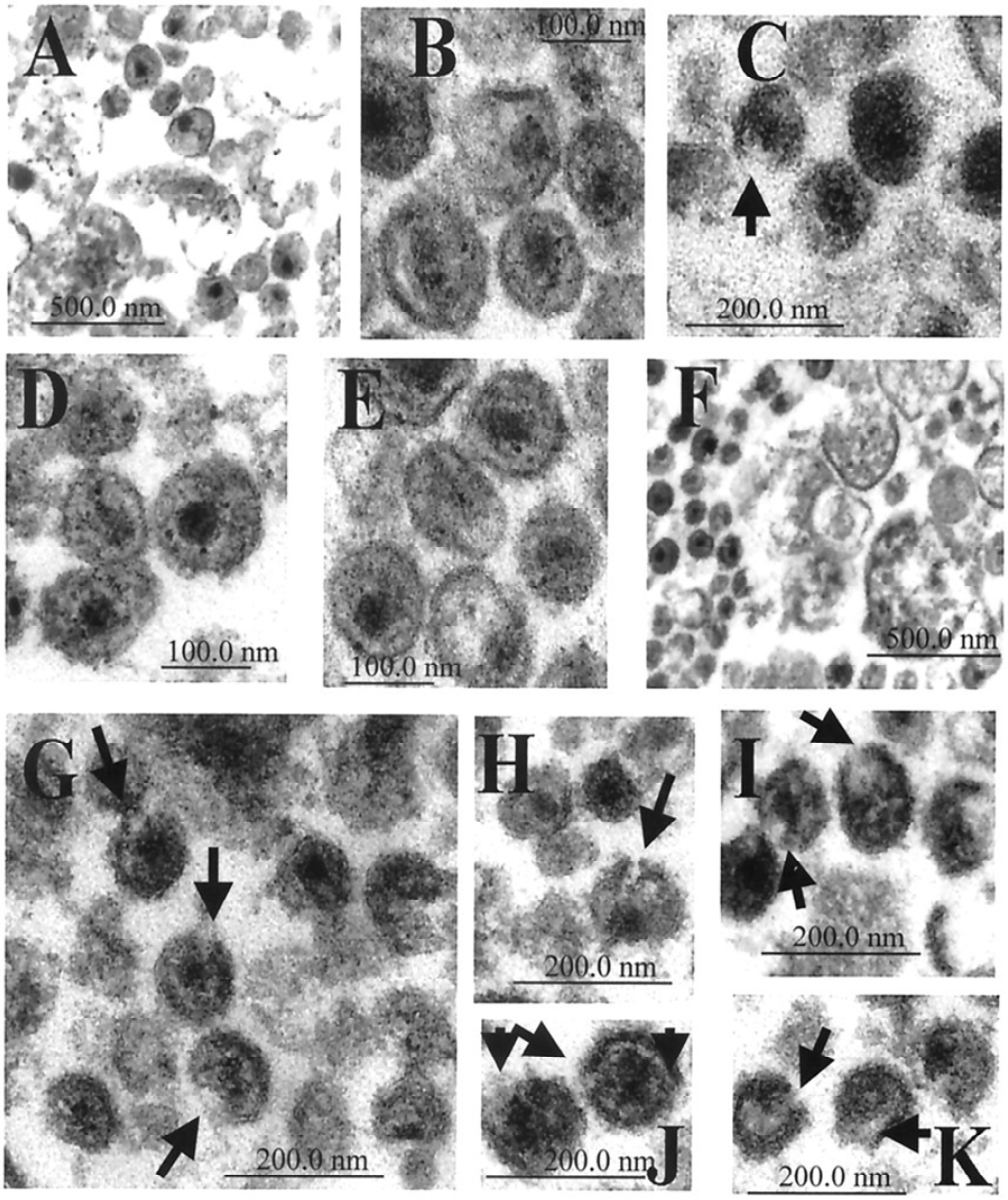

Figure 4. The role of lipids in maintaining retrovirus particle integrity and morphology.
Electron microscopy of HIV-1 treated under permeabilizing conditions revealed holes in the membrane of the virus. HIV-1 samples that were untreated (A and D), treated under non-permeabilizing conditions (B and E), or treated under permeabilizing conditions (C and F to K) were examined by transmission electron microscopy. Magnifications: x4,000 (A and F) and x20,000 (B to E and G to K). Figure taken from (Graham et al., 2003).

1.2.2 Retrovirus proteins interact with membrane lipids to determine assembly and budding site

1.2.2.1 The viral proteins

One of the key questions in retrovirus research pertains to the selection of the assembly and budding site. It has been noted that the expression of retrovirus Gag alone is enough to produce the assembly and release of non-infectious virus-like particles (Demirov and Freed, 2004). The Gag precursor protein can be generally subdivided into four different domains, each with a unique function: MA domain contains the membrane targeting signal for Gag; CA domain contains sequences responsible for Gag-Gag multimerization that drives the assembly process; nucleocapsid NC domain is involved in the interaction of Gag with the viral RNA genome; L domain functions in recruiting the ESCRT machinery and is responsible for the final release of the virus particle from the cell. It is interesting to note that there are analogous structural proteins found in other virus families like Rhabdoviridae (Vesicular Stomatis Virus) (Swinteck and Lyles, 2008), Orthomyxoviridae (Influenza Virus) (Nayak et al., 2004) and Paramyxoviridae (Respiratory Syncytial Virus) (Marty et al., 2004) that also use the plasma membrane site for budding.

Other viral factors besides Gag may influence site selection. For instance, in polarized epithelial cells, Gag that is expressed alone localizes to both apical and basolateral surfaces, while Gag that is co-expressed with Env is directed only to the basolateral surface (Lodge et al., 1997b; Lodge et al., 1997a). On its own, retrovirus Env glycoprotein appear to be trafficked to lipid rafts because its transmembrane domain bears either cysteine residues which are targets for palmitoylation or contains residues with bulky hydrophobic side chains (Bhattacharya et al., 2004; Rousso et al., 2000). More recently, it was shown that Gag

interaction with Env through the MA domain is also essential for promoting Env localization to detergent resistant membranes (DRMs) or lipid rafts (Bhattacharya et al., 2006).

1.2.2.2 Lipid rafts

The general idea that retroviruses and other enveloped viruses are targeted to and bud from lipid rafts has gained widespread acceptance (Briggs et al., 2003; Ono and Freed, 2005; Rajendran and Simons, 2005). Lipid rafts are ordered domains that exist within the disordered phase of the bulk cell membrane. These dynamic lipid-protein assemblies are characterized by the relative enrichment of cholesterol, sphingolipids, saturated glycerophospholipids and protein molecules with a high inherent affinity for ordered lipid domains. Raft lipids are believed to be held together weakly, establishing a dynamic equilibrium of raft and non-raft regions within the plasma membrane (Harder and Simons, 1997). The sphingolipids interact laterally through van der Waals interactions and extensive hydrogen bonding between the sphingosine backbones and between the sugar head groups (Ramstedt and Slotte, 2006). Moreover, the majority of sphingolipids have saturated, and therefore unkinked, acyl chains that allow tighter packing of laterally associated lipids and a higher gel-liquid phase transition temperature (Ramstedt and Slotte, 2002). These interactions lead to segregation of sphingolipid rich domains from their glycerophospholipid-rich surroundings. The degree of lateral association is further increased by the presence of cholesterol. The 3-β-hydroxyl group of cholesterol hydrogen bonds with the ceramide group of sphingolipids, while its planar sterol ring interacts with the saturated acyl chain (Ramstedt and Slotte, 2006; Xu and London, 2000).

It should be noted that the molecular features of lipid rafts described above are mainly based on data obtained from *in vitro* model membrane experiments, and is probably an

oversimplification of actual biological interactions. Nevertheless, it is clear that the lipid and protein composition of lipid rafts are restricted by the biophysical properties of their individual molecules. This means that newly formed rafts tend to recruit other molecules by their affinity for the initial raft molecules, resulting in an increasing concentration of ordered lipids and proteins in a larger raft platform on the membrane. The molecular signal for the raft affinity of peripheral and transmembrane proteins is based on myristoyl and palmitoyl covalent modifications respectively (Brown, 2006). Thus, the observation that retrovirus Gag and Nef proteins are typically myristoylated while Env glycoproteins are palmitoylated (Resh, 1999) suggests that these proteins are targeted to lipid rafts during assembly.

The involvement of lipid rafts in retrovirus assembly offers a convenient model for visualizing how retrovirus assembly may occur (Briggs et al., 2003 and Figure 5). Retrovirus infection leads to the production of retroviral Gag and Env proteins and their trafficking to pre-existing rafts at the cell surface. The affinity of the viral proteins for a particular lipid population leads to an increase in recruitment of more host lipids and proteins of similar affinity, resulting in their enrichment at a focal point where budding is to take place. This process would continue until the collection of viral proteins and host proteins, and their interaction with the inner leaflet of the membrane results in curvature and budding of the retrovirus particle. There exist numerous lines of evidence that retroviruses assemble and bud through lipid rafts, including (1) co-flotation of Gag proteins with DRMs and associated marker proteins in density gradients after cold detergent treatment (Lindwasser and Resh, 2001), (2) blocking of virus assembly and budding after raft disruption by cholesterol depletion (Ono and Freed, 2001), and (3) observing punctuate co-localization of viral proteins with raft markers in the plasma membrane by immunofluorescence microscopy (Nguyen and Hildreth, 2000). However, the most compelling evidence comes from the observation that purified virus particles are enriched in raft lipids including cholesterol, sphingomyelin (SM),

dihydrosphingomyelin (dhSM) and glucosylceramide (Glu-Cer), relative to the bulk cellular lipid composition (Aloia et al., 1993; Brugger et al., 2006).

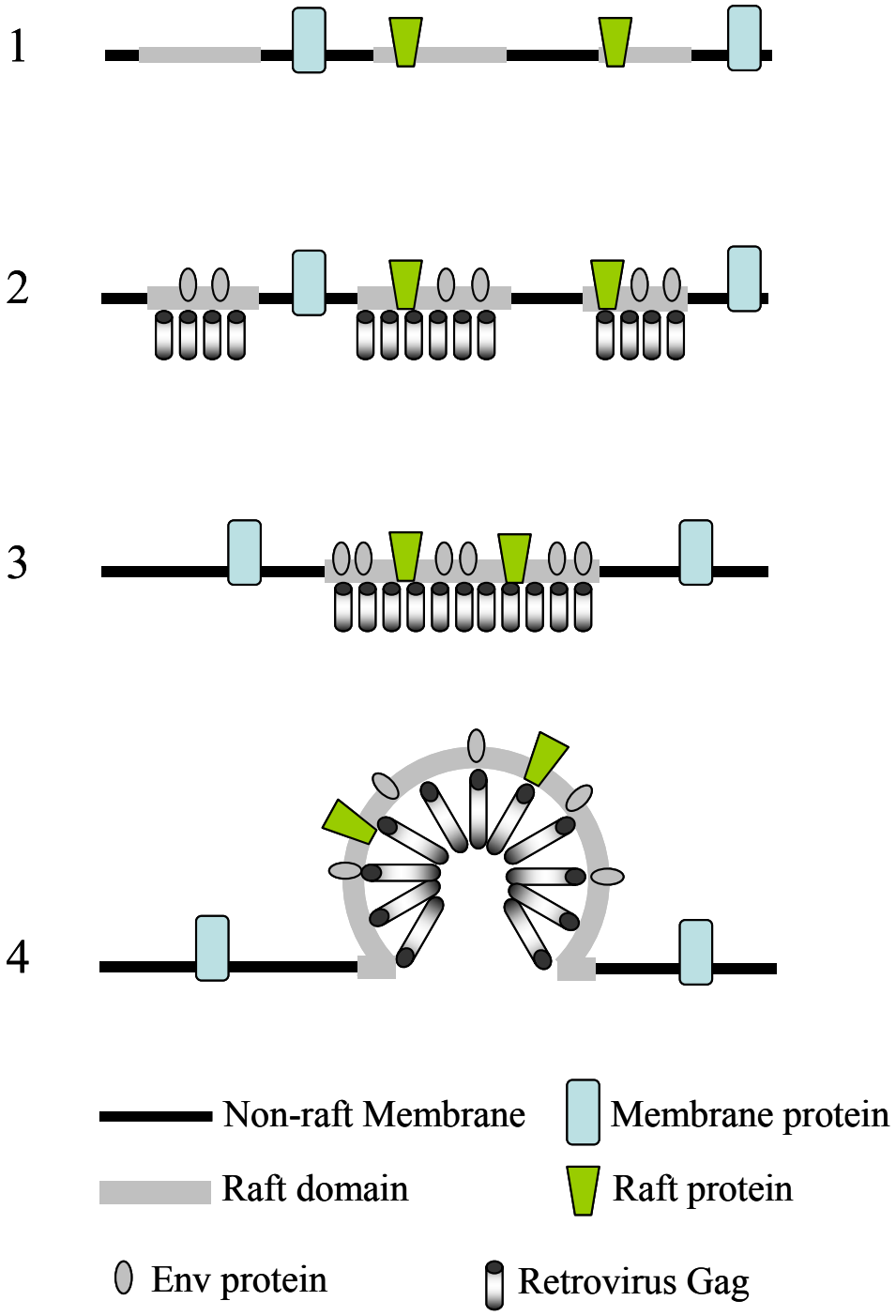

Figure 5. Involvement of lipid raft in retrovirus budding.
Step 1: Pre-existing rafts are found on the plasma membrane. Step 2: Retrovirus infection results in the expression of Gag and Env protein which are targeted to the plasma membrane rafts due to their intrinsic raft affinity. Step 3: Aggregation of Gag pulls the separate rafts together. Non-raft membranes and membrane proteins without a raft affinity become excluded from the enlarged raft structure. Step 4: The budding process is initiated, carrying along not only retrovirus protein but also raft associated host proteins. Adapted from (Briggs et al., 2003).

1.2.2.3 Phosphoinositides

While the lipid raft theory provides an attractive description of how viral membranes are formed, the precise molecular interaction between viral protein and the membrane is less evident. An early clue to this issue was provided by the observation that MA domain of Gag directs the polypeptide precursor to the plasma membrane via a bipartite motif consisting of an N-terminal myristic acid that is covalently attached (Bryant and Ratner, 1990) and a highly basic cluster of amino acid residues (Yuan et al., 1993). However, myristoylation modification alone cannot be solely responsible for Gag transport to the plasma membrane since not all myristoylated proteins are associated with the plasma membrane (Resh, 1999; Schultz et al., 1988). Moreover, non-myristoylated Gag from retroviruses like rous sarcoma virus (RSV) and EIAV, are still targeted to the plasma membrane for assembly and budding (Conte and Matthews, 1998). Hence, the additional signal for plasma membrane binding must reside within the basic cluster of positively charged amino acid residues.

The cytosolic surface of the plasma membrane carries an appreciable negative charge due to the large proportion of negatively charged acidic phospholipids relative to other intracellular membranes. The most abundant of these phospholipids is the monovalent acidic phosphatidylserine (PS), which represent 10-20% of plasma membrane lipids (Vance and Steenbergen, 2005). Plasma membrane localization of a number of cellular proteins seem to depend on PS re-distribution in certain cellular events including calcium influx (Yeung et al., 2008) and phagocytosis (Yeung et al., 2006). In addition to PS, other negatively charged phospholipids appear to be enriched in the inner leaflet of the plasma membrane including phosphatidic acid (PA), phosphatidylinositol (PI) and their polyphosphorylated derivatives (collectively termed as phosphoinositides) such as phosphatidylinositol-4,5-bisphosphate ($PI(4,5)P_2$) and phosphatidylinositol-3,4,5-triphosphate ($PI(3,4,5)P_3$). While $PI(4,5)P_2$ and

$PI(3,4,5)P_3$ represent only a minor fraction of the plasma membrane lipids, they play multiple vital roles in diverse cellular functions (Rusten and Stenmark, 2006). Therefore, their concentration is tightly regulated enzymatically by a significant number of kinases and phosphatases (Downes et al., 2005) and spatially by reversible phosphoinositide binding proteins such as MARCKS (McLaughlin and Murray, 2005).

The complementary charge state of Gag MA and inner plasma membrane surface intuitively suggests an electrostatic mechanism by which Gag interact with the membrane. This early hypothesis was supported by liposome pull-down assays showing that Gag can be enriched by liposomes containing PS (Zhou et al., 1994). A link between phosphoinositides and retrovirus assembly was provided by the observation that inositol polyphosphate molecules are able to promote cell free assembly of virus like particles from recombinant HIV-1 Gag molecules (Campbell et al., 2001). More recently, it was shown that depletion of $PI(4,5)P_2$ inhibits HIV assembly and leads to accumulation of Gag at late endosomes and MVBs (Ono et al., 2004). The work of Saad et al. provided a structural framework (Figure 6) in which both $PI(4,5)P_2$ association and myristic switch work cooperatively during HIV-1 assembly (Saad et al., 2006). By nuclear magnetic resonance structural analysis, the authors reported that myristylated MA binds directly to $PI(4,5)P_2$ and that this binding is highly specific. Furthermore, it was proposed that the inositol headgroup and the 2' fatty acid chain of the lipid molecule fit directly into a hydrophobic cleft in MA, thus allowing the negatively charged phosphates to form salt bridges with basic residues in MA. This interaction causes the MA myristic acid moiety to flip out from a sequestered to an exposed conformation thereby increasing Gag membrane partitioning.

An interesting feature of this myristic switch model is that it also reconciles an apparent conflict with the lipid raft model (Freed, 2006). As mentioned above, lipid rafts are concentrated in saturated glycerophospholipids. Because the predominant form of $PI(4,5)P_2$

in cells contains a saturated 1' fatty acid side chain (C18:0) and also a poly-unsaturated 2' side chain (C20:4), $PI(4,5)P_2$ may equilibrate between raft and non-raft domains in the membrane. During Gag binding, the 2' side chain is extruded from the lipid bilayer and packed into MA, with myristic acid taking its place in the bilayer. Thus, only the fully saturated 1' fatty acid and myristic acid remains in the plasma membrane, thus increasing the affinity of $PI(4,5)P_2$ and its associated Gag molecule for the lipid raft.

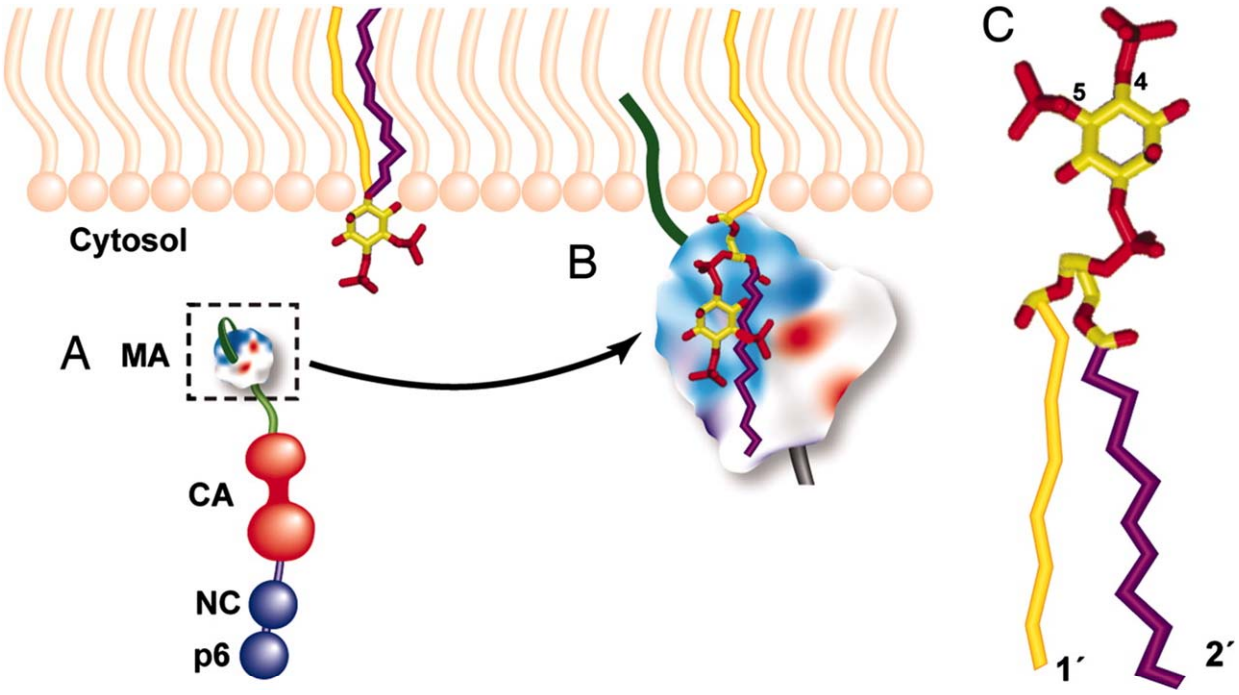

Figure 6. Binding of MA domain to Pr55 Gag to PI(4,5)P2.
Gag precursor protein showing the four different functional domains (A). The MA domain is covalently attached with a sequestered myristic acid moiety (green) and a highly basic binding pocket (blue). Gag is targeted to the MA domain via the electrostatic interaction between the basic binding pocket and the negatively charged PI(4,5)P2 head group (B). According to the model of Saad *et al.*, binding between MA and PI(4,5)P2 leads to the flipping out of the sequestered myristic acid moiety into the plasma membrane while the 2' poly-unsaturated fatty acid of PI(4,5)P2 is flipped out of the plasma membrane and into the hydrophobic domain originally occupied by myristic acid. (C) Illustrative cartoon of PI(4,5)P2 structure, with phosphates on the 4 and 5 position (red) of the inositol ring (yellow) and the 1' – and 2'- acyl chain indicated. Note that the 2' acyl chain is more kinked than the 1' chains, indicating a higher degree of poly-unsaturation. Figure taken from (Freed, 2006).

While such specific mechanisms have not been established for other retroviruses, the electrostatic homology between all retrovirus Gag MA domains predicts a commonly evolved pathway for Gag targeting to the plasma membrane during retrovirus assembly (Murray et al.,

2005; Riffel et al., 2002). This would likely involve interactions with $PI(4,5)P_2$ and/or $PI(3,4,5)P_3$, the predominant phosphoinositide species in the plasma membrane (Rusten and Stenmark, 2006).

1.2.3 Lipids as alternative receptors for retrovirus entry

In order to enter its host, a retrovirus needs to first bind to specific receptors on the cell surface through its Env glycoprotein. However, this seems to contradict clinical observations that HIV can also infect CD4 negative cells found in the brain and gastrointestinal tract. This has contributed to investigations directed at the role played by non protein molecules such as lipids in retrovirus entry.

1.2.3.1 Glycosphingolipids as alternative receptors for retrovirus entry

Cell associated glycosphingolipids (GSLs) have been widely investigated for their role in retroviral entry. GSLs are ubiquitous constituents of mammalian plasma membranes, with diverse cellular roles including cell recognition, growth control, differentiation and tumorigenesis (Tettamanti, 2004). Structurally, GSLs contain a lipid group linked to a carbohydrate group via a glycosidic bond. In mammalian cells, the lipid group is typically made up of a ceramide molecule containing a sphingoid base that is derivatized on the 2-amino group with a fatty acid. The fatty acids vary in chain length and degree of saturations, though the most common in mammalian cells appear to be 16:0, 24:1 and 24:0. The attached carbohydrate group can take the form of uncharged sugars such as glucose, galactose and *N*-acetylglucosamine (GlcNAc) or may contain ionized functional groups such as phosphate, sulfate or charged carbohydrate residues such as sialic acid (N-acetylneuraminic acid) in

gangliosides. Because of such structural diversity, GSLs may exhibit numerous functions in cellular physiology.

GSL levels appear to regulate virus entry differently depending on the viral receptor status of the cell. In cells that do not express CD4 such as neuronal cells (Harouse et al., 1989) and colonic epithelial cells (Fantini et al., 1993), HIV appears to use GSLs as substitute receptors to gain entry. A binding site for galactosyl ceramide has been mapped to the HIV Env gp41 residues 650-685 thereby providing a structural basis for GSLs in HIV entry (Alfsen and Bomsel, 2002). In cells producing functional retroviral receptors, a direct association between the HIV receptor CD4 (Popik et al., 2002; Sorice et al., 2000), co-receptors CCR5 (Nguyen et al., 2005; Nguyen and Taub, 2002) and CXCR4 (Sorice et al., 2001) with GSL enriched lipid rafts has been observed. When cells express low endogenous levels of viral receptors, cell surface GSLs are known to be involved in promoting receptor aggregation, thus increasing the potential of receptor interaction (Rawat et al., 2004b; Rawat et al., 2006). On the other hand, when GSLs are expressed in excess in certain cell lines, they become a barrier to prevent virus receptor clustering, thus blocking subsequent events necessary for the formation of a functional fusion pore and infection (Rawat et al., 2004b). Conversely, one would predict that enrichment of GSLs on the retrovirus envelope (Nguyen and Hildreth, 2000) can also contribute to the attachment of the virus to the host. However, there is no experimental evidence suggesting this.

1.2.3.2 Role of PS in viral entry

So far, there have been limited reports regarding the involvement of PS in retrovirus entry. Lipid asymmetry exists in all cells, whereby PS and PE are cytoplasmic while PC and SM are exoplasmic facing lipids (Figure 3). During HIV infection of macrophage cells,

apoptosis occurs and PS becomes externalized (Callahan et al., 2003). Thus HIV virions produced from macrophages are known to be decorated with PS on the surface on their envelopes. In this system, the addition of PS-specific binding protein Annexin V or PS vesicles is able to reduce HIV-1 infection of macrophages but not T cells. This suggests that PS is an important cofactor specifically in HIV-1 infection of macrophages (Callahan et al., 2003), although the molecular mechanism at work is unknown. One possibility stems from a recent study of Vaccinia virus, which appear to use externalized PS in apoptotic mimicry as a way to infect macrophages (Mercer and Helenius, 2008).

Cell associated PS can also regulate retrovirus entry. When target cells bearing functional retrovirus receptors are treated with PS liposomes, which results in an increase of cell surface PS levels, retrovirus infectivity is non-specifically enhanced by up to 20-fold (Coil and Miller, 2005a). In some cases, cell specific glycosylation of viral receptors near the active virus binding site result in a block to functional receptor-virus interactions. However, with pre-treatment of PS liposomes, such blocks are relieved and the cells become susceptible to retrovirus infection. This effect is referred as “glycosylation-specific enhancement” by PS (Coil and Miller, 2005b).

1.2.4 Virus fission and fusion

An equally intuitive role of the retrovirus envelope is to provide the means by which the nascent retrovirus can form a protrusion at the assembly site before finally budding from the site through fission (Figure 7A). This envelope composition must subsequently allow efficient fusion of the mature virus with the membrane of a new host cell. For both events to occur, both cell and virus associated membrane bilayers must generate membrane curvature through a coordinated sequence of events involving membrane proteins and lipids to provide

the physical forces required to disrupt the original bilayer membrane structures (McMahon and Gallop, 2005; Zimmerberg and Kozlov, 2006). A part of this energy is provided by the interaction of specific retroviral proteins with their host counterparts, i.e. Gag with the ESCRT machinery and Env with the host surface receptors like CD4 (HIV) and mCAT-1 (MLV) (Goff, 2007). Another aspect of this energy is provided by the presence of particular lipids that are capable of producing curvature spontaneously or through interaction with protein partners.

1.2.4.1 Curvature inducing lipids

The underlying basis of lipids producing spontaneous curvature depends very much on their individual molecular geometry (Figure 7B). Lipids that have conical and inverted-conical shapes promote negative and positive spontaneous curvature respectively. Conical lipids are characterized by a relatively small head group compared to its fatty acyl portion and are represented by PA, cholesterol, ceramide, diacylglycerol (DG) and phosphatidylethanolamine (PE). Inverted conical lipids are characterized by a large head group compared to its fatty acyl portion and are represented mainly by lysolipids, i.e. lipids with a single fatty acyl chain. On the other hand, PS and phosphatidylcholine (PC) have relatively low spontaneous curvature because their large head group compensates for the double fatty acyl chains, giving these lipids a cylindrical shape. In theory, membrane in a state of dynamic flux should exhibit local accumulations of curvature forming lipids and a concomitant decrease in cylindrical lipids in membrane regions with a highly bent structure (Figure 7A). This would lead to an energetically favorable state that allows membrane rupture and mixing needed to complete fusion or fission activities.

There are a number of ways that changing lipid composition can drive curvature in a biological system. Common enzymatic reactions such as the production of lysoPA and PA, which are interconverted by lysophophasphatidic acid acyl transferase and phospholipase A2 activity respectively, favor opposite membrane curvatures (McMahon and Gallop, 2005). On the other hand, lipids may respond to curvature by concentrating in domain curvatures that they energetically prefer. A direct demonstration of this effect was recently shown by the accumulation of PE in the membrane fusion stalk of mating Tetrahymena cells (Ostrowski et al., 2004). Lastly, when flippases and scramblases change the topology of lipids like PS and PE, it effectively changes asymmetry of a membrane bilayer and the net curvature energy along a lipid plane. This results in spontaneous membrane curvature and vesicle formation required during endocytosis (Farge et al., 1999; Hua and Graham, 2003).

One would expect lipids to play a major role in directing membrane activity in viruses during budding and fusion (Figure 7A). Recently lipidomics analysis of HIV particles found high levels of plasmalogen PE (pPE) molecules, a lipid class with strong fusogenic activity (Nagan and Zoeller, 2001), compared to total cellular levels. The loss of carbonyl oxygen and the presence of the vinyl ether double bond give pPE different physical properties when compared to their diacyl PE counterparts. For instance, pPE tends to form non-bilayer Hex II structures at or below 30°C, while diacyl analogues form these structures at much higher temperatures (Glaser and Gross, 1994; Lohner, 1996). Energetically, this would mean easier formation of the hemi-fusion stalk-like state so that budding and entry become less challenging for the retrovirus. Consistent with this idea, it has been shown in both class I (Chernomordik et al., 1998; Gunther-Ausborn and Stegmann, 1997; Martin and Ruysschaert, 1995) and class II (Stiasny and Heinz, 2004) viruses, the presence of inverted-cone shaped lipids in the target membrane severely inhibit the fusion mechanism while cone shaped lipids enhance it.

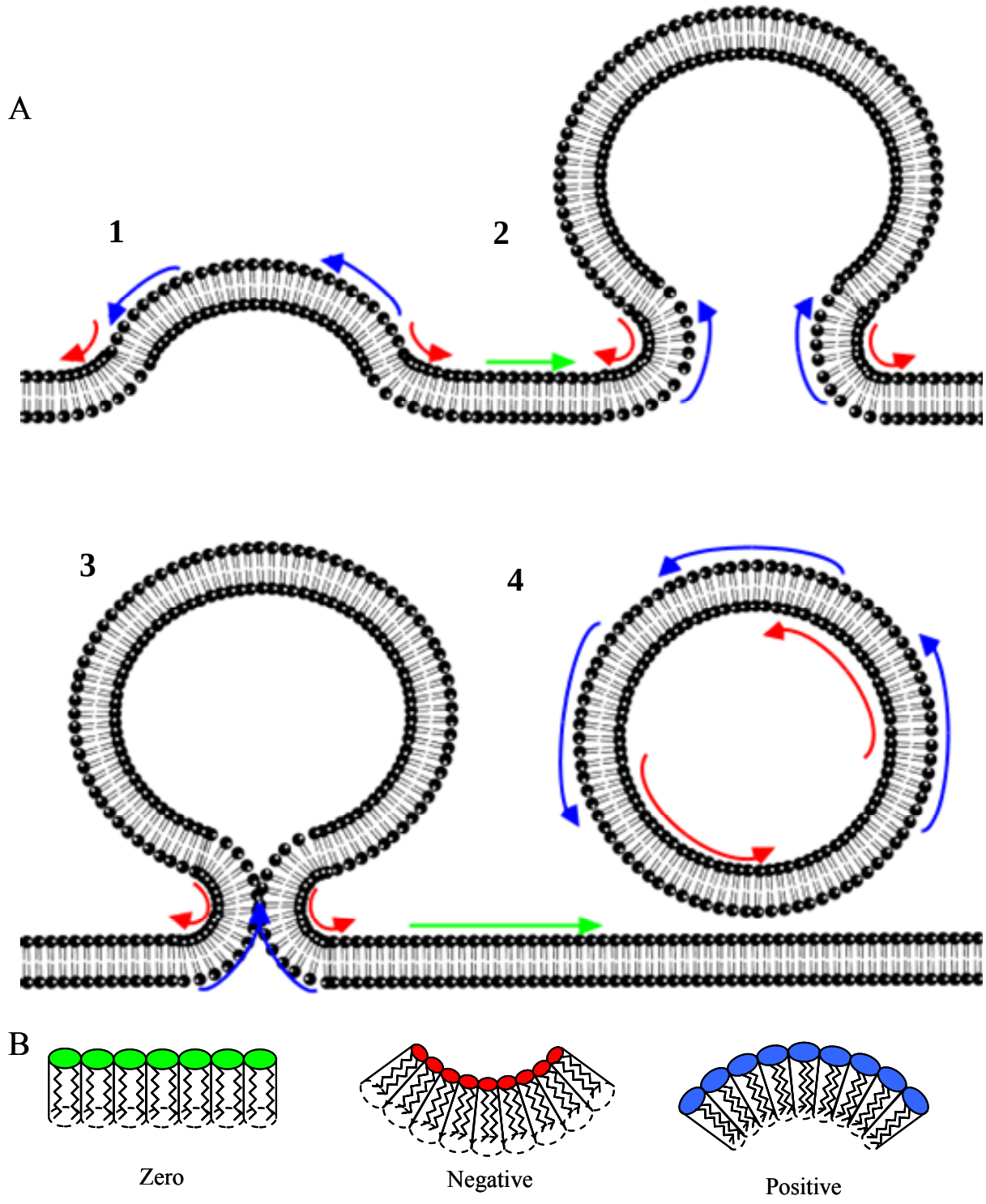

Figure 7. Progression of membrane invagination and dynamics involved in viral budding.
(A). Step 1: Early stage budding of plasma membrane triggered by invagination of membrane. Step 2: Hemifusion state characterized by the formation of the vesicle and the pulling of adjoining membranes together. Step 3: Late stage stalk formation, characterized by the two adjoining membranes merging their outer leaflet together. Step 4: Fission of membrane stalk to form complete virus vesicle. Red, blue and green arrows show bilayer regions expected to accumulate lipids exhibiting negative, positive and zero curvature respectively. Membrane curvature formed by accumulation of lipids with inherent geometrical shapes (B). Cylindrical shaped lipids (green) produces zero curvature, conical lipids (red) produces negative curvature while inverted-conical lipids (blue) produces positive curvature.

1.2.5 Lipid expression is modified to support retrovirus replication

The replication of an obligatory retrovirus would undoubtedly place some burden on the host cell lipid metabolism. In fact, an increased risk of arthrosclerosis and coronary artery disease due to dyslipidemia is a recognized clinical problem in HIV-infected patients (El-Sadr et al., 2005; Escaut et al., 2003) as is the appearance of antibodies against GM2 (Wu et al., 1999), GM3 (Griggi et al., 1994), and PS (Silvestris et al., 1996). At the cellular level, it was found that changes in cellular morphology including the appearance of lipid bodies in macrophages, led to the formation of foam cells common in arthrosclerosis (Mujawar et al., 2006).

Gene expression analysis of both MLV and HIV infected cell lines and primary cells indicated that numerous genes involved in cholesterol metabolism and trafficking are altered by infection (Beer et al., 2003; Giri et al., 2006). In the case of HIV, it was found that expressing the Nef accessory protein of HIV alone is able to simultaneously increase cholesterol biosynthesis and impair ATP-binding cassette transporter A1 (ABCA1)-dependent cholesterol efflux from human macrophages. Furthermore, Nef contains a cholesterol binding sequence in its C terminus which allows it to transport cholesterol to lipid rafts and progeny viruses to allow proper HIV release (Zheng et al., 2003).

1.3 Motivation and objectives of study

1.3.1 Past studies on retroviruses

It is clear from literature review that lipids play important roles in the replication cycle of retroviruses to support of virus propagation. Therefore, detailed knowledge pertaining to the molecular composition of the retroviral lipid envelope would provide

important information about its role in the replication cycle, particularly regarding the nature of the budding site.

Previously published works compared the lipid composition of HIV with that of plasma membrane and total cell membrane of their host cell respectively and suggested that HIV buds from microdomains or lipid rafts (Aloia et al., 1993; Brugger et al., 2006). While both of these studies were fundamentally important, they were hampered by two main deficiencies. Firstly, both studies presented data on only a limited number of lipid classes despite the wide diversity of lipids found in mammalian cells. Because of this, we expect that lipids of significant biological properties would have been missed from these studies. Secondly, both studies only utilized HIV produced from a single cell type. One possible outcome is that this may lead a biased interpretation of results since different cell types, and by extension viruses produced from them, are expected to contain different lipid composition. In addition, the previous studies were HIV-specific and thus cannot sufficiently address the role of lipids on general retrovirus phenomenon.

1.3.2 Lipidomics model system

Given this context, it is clear that a more systematic and broad scoped lipid analysis of HIV and other retroviruses is needed. This would enable us to identify lipid targets for further functional characterization in the context of the retrovirus replication cycle. In this regard, we propose the use of a lipidomics approach to study retrovirus lipids (Figure 8). The methodology of lipidomics, defined as the systems level analysis and characterization of lipids and their interacting moieties, consist of a four steps approach: 1) identify the conditions required and sample preparation, 2) lipid extraction, 3) lipid analysis and 4) functional analysis of candidate lipid pathway metabolism (Wenk, 2005). Such a framework

provides a convenient and logical way by which to visualize the experimental design that we will be using in this study and the intended objectives of these experiments.

1.3.3 Experimental approach and intended outcomes

The first step begins with identifying and preparing the conditions to analyze, which in our case consists of purified retrovirus particles (Figure 8) and a suitable reference. Retroviruses were propagated to high titers and purified from host cells using standard biochemical protocols. This work was done in collaboration with our collaborators Walther Mothes (Yale University School of Medicine, Department of Microbial Pathogenesis) and David Ott (AIDS and Cancer Virus Program, SAIC-Frederick, Inc., National Cancer Institute at Frederick). We used both total cell membrane and plasma membrane fractions as a basis of comparison for the retrovirus lipid data. The purity of virus isolates and plasma membrane fractions were judged by electron microscopy and western blotting techniques against membrane markers respectively. With the total cell membrane control, we are looking to recapitulate the results of Brugger et al, thus proving that our methods of analysis are comparable. On the other hand, purified plasma membrane fractions would serve as a more relevant control since retroviruses use the plasma membrane as their budding site.

Next, lipids from the viruses and control samples must be extracted using the appropriate extraction solvent composition (Figure 8). Unlike nucleic acids and proteins, lipid molecules are diverse in structure and hence also widely varying in their biochemical and biophysical properties, including differences in solubility in different types of solvents. Because of this, there is currently no extraction method that can efficiently recover all classes of lipids in a single protocol. For our intention of detecting and measuring all lipids found in

the retrovirus envelopes, we will be investigating the use of different extraction methods to sufficiently cover most lipid classes.

In the third step, lipid extracts were analyzed mainly via liquid chromatography (LC) and electrospray ionization mass spectrometry (ESI-MS) (Figure 8). In ESI-MS, the ionization and fragmentation pattern of a lipid extract can be finely controlled and used in both profiling and structural identification of lipids. Almost all of the major lipid classes that we are interested in including phospholipids, sphingolipids and neutral lipids, can be readily detected. The fragmentation patterns of many lipid classes has been resolved via tandem mass spectrometry and will allow us to quantify lipid classes based on their specific product ions (Brugger et al., 1997; Han and Gross, 2005). While the ESI-MS ion source enables the convenience of direct infusion of crude lipid extracts (Han and Gross, 2005), there is also the option of coupling HPLC separation with ESI-MS analysis (Camera et al., 2004; Isaac et al., 2003; MacPherson et al., 1996; McDonald et al., 2007; Merrill, Jr. et al., 2005; Shui et al., 2007a). This increases the sensitivity of the instrument by decreasing the chemical suppression in the ion source and also allows the separation of lipid molecules with the same m/z value but different physical properties. The objectives of these experiments will be to identify lipid molecules which are enriched or de-enriched in the retrovirus envelope with respect to the control membrane fraction. We hypothesized that lipid enrichment in the retrovirus envelope may imply that the particular lipid class plays an important functional role in the biogenesis of the virus.

Lastly, based on the results of the detailed lipid analysis, we investigated the biological activity of specific lipid classes including phosphoinositides, GSLs and aminophospholipids in the context of the retrovirus replication (Figure 8). It is envisioned that such experiments will help to validate the importance of the biochemical data obtained through initial comprehensive lipid profiling.

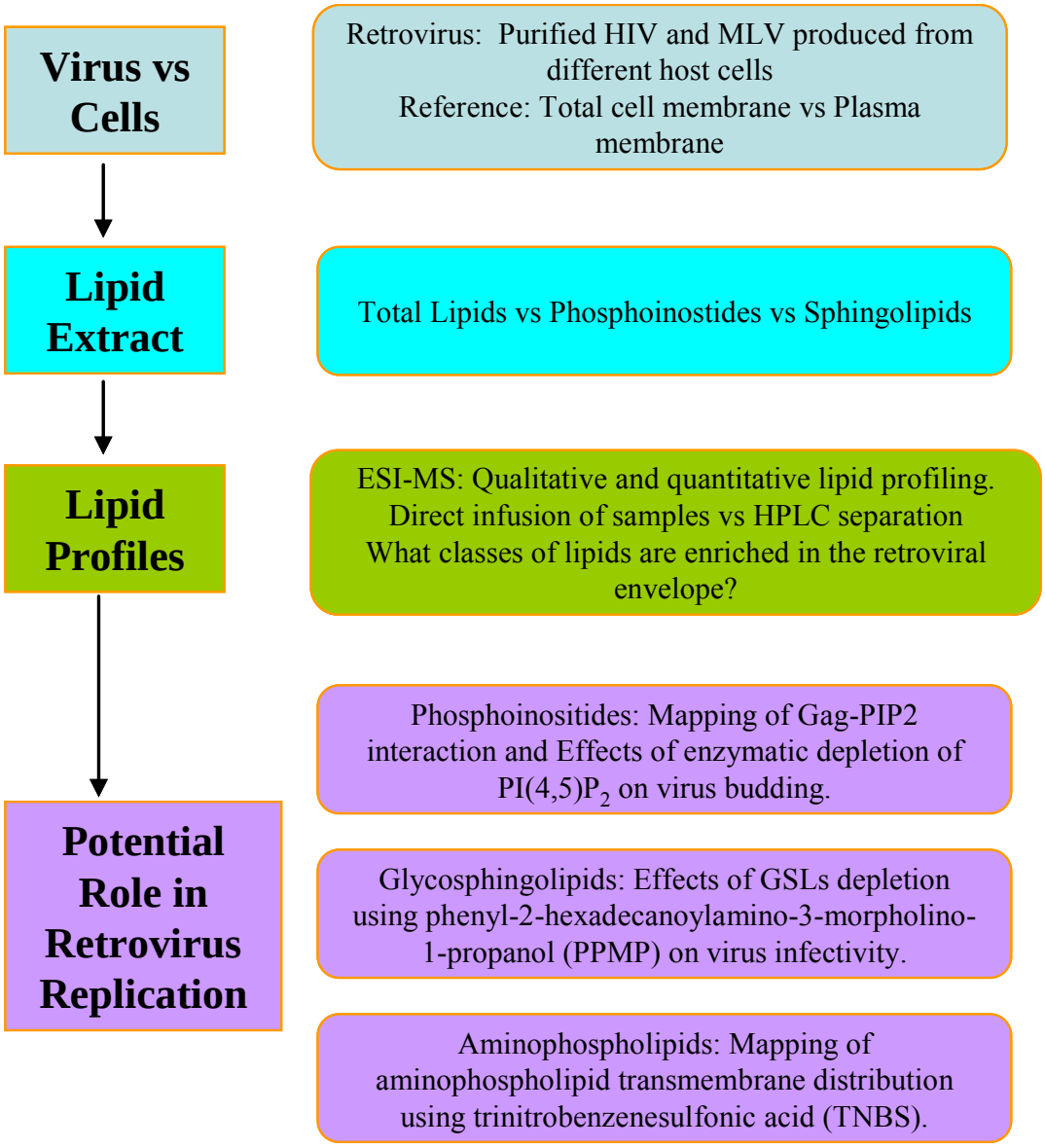

Figure 8. An illustrative framework for the functional lipidomics analysis of retrovirus envelope lipids. Adapted from (Wenk, 2005).

Chapter 2 – Lipidomics analysis of retrovirus envelopes

2.1 Introduction

In this study, we anticipate that a detailed analysis of the lipid composition of retrovirus envelopes compared to the host cell membrane may provide important information about the assembly and budding process, especially regarding the nature of the budding site. We built upon previous analyses of HIV lipid composition (Aloia et al., 1993; Brugger et al., 2006) and analyzed the lipid composition of highly purified samples of retroviruses including HIV and MLV by mass spectrometry. Comparisons were made not only to total cell membrane but to that of the membrane from which these viruses bud, the plasma membrane (Figure 9). In order to minimize biased interpretation that may result from the unique lipid composition of a host cell, we expanded the host range where possible, i.e. HIV was produced from both H9 cell line (Ott et al., 1995) and monocyte-derived macrophages (MDM) (Freed et al., 1995) while MLV was produced from both Rat Embryonic Fibroblast cell line (REF) and avian embryonic fibroblast cell line expressing the murine ecotropic receptor MCAT-1 (DFJ8) (Barsov et al., 2001). Given the scope of lipid diversity present in mammalian cells, we attempted to provide a broader coverage of lipids compared to Aloia et al. and Brugger et al. These include important lipid classes involved in lipid signaling and immunological responses such as phosphatidylinositol (PI), phosphatidylinositol phosphate (PIP), phosphatidylinositol bisphosphate (PIP_2), ether phosphatidylcholine (ePC), glycosphingolipids GM3 and neutral lipids including diacylglycerols (DG), triacylglycerols (TG), cholesterol (Chol) and cholesterol esters (CE).

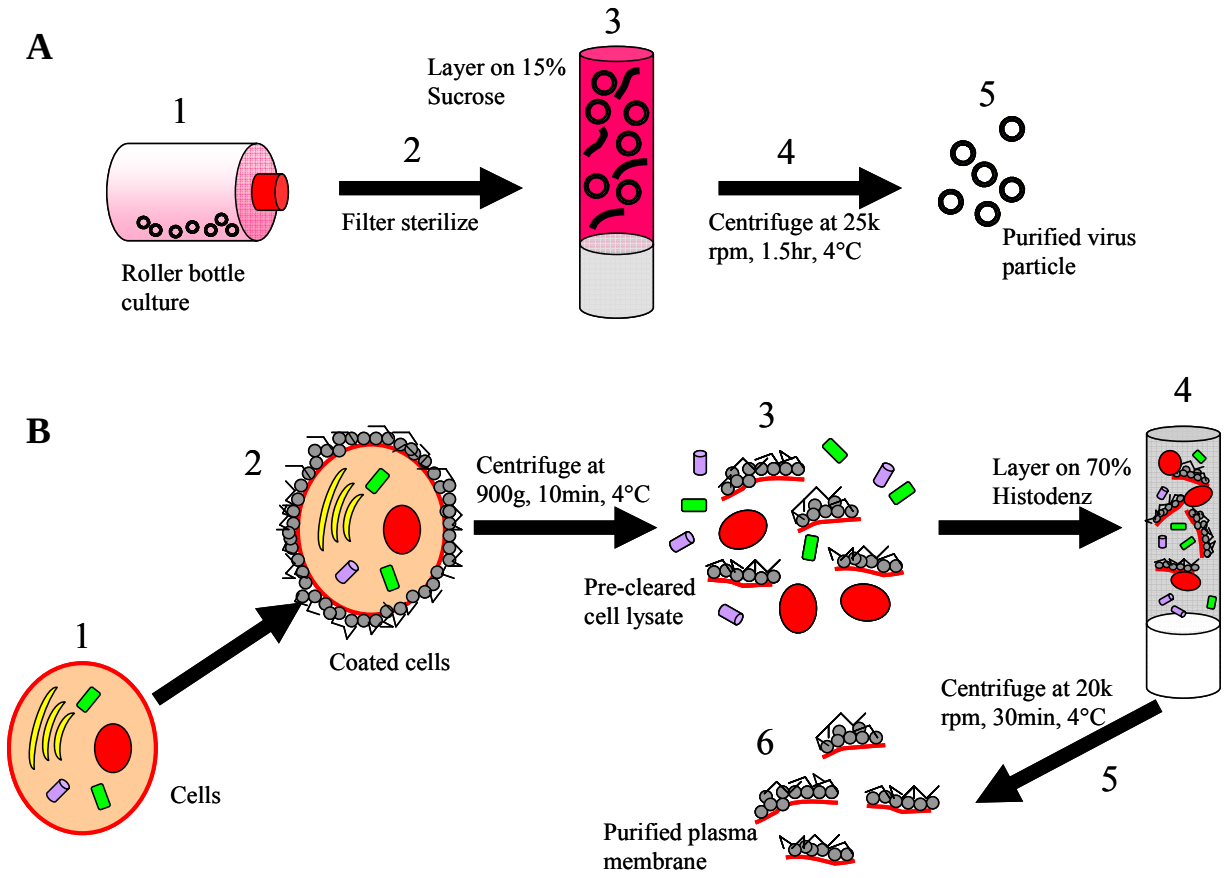

Figure 9. Experimental setup for comparative lipid profiling of retrovirus envelopes.
(A) Purification of retrovirus particles. Step 1: Roller bottle culture of adherent cells to concentrate retrovirus production. Step 2: Filter sterilize culture supernatant using 0.45µM filter. Step 3: Layer culture supernatant on a 15% sucrose cushion. Step 4: Centrifuge at 25,000rpm for 1.5hr at 4°C. Step 5: Remove supernatant and sucrose cushion to obtain pure virus pellet ready for lipid analysis. Purification of HIV requires an additional step using anti-CD45 immunodepletion. (B) Isolation of plasma membrane fraction. Step 1: Culture and collect producer cells. These cells are either used for total membrane reference or for further isolation of plasma membrane. Step 2: Coat cells with cationic silica beads (positive charge) followed by an outer layer of polyacrylic acid solution (negative charge). Step 3: Lyse cells and carry out a pre-clearing centrifugation step on the lysate to remove internal vesicles. Step 4: Layer the cell lysate on a 70% Histodenz cushion. Step 5: Centrifuge at 20,000rpm for 0.5hr at 4°C. Step 6: Remove supernatant and 70% Histodenz to obtain purified plasma membrane fraction.

2.2 Materials and Methods

2.2.1 Reagents

All cell culture media and supplements were purchased from GIBCO, Invitrogen (Carsbad, CA, USA) or from the National University Medical Institute (NUMI, Singapore) supply store. Lipid standards were purchased from Avanti Polar Lipid Inc (Alabaster, AL, USA) and Echelon Biosciences Inc (Salt Lake City, UT, USA). All other reagents and chemicals including HPLC grade methanol, chloroform, piperidine were purchased from Sigma Aldrich (St Louis, MO, USA) unless stated otherwise. Antibodies were either purchased from Zymed Laboratories (South San Francisco, CA, USA), BD Biosciences (Franklin Lakes, NJ, USA), Abcam (Cambridge, UK) or Santa Cruz Biotechnology (Santa Cruz, CA, USA).

2.2.2 Cell culture

Uninfected H9 and the chronically HIV-1-infected H9 cell line, Clone 4 (Ott et al., 1995) were cultured in RPMI 1640 media with 10% fetal bovine serum, 2mM L-glutamine, penicillin G at 100U/ml, and streptomycin sulfate at 100µg/ml (complete media). Uninfected and chronically infected rat embryonic fibroblast (REF) cell lines were cultured in DMEM media with 10% fetal bovine serum, 2mM L-glutamine and penicillin G at 100U/ml, and streptomycin sulfate at 100µg/ml (complete media). Avian embryonic fibroblast cell line expressing the murine ecotropic receptor MCAT-1 (DFJ8), were grown in the same media supplemented with G418 at 200µg/ml to maintain stable expression (Barsov et al., 2001). During virus production, DFJ8 cells were cultured without G418 as it was suspected that G418 may interfere with the viral budding process.

2.2.3 Isolation and culture of macrophages

Elutriated monocytes from HIV-negative donor leukopacs were obtained from the NIH Transfusion Branch and cultured at 2-3x10^6 cells per well on ultralow-attachment six-well Costar plates (catalog # 3471, Corning, Acton, MA) in RPMI 1640 media as supplemented above for 7 days to generate monocyte-derived macrophages (MDMs). MDMs were infected with the CCR5-tropic NLAD8 (Freed et al., 1995) overnight followed by two PBS washes to remove non-adhered virus. The infected cultures were then cultured and supernatants were periodically removed for virus isolation.

2.2.4 Virus stock preparation

Concentrated MLV stocks were produced in roller culture bottles from chronically infected REF and DFJ8 cells. The culture supernatants were collected and passed through a 0.45μm filter, centrifuged at 25,000rpm at 4^{o}C for 90min through a 15% sucrose layer to obtain purified virus. For HIV produced from Clone 4 and MDMs, the culture supernatants were passed through a 0.45μm filter, centrifuged through 15% sucrose cushion and the resulting HIV pellet further purified away from contaminating microvesicles using anti-CD45 depletion (Trubey et al., 2003). The purity of our virus was either checked via electron microscopy or western blots against the retrovirus Gag proteins. All virus and microvesicle stocks were stored at -80°C until further use.

2.2.5 Plasma membrane extraction using cationic silica beads[1]

Plasma membrane fractions were purified using cationic colloidal silica beads (Harila et al., 2006; Mason and Jacobson, 1985; Stolz and Jacobson, 1992). At least 10^6 cells were typically used for each extraction experiment. Adherent cells were washed with PBS and trypsinized at 37°C for 3-4min to detach them from the tissue culture plate. The trypsin was inactivated by washing the detached cells with complete cell culture media. The cells were finally washed with PBS and pelleted with centrifugation carried out at 300g for 3min at 4°C. Suspension cells were also washed with PBS in the same way. These steps prepared cell pellets that were ready for silica beads coating. All subsequent steps hereafter were performed at 4°C.

The cell pellet was re-suspended in 1ml of plasma membrane coating buffer (PMCB). The cell suspension was added drop-wise into 5ml of 1% (wt/vol) cationic colloidal silica beads (kindly provided by Donna Beer Stolz, University of Pittsburgh School of Medicine) in PMCB. To remove excess unbound cationic silica, the cells were then washed with 20ml total volume of PMCB by pelleting through centrifugation carried out at 300g for 3min, repeated three times. After the third wash, the cells, now bound with cationic silica beads, were again resuspended in 1ml of PMCB. The cells were added drop-wise into 5ml of polyacrylic acid in PMCB (PAA/PMCB). The cells were washed twice with 20ml total volume of PMCB followed by to remove excess PAA/PMCB solution. The bound cells were then incubated in a hypotonic lysis buffer, supplemented with protease inhibitors (Roche, IN, USA) for 30mins, with gentle agitation. The hypotonic condition resulted in swelled cells that were then lysed using 20-30 strokes of a tight fitting Dounce homogenizer. Cell disruption was verified by trypan blue (Gibco) exclusion using a light microscope. The suspension was then centrifuged

[1] Refer to Appendix 1 for the recipes of reagents used under the section *"Plasma membrane extraction from cells using cationic silica beads"*.

at 900g for 10min to remove internal membranes released; leaving behind a pellet that contains nuclei and silica bound plasma membrane fragments. The plasma membranes in the resulting pellet were purified away from the nuclei by sedimentation through a 70% (wt/vol) Histodenz (Sigma) in lysis buffer cushion using a TW41 rotor at 20,000 rpm for 30mins. The purified plasma membrane pellet, which appeared as a glassy membranous disc, was collected into a microfuge tube and washed 3 times with the lysis buffer at 14,000rpm for 5mins to remove any residual Histodenz as Histodenz is known to interfere with subsequent protein analysis. The purified PM was stored at -80°C before further use.

2.2.6 Plasma membrane extraction from cells using Optiprep gradient[2]

Plasma membrane was also extracted using a 5-20% (wt/vol) continuous Optiprep (Axis-Shield, Sigma) gradient, as described in the Optiprep application sheet S23. Optiprep is a 60% solution of iodixanol in water. A 40% iodixanol working solution (WS) was prepared by mixing 2 volumes of Optiprep with 1 volume of Optiprep diluent. Subsequent dilutions of the WS were carried out using a WS diluent. The continuous gradient was prepared by layering equal layers of 5% (top), 10%, 15% and 20% (bottom) of iodixanol in the ultracentrifuge tube and allowing passive diffusion to occur at room temperature over a period of 3h to 4h prior to use. At least 10^6 cells were harvested in 250µl of homogenization buffer, supplemented with protease inhibitor (Roche) and lysed using 20-30 strokes of a Dounce homogenizer. Homogenates were centrifuged at 1000g for 5min to pellet nuclei and cell debris. Postnuclear supernatant was loaded onto the preformed 5 to 20% continuous Optiprep gradient and centrifuged at 150,000g at 4°C for 20h using a SW41 ultracentrifuge

[2] Refer to Appendix 1 for the recipes of reagents used under the section *"Plasma membrane extraction from cells using Optiprep"*.

rotor. 13-15 fractions (800µl) were sampled from the top of gradient and subsequently stored at -80°C before further use.

2.2.7 Protein analysis to check for plasma membrane purity[3]

The purity of the plasma membrane preparations was checked via western blotting. Proteins from the plasma membrane preparations were extracted using RIPA buffer (Pierce, IL, USA) supplemented with protease inhibitor (Roche). PM fractions in the extraction buffer was agitated for 30min at 4°C and then centrifuged at 12,000 rpm for 30min at 4°C. The supernatant was then collected and used for further protein analysis. The protein amount was quantified using the Bio-Rad (Hercules, CA, USA) Protein Assay, based on the method of Bradford. The protein samples were loaded onto either a 10% or 12% SDS-PAGE gel and the proteins were separated by electrophoresis at 120V for a period of about 2h. The molecular weight marker used was the Precision Plus Protein Dual Color Standards from Bio-Rad. After protein separation, the proteins were transferred onto a PVDF membrane (Pall, Northern Boulevard East Hills, NY, USA) via wet transfer at 100V for 2h or 20V for O/N. Prior to the transfer reaction the PVDF membrane was activated by soaking in methanol for 15 min, followed by washing with the transfer buffer for 5 min prior to use.

To ensure proper protein transfer reaction, the membrane was reversibly stained by Ponceau S (Bio-Rad) solution before washing off the stain using Milli-Q water. The immunodetection reaction was initiated by blocking non-specific binding by immersing the membrane in blocking solution for 30min. Next, the membrane was immersed in primary detection antibody that was diluted in the blocking solution for at least 2h at room temperature or overnight at 4°C. The primary antibodies used included anti-TrF (Zymed

[3] Refer to Appendix 1 for the recipes of reagents used under the section *"Protein analysis"*.

Laboratories), anti-Flotillin (BD Biosciences or Abcam), anti-Caveolin, (Abcam), anti-Actin (Abcam), anti-Rab5 (Abcam), EEA1 (Santa Cruz) and Lamp1 (Santa Cruz) and these were diluted according to the manufacturer instructions. This was followed by two membrane washes in 3x changes of wash solution, 5min per wash. The membrane was then transferred to the appropriate secondary antibody solution for at least 2h at room temperature or overnight at 4°C. The antibody was diluted according to the manufacturer instructions to ensure proper staining without background. After secondary detection, the membrane was washed 3x with the wash solution. The antibodies were detected using SuperSignal West Dura Pico Substrate solution from Pierce Biotechnology (Rockford, IL, USA) according to the manufacturer instructions. The blots were re-used up to 3 times by stripping away the binding antibodies using Restore PLUS Western Blot Stripping Buffer (Pierce). Refer to Appendix 1 for recipe of solutions used.

2.2.8 Lipid preparation

Total lipid samples were prepared using a modified version of Bligh and Dyer method (Bligh and Dyer, 1959). All buffers and reagents were pre-chilled in an ice-bath. Virus or cells were washed and re-suspended in 50µl PBS. 0.6ml of a chloroform:methanol (1:2) mix was added to the sample and the mixture was vortexed vigorously for 3x1 min with a 5 min interval in between. Next, 0.3ml chloroform and 0.2ml 1M KCl was added to the tube and the mixture was again vortexed, three times for 30 s with intervals of 1 min in between. The mixture was then centrifuged for 2 min at 9,000 rpm to separate the phases. The lower organic layer was transferred to a clean microfuge tube and was dried under a stream of N_2 gas or via speed vacuum. Phosphoinositide enriched lipid samples were prepared by replacing the 1M KCl solution with 1M HCl (Wenk et al., 2003). Sphingolipid samples were

prepared via the alkaline hydrolysis method described by Merill (Merrill, Jr. et al., 2005). Briefly, 0.75ml of chloroform:methanol (1:2) was added to the sample and sonicated until they appeared evenly dispersed, then incubated overnight at 48°C. Next the tubes were cooled and mixed with 75µl of 1 M KOH in methanol, and incubated for 2 hr at 37°C with shaking. The sample was then neutralized with 6µl of glacial acetic acid. Lastly, 0.5ml of chloroform and 0.3ml of water was added to the tube and the mixture was then centrifuged for 2 min at 9,000 rpm to separate the phases. The lower organic layer was transferred to a clean microfuge tube and was dried under a stream of N_2 gas or via speed vacuum. A summary of the methods used are provided in Table 3.

Sample Type	**Method**	**Lipids measured by ESI-MS**	**Remarks**
Total lipid extract	Modified Bligh and Dyer with 1M KCl break phase	All lipids except DHSM, PIP and PIP_2	General lipid extraction protocol
Phosphoinositide extract	Modified Bligh and Dyer with 1M HCl break phase	PI, PIP and PIP_2	Acid labile plasmalogens and ether phospholipids are hydrolyzed
Sphingolipid extract	Modified Bligh and Dyer extraction follow by KOH hydrolysis	SM, DHSM, sphigosine, ceramides, hexosyl ceramides and GM3	Glycerophospholipids are hydrolyzed

Table 3. Lipid extraction protocols used in this study.

2.2.9 Analysis of lipids using high performance lipid chromatography/electrospray mass spectrometry

Qualitative lipid profiling via electrospray ionization mass spectrometry (ESI-MS) was carried out with a Waters Micromass Q-TOF mass spectrometer with an upfront Waters CapLC inlet (Waters Corp., Milford, MA) as described previously (Shui et al., 2007b). The capillary voltage and sample cone voltage were maintained at 3.0kV and 50V, respectively. The source temperature was 80°C, and the desolvation temperature was set at 250°C. Mass spectra were acquired in the negative ion mode with an acquisition time of 3 min.

Chloroform-methanol (1:1, vol/vol) at a flow rate of 15µl/min was used as the mobile phase. Typically, samples were dissolved in the mobile phase to give an appropriate concentration and 2µl of sample was injected for analysis.

For quantitative analysis, we used a triple quadrupole instrument ABI 4000 Q-Trap (Applied Biosystems, Foster City CA) in the multiple reactions monitoring (MRM) mode. In our experiments, the internal standards used included 1,2-dimyristoyl-glycero-phosphoserine (DMPS), 1,2-dimyristoyl-glycero-3-phosphoethanolamine (DMPE), 1,2-dimyristoyl-glycero-3-phosphocholine (DMPC), lauroyl sphingomyelin (L-SM), N-heptadecanoyl-d-*erythro*-sphingosine (C17 Ceramide) and d-glucosyl-ß1-1'-N-octanoyl-d-*erythro*-sphingosine (C8 Glucosyl Ceramide) (Avanti Polar Lipids) which allowed the measurement of phosphatidylserine (PS), phosphatidylethanolamine (PE) and plasmalogen phosphatidylethanolamine (pPE), phosphatidylcholine (PC) and ether phosphatidylcholine (ePC), sphingomyelin (SM) and dihydrosphingomyelin (dhSM), ceramide (Cer) and glucosylceramide (GluCer) respectively. PI, PIP and PIP_2 levels were referenced to 1,2-dioctanoyl-glycero-3-phosphoinositol (C8-PI), 1,2-dioctanoyl-glycero-3-[phosphoinositol-4-phosphate] (C8-PI(4)P) and 1,2-dioctanoyl-glycero-3-[phosphoinositol-4,5-bisphosphate] (C8-PI(4,5)P_2) (Echelon Biosciences Inc) respectively. Since a suitable standard was not available for GM3, we normalized GM3 levels to SM levels. In other instances where no internal standards were used, the individual lipid species were normalized to the total measured signal intensity of the sample. The total lipid and sphingolipid extracts were dissolved in chloroform:methanol (1:1, vol/vol) and typically, 10 to 15µl of the sample was injected via autosampler. For the phosphoinositide samples, the lipids were dissolved in chloroform:methanol (1:1), spiked with 1/10 volume of 300ppm piperidine solution and directly infused into the mass spectrometer (Wenk et al., 2003). The m/z transitions used were published previously (Brugger et al., 1997; Merrill, Jr. et al., 2005; Wenk et al., 2003)

and we optimized the declustering potential and collision energy using the Quantitative Optimization function available on the Analyst 1.4.1 software. The optimized parameters used in these experiments are displayed in Appendix 2 to 4. The instrument was calibrated using PPG standards provided by ABI and the mass tolerance was adjusted to ~100ppm or 0.1Da. The signal intensity obtained for each lipid species was converted to their mol level in each fraction by normalization to the appropriate internal standard. The final lipid molar percentages of each sample were obtained by cross normalizing the lipid levels of each fraction measured as described below (Ivanova et al., 2001). The standard deviations shown represent the variation in at least 3 replicate experiments, i.e. $n \geq 3$, unless stated otherwise.

For the measurement of neutral lipids, we employed a triple quadrupole instrument ABI 3200QT (Applied Biosystems, Foster City CA) connected with a high performance liquid chromatography (HPLC) system using a sensitive HPLC/ESI-MS method (Shui G et al, manuscript in preparation). Briefly, lipids were separated on an Agilent Zorbax Eclipse XDB-C18 column with dimensions 4.6x150mm (Agilent Technologies, Santa Clara CA) at 30°C using chloroform:methanol:2% 0.1M NH_4OAC (100:100:4 vol/vol/vol) as a mobile phase at a flow rate of 250µL/min and an injection volume of 30µl. Mass spectrometry was recorded at both positive and negative ESI modes in enhanced MS (EMS) scan mode for overall spectrum profile and Q3 scan mode for targeted lipid profile. The relevant instrument conditions included a turbo spray source voltage of +5000V and -4500V for positive and negative respectively and a source temperature of 250°C. A total run time of 30min was utilized to elute both polar lipids and neutral lipids. The elution profile of the various lipid classes are in the following order: MG (5.5-6min), free Chol (7-7.5min), CE (12-20min), DG (7-10min), TG (12-26min), phospholipids (7-12min). Due to the lack of relevant internal standards for the neutral lipids, the intensity level measured in each class of neutral lipids obtained was normalized to the total Q3 signal intensity obtained from each analysis. Chol-

to-PC ratio was also used to compare the cholesterol levels between the samples as carried out previously by Brugger et al. The cholesterol levels were calculated by normalizing the 369 m/z peak intensity to the total PC peak intensity, both of which were measured at positive mode.

2.2.10 Calculation of total lipid levels

For each of these different extracts, the quantity of each relevant lipid species was measured by following their MRM transition. The signal intensity obtained for each lipid species was converted to their mole levels using Eqn (1). The assumption we have made here is that the standards and the lipids being measured are found within the linear concentration to signal intensity range.

$$\frac{No\ of\ Moles\ of}{Lipid\ Species} = \frac{No\ of\ Moles\ of\ Internal\ Standard}{Signal\ Intensity\ of\ Internal\ Standard} \times \frac{Signal\ Intensity}{of\ Lipid\ Species} \quad \text{------ (1)}$$

Next, we then calculated the molar fraction of the lipid species measured within each extract using the Eqn (2).

$$\frac{Molar\ Fraction\ of}{Each\ Lipid\ Species} = \frac{No\ of\ Moles\ of}{Lipid\ Species} \div \sum \frac{No\ of\ Moles\ of}{All\ Lipid\ Species\ Measured} \quad \text{------ (2)}$$

Subsequently, the molar fraction of the lipids measured with the sphingolipid extract (SLE) and phosphoinositide extracts (PIE) were scaled to that of the total lipid extracts (TLE) by using SM and PI respectively as common denominator levels (3). An example is given below for the scaling of lipids from the SLE levels to TLE levels.

$$\frac{Scaled\ Molar\ Fraction\ of}{Each\ Lipid\ Species\ in\ SLE} = \frac{Molar\ Fraction\ of\ Each}{Lipid\ Species\ in\ SLE} \times \frac{Molar\ Fraction\ of\ SM\ in\ TLE}{Molar\ Fraction\ of\ SM\ in\ SLE} \quad \text{------ (3)}$$

This would allow the addition of the molar fractions of lipids measured in the SLE and PIE to that of TLE to obtain a cumulative molar fraction of all the lipids measured by MRM (4).

$$\begin{matrix}\textit{Cummulative Molar Fraction}\\ \textit{of All Lipids Measured}\end{matrix} = \sum \begin{matrix}\textit{Molar Fraction of All Lipids from TLE (except SM and PI)},\\ \textit{Scaled Molar Fraction of All Lipids from SLE and PIE}\end{matrix} \quad \text{------ (4)}$$

The final normalized molar fraction of each lipid class measured is then calculated as in Eqn (5).

$$\begin{matrix}\textit{Normalized MolarFraction}\\ \textit{of Each Lipid Class}\end{matrix} = \begin{matrix}\textit{Molar Fraction of}\\ \textit{Lipid Class Measured}\end{matrix} \div \begin{matrix}\textit{Cummulative Molar Fraction}\\ \textit{of All Lipids Measured}\end{matrix} \quad \text{------ (5)}$$

2.3 Results

2.3.1 Preparation of pure retrovirus particles

In order to analyze retroviral lipids, we purified HIV and MLV from culture supernatants of chronically infected cells by ultracentrifugation through 15% sucrose cushions. Electron microscopy inspection showed that this resulted in highly purified MLV particles with an electron dense core (Figure 10A). More importantly, the MLV preparation lacked any detectable microvesicles (MV) particles that appear as pleomorphic vesicles with a transparent centre that range in size from about 50 to 500nm (Bess, Jr. et al., 1997; Gluschankof et al., 1997) (Figure 10B). In contrast, HIV preparations isolated from culture supernatants of Clone 4 cells (Ott et al., 1995), a chronically infected H9 T-cell line, and monocyte derived macrophages (MDM), were previously shown to contain contaminating non-viral particles of MV (Bess, Jr. et al., 1997; Gluschankof et al., 1997). Proteomic analysis of these particles found that MV were enriched for CD45, T200 leukocyte common antigen, in its membrane while HIV specifically excluded CD45 from its membrane (Esser et al., 2001). Therefore, pure HIV particles were obtained by further purification of the culture supernatant after the 15% sucrose cushion step, using anti-CD45 immunodepletion to remove the contaminating MV (Trubey et al., 2003) (Fig 10B).

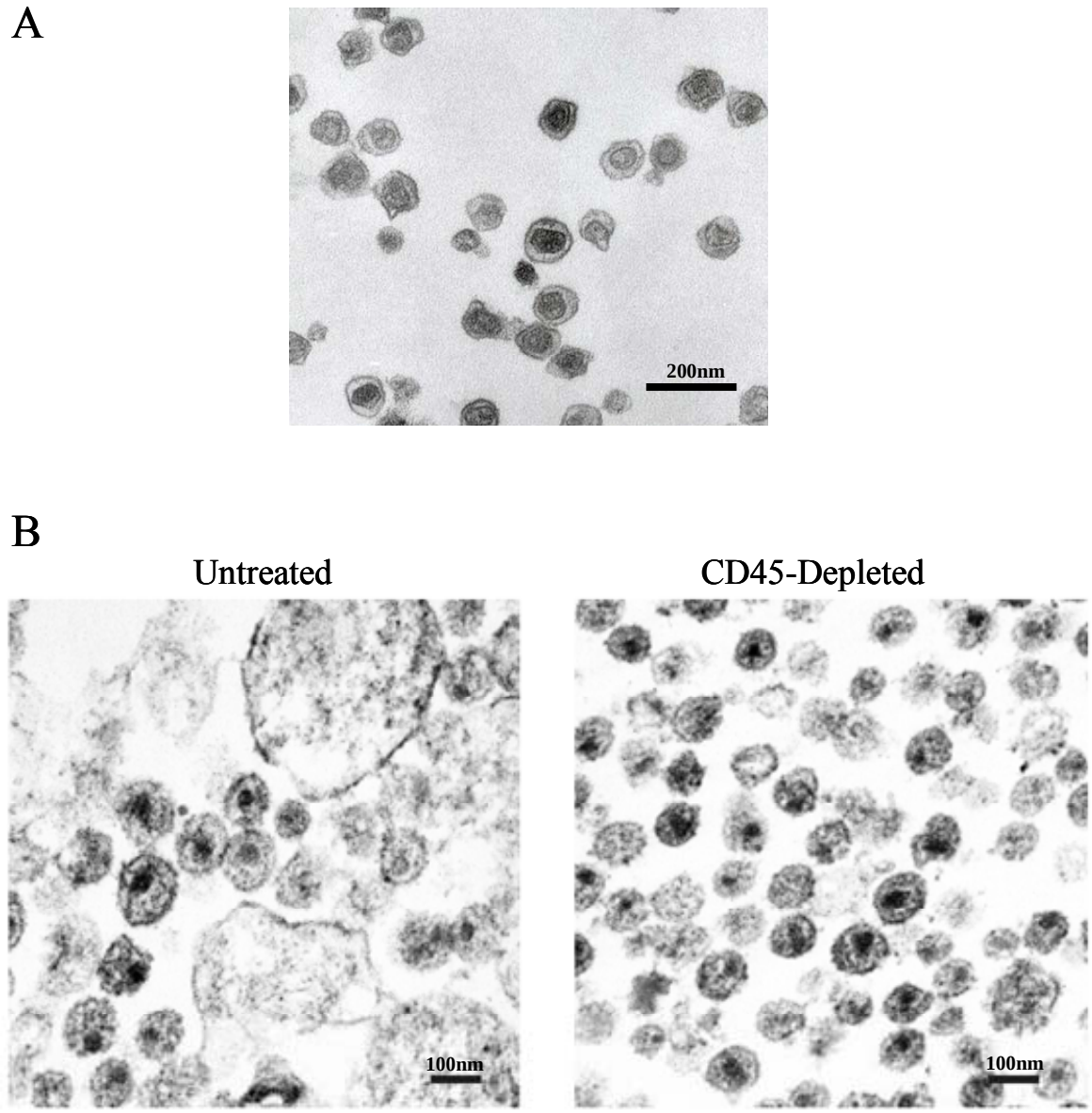

Figure 10. (A) Electron microscopy of purified MLV particles. (B) Electron microscopy images of purified HIV particles before and after anti-CD45 immunodepletion.

2.3.2 Methodology for lipid analysis

Due to the varying chemistry and solubility of different lipid classes, we prepared our samples in three different fractions using a variation of the chloroform:methanol extraction method (Bligh and Dyer, 1959) (Table 3). Total lipid (PS, PC, ePC, PE, pPE, PI, and SM) fractions were prepared using a slightly modified version of the standard Bligh and Dyer method, using 1M KCl instead of water for phase separation. This is thought to prevent some

acidic lipids from binding to denatured proteins during phase separation. Phosphoinositides (PI, PIP and PIP_2) are known to bind even more strongly to denatured protein, thus had to be extracted by partitioning into the organic phase at low pH using 1M HCl (Wenk et al., 2003). Sphingolipids (SM, dhSM, Cer, GluCer) were made accessible following mild alkaline hydrolysis of the total lipid extract (Merrill, Jr. et al., 2005). This treatment releases esterified fatty acid from the "contaminating" phospholipids in the mixture, leaving amide linked acyl groups in sphingolipids unaffected. This resulted not only in higher sphingolipid detection levels (Jiang et al., 2007), but also allowed the discrimination of SM species signal intensity from PC isomeric species signal intensities that have overlapping m/z values.

Finally, we employed a combination of electrospray ionization mass spectrometry (ESI-MS) methods to profile our lipid samples. Using the Waters Micromass Q-TOF instrument, our analyses were useful in providing a qualitative perspective of the lipid samples and also in identifying the different classes of lipids found in the sample due to its excellent peak resolution. However, it is important to note that the nature of these results provided only semi-quantitative data of the amount of lipids present in the samples. There are two reasons for this – (1) due to the different chemistries of the two different extracts, commonly known as the matrix effect of the sample, one can expect different ionization even of the same ions in the two different samples. This was most clearly shown by the differences in ionization of internal standards spiked into the samples (data not shown). (2) Beside this problem, another difficulty was trying to obtain a similar concentration of lipid extract to inject during the experiment. Differences in sample lipid concentration may result in differences in ionization efficiencies and ionic suppression. This problem was partially solved by using a crude method of spotting the samples on a TLC silica plate to check for their concentration and then re-dissolving them to the appropriate concentrations before carrying out the Q-TOF experiments (data not shown). We addressed this problem by using the ABI

4000 Q-Trap instrument for multiple reactions monitoring (MRM) measurements. This method is optimized to detect only specified ions of interest, thus increasing sensitivity and selectivity of detection, without being affected by the different chemistries of the samples (Fei et al., 2008; Merrill, Jr. et al., 2005). In total, ~250 individual lipid species were detected and quantified in the complex sample mixtures. To allow for the quantification of the relative amounts of lipids, each sample was spiked with a relevant cocktail of internal standards. The inclusion of the internal standards normalized for differences in ionization and fragmentation patterns of different lipid classes. By referencing to these internal standards, we were able to calculate the molar percentages of the individual lipid classes in each fraction, and then, through cross normalization to common lipid classes in each of the different extracts (described in Materials and Methods), the total molar percentages of all detectable lipid classes were obtained (Table 4, 5A and 6A).

	This Study					Brugger et al, 2006	Aloia et al, 1993
Virus	**HIV**	**HIV**	**CD45 MV**	**MLV**	**MLV**	**HIV**	**HIV-1**
Cell Line	**H9**	**MDM**	**MDM**	**REF**	**DFJ8**	**MT4**	**H9**
PS	13.4 ± 1.5	10.5 ± 1.4	9.4 ± 1.2	15.7 ± 1.9	15.1 ± 1.9	15.5 ± 2.2	9.0
PI	2.7 ± 1.3	3.0 ± 1.4	2.7 ± 0.6	1.5 ± 0.4	2.2 ± 0.4	n/a	0.4
PIP	2.1 ± 0.4	3.1 ± 0.4	0.7 ± 0.1	1.8 ± 0.3	3.1 ± 0.7	n/a	n/a
PIP_2	2.6 ± 0.7	3.6 ± 0.8	0.6 ± 0.1	7.3 ± 0.4	0.8 ± 0.4	n/a	n/a
PE	8.0 ± 2.5	5.3 ± 2.2	3.8 ± 0.9	7.3 ± 2.4	7.2 ± 1.2	8.2 ± 1.3	24.6
pPE	13.6 ± 3.9	12.6 ± 3.2	13.9 ± 3.0	16.0 ± 3.0	13.5 ± 2.2	27.0 ± 3.3	
PC	22.4 ± 3.8	17.0 ± 2.6	21.7 ± 1.5	15.6 ± 3.1	21.8 ± 1.8	16.0 ± 1.0	29.9
ePC	5.4 ± 0.9	4.6 ± 0.9	7.1 ± 0.9	3.4 ± 1.2	5.4 ± 1.2	n/a	
SM	20.7 ± 3.0	26.7 ± 2.3	28.9 ± 1.8	22.5 ± 3.1	26.6 ± 0.9	33.1 ± 1.2	24.1
dhSM	3.1 ± 0.2	8.3 ± 0.5	6.7 ± 0.3	5.6 ± 0.6	3.8 ± 0.1		
Cer	1.5 ± 0.4	1.6 ± 0.3	2.3 ± 0.3	1.4 ± 0.6	0.3 ± 0.2	n/a	n/a
GluCer	4.4 ± 1.0	3.7 ± 1.8	2.3 ± 0.4	2.0 ± 0.9	0.3 ± 0.2	n/a	n/a
PA	n/a	n/a	n/a	n/a	n/a	n/a	1.2
Others	n/a	n/a	n/a	n/a	n/a	n/a	8.3
Chol	0.14 ± 0.04	0.12 ± 0.03	0.36 ± 0.03	0.11 ± 0.01	0.09 ± 0.03	n/a	n/a
GM3	0.08 ± 0.01	0.12 ± 0.04	0.04 ± 0.00	0.35 ± 0.10	0.012 ± 0.005	n/a	n/a

Table 4. Lipid composition of different retrovirus envelopes produced from various cell types.
Values for all lipid classes except cholesterol (Chol) and GM3 are expressed as molar percentages of a given lipid to total lipids measured. Chol and GM3 are expressed as ratios of its signal intensity to total PC level and total SM level respectively. The data represents the average and standard deviation of at least three independent samples, $n \geq 3$. The lipid composition of HIV from previous studies by Aloia et al. and Brugger et al. are shown for comparison.

A

Cell Line	H9	REF	DFJ8
PS	4.7 ± 0.4	6.3 ± 1.3	7.9
PI	7.7 ± 0.7	16.6 ± 8.3	13.7
PIP	1.5 ± 0.1	1.6 ± 0.2	0.3
PIP2	1.1 ± 0.2	1.2 ± 0.3	0.2
PE	5.0 ± 0.6	8.4 ± 2.8	8.6
pPE	6.2 ± 0.6	12.8 ± 6.6	10.9
PC	30.2 ± 1.2	26.6 ± 4.0	31.2
ePC	20.4 ± 1.2	6.0 ± 1.5	8.4
SM	9.8 ± 1.1	12.3 ± 0.9	14.4
dhSM	1.2 ± 0.2	2.4 ± 0.0	2.0
Cer	5.3 ± 1.4	4.2 ± 0.7	1.9
GluCer	6.9 ± 0.8	1.7 ± 0.3	0.5

B

	This Study			Brugger et al, 2006
Virus	**HIV**	**MLV**	**MLV**	**HIV**
Cell Line	**H9**	**REF**	**DFJ8**	**MT4**
PS	2.8***	2.5***	1.9	2.1
PI	-0.4***	-0.1*	-0.2	n/a
PIP	1.4*	1.2	10.3	n/a
PIP_2	2.4**	5.9***	4.0	n/a
PE	1.6	-0.9	-0.8	-0.5
pPE	2.2**	1.3	1.2	1.7
PC	-0.7**	-0.6**	-0.7	-0.4
ePC	-0.3***	-0.6*	-0.6	n/a
SM	2.1***	1.8***	1.8	3.2
dhSM	2.5***	2.3***	1.9	
Cer	-0.3**	-0.3***	-0.2	-0.3
GluCer	-0.6**	1.2	-0.6	2.6

Table 5. Comparative lipid analysis of retroviruses versus total cell membrane.
(A) Lipid composition of various total cell membrane used in this study. Values are expressed as molar percentages of a given lipid to total lipids measured for the sample. The data represents the average and standard deviation of at least three independent samples, n≥3, except DF1 cells. (B) Ratio of retroviral lipids to total membrane lipid composition of host cells. Lipids which are significantly enriched (>1.5 fold) or excluded (<1.5 fold) in viral envelopes are highlighted in red and green, respectively. The data represents the average of at least three independent samples, i.e. n≥3. Statistical significance was calculated using unpaired student's T test, where *, ** and *** denotes $p < 0.05$, $p < 0.01$ and $p < 0.001$ respectively.

2.3.3 Phospholipids and sphingolipids profile of HIV and other retroviruses

The HIV lipid composition data obtained in this analysis was in close agreement with data generated in previous studies by Aloia et al. and Brugger et al (Aloia et al., 1993; Brugger et al., 2006) (Table 4). To reveal the potential enrichment or exclusion of lipids in retroviruses, we compared viral lipids to total cellular lipids of their uninfected producer cells (Table 5). The comparative ratio of HIV lipids to H9 total cellular lipids confirmed the enrichment of PS, pPE, Chol, SM, dhSM and GluCer previously reported Brugger et al. (Brugger et al., 2006), while PC and Cer are excluded (Table 5B) (Aloia et al., 1993; Brugger et al., 1997; Brugger et al., 2006). By recapitulating this result, we confirmed that even though our methods of analysis are different[4], we were able to yield similar results when the conditions under study were the same, thus validating our comparative data shown in later experiments. Interestingly, PI levels were consistently low while phosphoinositides were highly elevated in HIV envelopes.

Qualitatively, parallel experiments with virions produced from H9 cells infected with a mutant construct found that the lipid composition of HIV was not changed in the absence of the viral envelope glycoprotein (Env) (Figure 11A and Figure 12B-C), suggesting that, even though the Env is thought to be associated with lipid rafts (Rousso et al., 2000), Env does not assist the specific incorporation of any lipid. Instead, our data suggests that Gag alone dictates the major lipid components incorporated into HIV, consistent with the fact that Gag alone is responsible for lipid raft association (Bhattacharya et al., 2006) and is sufficient for particle assembly and release (Morita and Sundquist, 2004).

HIV derived from either H9 cells or MDM cells were also virtually identical, with the exception that dhSM is elevated in HIV from MDM cells (Table 5 and Figure 12A). While

[4] Brugger et al. used precursor ion and neutral ion loss scans while we used MRM scans.

the differences are subtle, they could be a consequence of the precise site of assembly in both cell types. HIV from H9 cells buds at the plasma membrane while HIV budding from MDM may occur either at MVBs (Nguyen et al., 2003; Ono and Freed, 2004) or at deeply invaginated membrane structures that appear to be derived from the plasma membrane in MDM (Deneka et al., 2007; Jouvenet et al., 2006; Welsch et al., 2007). Their overall similarity in virion lipid composition is in agreement with the emerging evidence that both assembly sites are continuous with the plasma membrane (Deneka et al., 2007; Jouvenet et al., 2006; Rudner et al., 2005; Welsch et al., 2007). Analysis of MV released from infected MDM cells (i.e. the CD45 enriched fraction) revealed that they exhibit similar lipid compositions to HIV released from these cells, albeit with much lower levels of phosphoinositides PIP and PIP_2 while HIV from the same cells contained these lipids (Table 4 and Figure 12D). Lipid profiles of MLV produced from REF and DFJ8 cells also showed remarkable similarity to that of HIV despite belonging to different retrovirus genus and being produced from different cell types (Table 4 and Figure 10B). This data suggested that the budding membranes of these different viruses are actually similar and likely to be the plasma membrane of the cell. We noted that MLV-DFJ8 exhibited an unusually high PIP content, possibly due a PIP_2 hydrolysis during their purification or a cell line specific effect or other cell specific effects (Table 4).

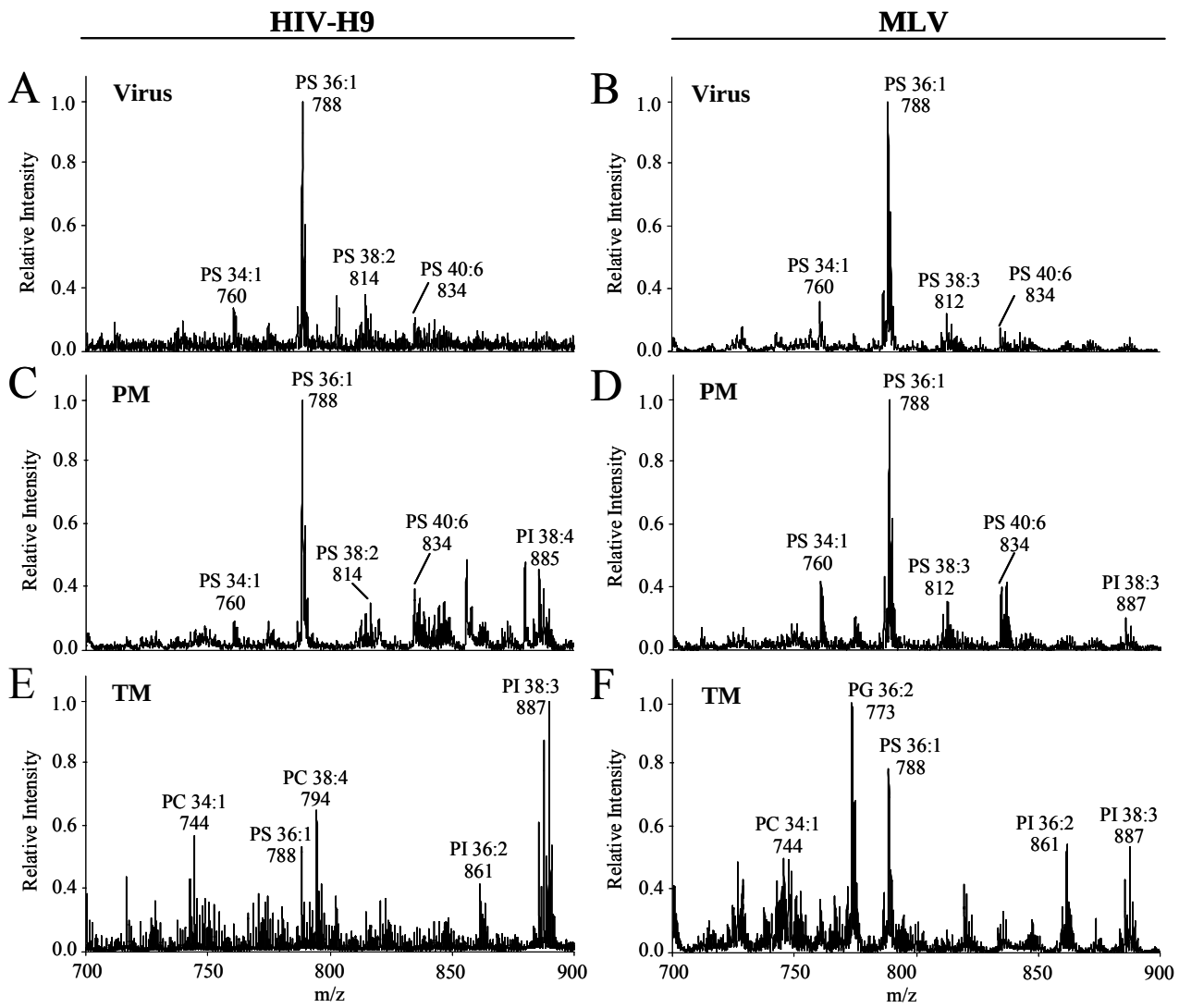

Figure 11. Qualitative lipid analysis of HIV, MLV and their respective host cell membrane.
ESI-MS spectra in the negative mode are shown for lipid mixtures from CD45 depleted HIV (A), H9 plasma membrane (PM) (C) and H9 total membranes (TM) (E). Similar analysis of lipids extracted from MLV (B), REF PM (D) and REF TM (F). The representative spectra shown are normalized to the highest peak within the m/z range. Prominent ions which were characterized by MS/MS are labeled.

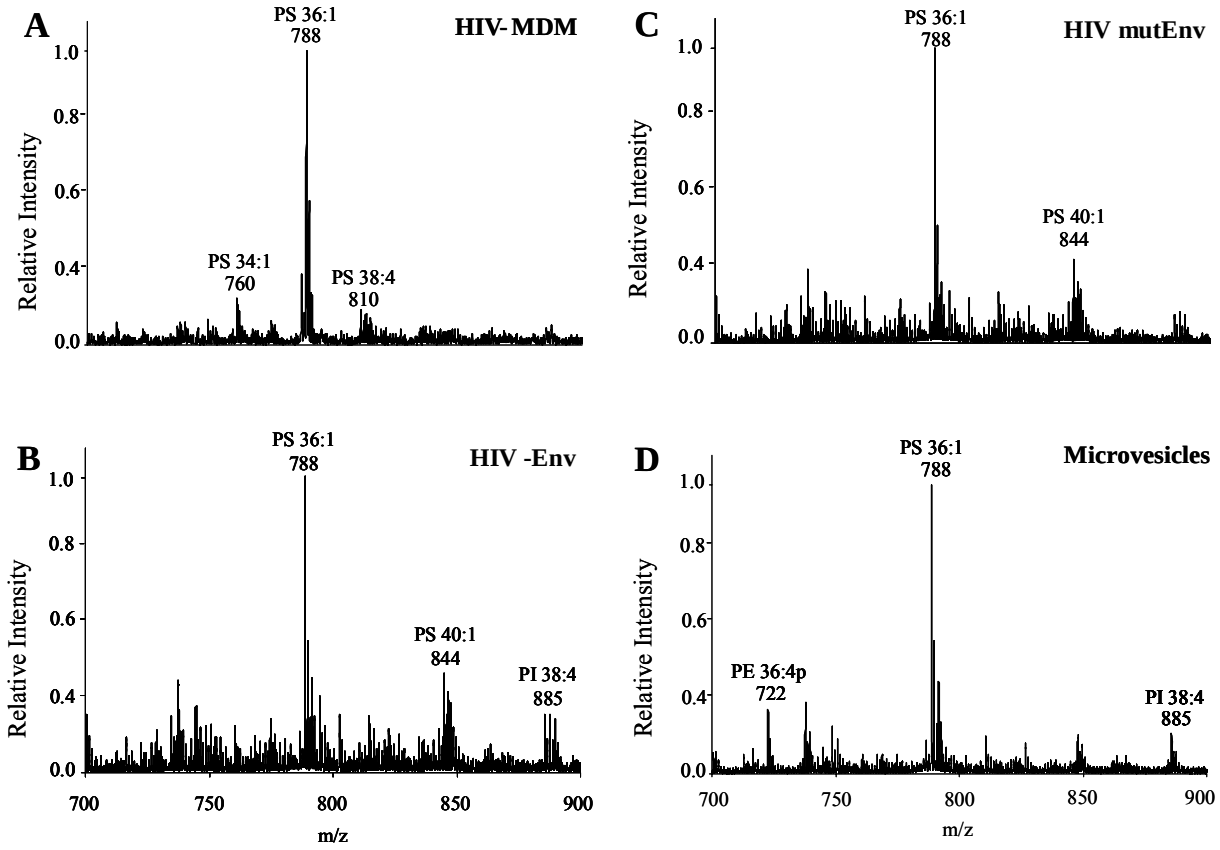

Figure 12. Qualitative lipid analysis of HIV and microvesicles.
ESI-MS analysis of lipids extracted from CD45 depleted HIV from monocyte derived macrophages (MDM) (A), HIV mutant that does not express Env from H9 cells (B), HIV with an endocytosis signal mutation in Env (Y712S in Tm) from H9 cells (C), CD45 enriched microvesicles from MDM (D). The representative spectra shown are normalized to the highest peak within the m/z range. Prominent peaks that were characterized by MS2 methods are labeled in the figure.

2.3.4 Purification of plasma membrane fractions

The lipid composition of the plasma membrane is distinct from that of other cellular membranes, exhibiting higher levels of cholesterol and sphingolipids (van Meer, 2005). Because HIV and MLV both use the plasma membrane for budding, we analyzed the lipids present in the plasma membrane rather than total cellular membrane to better assess enrichment. We enriched for plasma membrane via the use of cationic silica beads that adhere electrostatically to the plasma membrane (Harila et al., 2006; Mason and Jacobson, 1985; Stolz and Jacobson, 1992). To monitor the efficacy of these cationic beads for plasma membrane preparation, we followed the enrichment of raft (flotillin and caveolin) and non-

raft markers (transferrin receptor, TrF) (Figure 13A and 13B). Actin (cytoplasmic protein) and Rab5 (endosomal protein) served as indicators for plasma membrane purity (Figure 13A and 13B). Membranes are relatively plastic and can be altered by external agents. Therefore, before proceeding, we investigated if the concentration of cationic beads had any artificial effects on the membrane preparations that could lead to artifacts. At a low bead concentration of 1%, all three markers were present to a similar extent in adherent REF cells (Figure 13A). TrF levels in the plasma membrane fractions appear to be constant with increasing bead concentration and less abundant than total membrane levels. Since TrF recycles between plasma membrane and endosomes in a cell (Green et al., 1987), it explains why REF plasma membrane preparation will contain less TrF than observed in the REF total membrane preparations. Unexpectedly, the raft markers flotillin and caveolin appeared to be enriched over the non-raft marker TrF with increasing amounts of beads used, suggesting that these beads have a propensity for inducing lipid raft fractions at high concentrations (Figure 13A). This was confirmed by lipid analysis of the fractions showing that plasma membrane fraction extracted using 10% beads contained increased levels of SM (Figure 13C). Therefore, we decided to apply the 1% cationic bead solution which does not induce this artifact to prepare plasma membranes from all other adherent cell lines including DF1 and MDM. We found that the condition also works well for the suspension cell line H9 which showed equal levels of TrF and flotillin (Figure 13B).

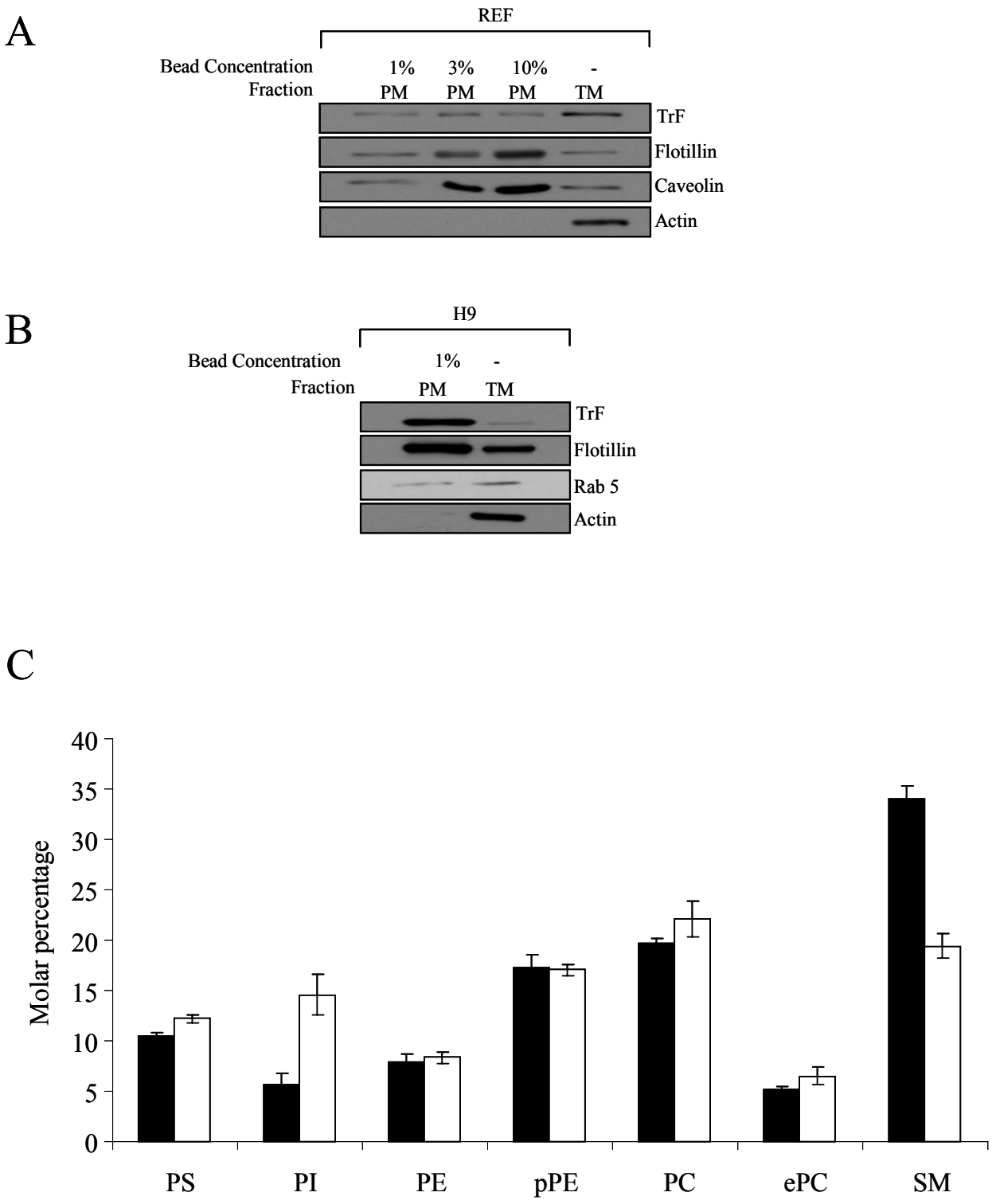

Figure 13. Purification of plasma membrane using cationic silica beads.
Plasma membrane (PM) fractions were isolated from (A) REF and (B) H9 cells using cationic beads and compared to total cell membrane (TM) fractions. Western blotting for raft (flotillin and caveolin) and non-raft markers (transferrin receptor, TrF) were used to assess plasma membrane characteristics while actin (cytoplasmic protein) and Rab5 (endosomal protein) served as indicators for plasma membrane purity. (C) Comparative lipid profile of REF PM isolated using 10% (■) and 1% (□) bead concentration. The standard deviation was derived from indepdent samples (n=3).

Considering the importance of the PM isolation to our analysis, we explored another PM isolation technique on the REF cell line using pre-formed Optiprep gradient procedure (Finzi et al., 2007; Sheff et al., 1999). Based on previous reports, it was found that the concentration of the PM would be found between fraction 4 and 5 based on 800µl sample volume from the lowest density gradient. We confirmed this result by recapitulating some of the western blot results showing an overlap of enrichment between TrF and early endosomal marker EEA1 (Sheff et al., 1999). Further lipid analysis of the various fractions of the gradient showed that the PM fraction is located in fraction 5&6 in our case (Figure 14B). More importantly, this result showed that both methods of PM isolation gave similar results (compare Figure 14B and 11D). Given the shorter preparation time required for the cationic silica method (<6hr) compared to the Optiprep method (>24hr), we elected to use the former method for the remainder of our experiments.

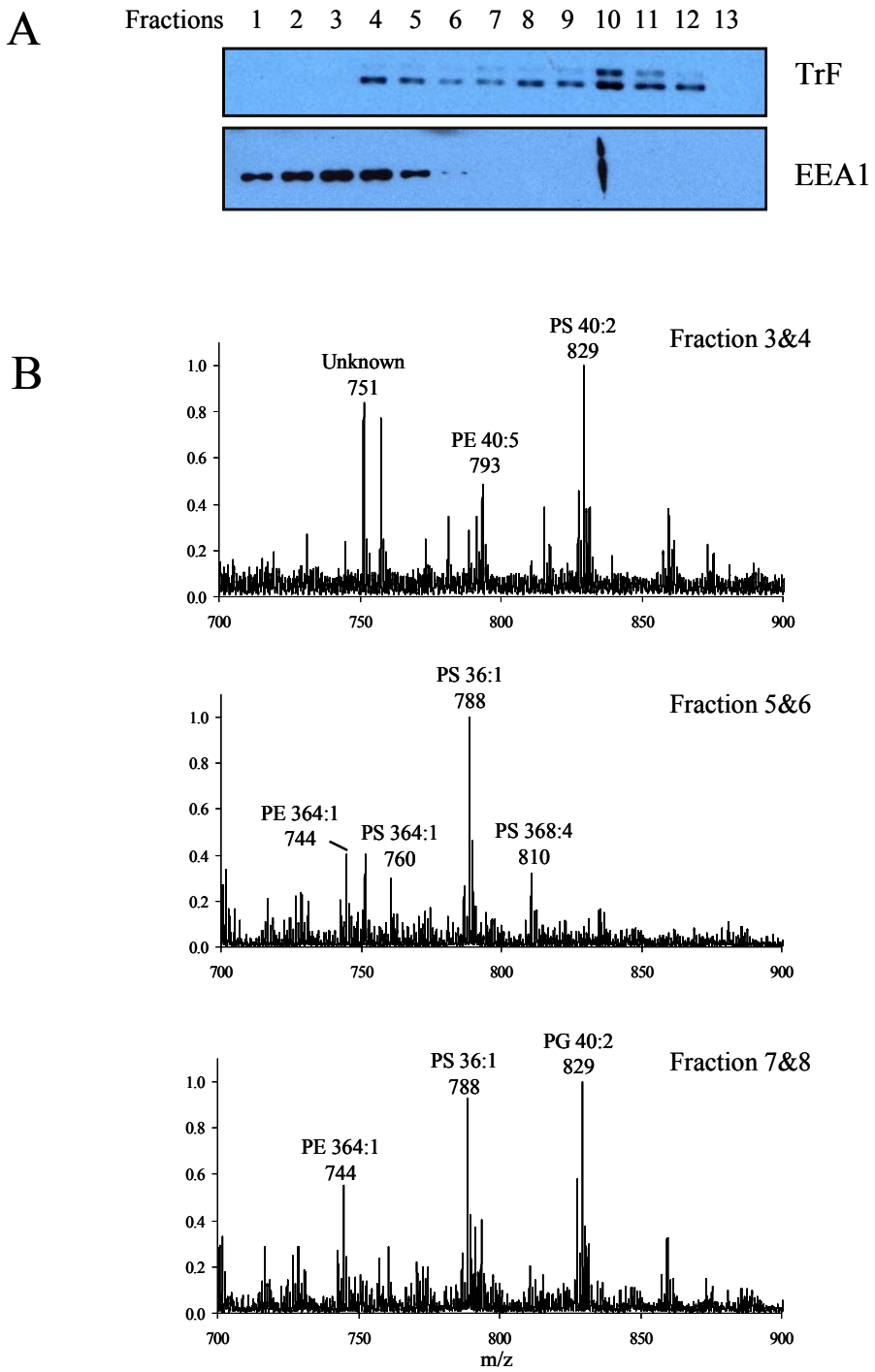

Figure 14. Purification of plasma membrane using Optiprep gradients
(A) Plasma membrane (PM) fractions from REF cells were isolated by centrifugation through a continuous Optiprep gradient. The fraction number refers to 800µl of gradient sampled from lower density to higher density. Membrane identity was confirmed by western blotting for various cellular organelles. TrF is a non-raft plasma membrane marker that also appears in the endosomal system while EEA1 is a marker for early endosomes. (B) ESI-MS analysis of fractions in negative modes are shown for three pooled fractions taken from the gradient. The representative spectra shown are normalized to the highest peak within the m/z range. Prominent peaks were labeled based on m/z identity.

2.3.5 The lipid composition of retroviruses resembles that of plasma membrane

Unbiased lipid profiling of purified viral particles and plasma membrane fractions revealed that the mass spectrometry patterns of MLV and HIV-H9 lipids were highly similar to their plasma membrane lipids, but not total cellular lipids (Figure 11A-F). Both virus and plasma membrane spectra were dominated by PS ions, namely PS 36:1, PS 34:1 and PS 38:3 or PS 38:2 in the negative polarity ESI mode (Figure 11A and B). This can be attributed to the abundance of PS in the lipid extract and the high ionization efficiency of PS as well as the exclusion of PI in viral envelopes. In addition to PS other minor ions in the mass spectra corresponded to numerous species of PE, pPE, PI, PA and GM3 which are not labeled in the spectra shown here. REF and H9 plasma membrane spectra were also similar to the viruses in having high PS levels, but differed in having higher levels of PI (Figure 11C and D). The absolute molar percentages of individual phospholipid and sphingolipid molecules are presented in Figure 15, 16, 17 and 18 for HIV-H9, MLV-REF, MLV-DFJ8 and HIV-MDM respectively. Detailed analysis of the head group charge and fatty acyl distribution indicates that retroviral envelopes have a tendency to harbor the more anionic lipids and shorter and more saturated fatty acyl chains compared to total cellular lipids (Figure 15-18). This distribution of retroviral lipid species is highly similar to the plasma membrane while being distinctly different from the total membrane of their respective host cell.

The comparison of viral lipids to plasma membrane lipids illustrates the striking similarity of retroviruses with plasma membrane lipids (Table 6B). In contrast, when total cell lipids are used for comparison, PS, pPE, SM, and DHSM are significantly enriched, while PI, PC, PE and Cer are excluded from viral envelopes (Table 5B). Thus, the plasma membrane is the appropriate cellular reference for comparison. In general, Chol, Cer and GM3 remain enriched in both retroviral envelopes as well as CD45-enriched MV over their

producer cell plasma membrane (Table 6B). More significantly, PIP and PIP_2 are enriched in the retrovirus envelopes compared to plasma membrane (Table 6B and Figure 19) and MV (Table 6B and Figure 18). These data suggest that while rafts lipids such as Chol, Cer and GM3 are generally important for the formation of both retroviruses and MV, the requirement for phosphoinositides is specific to retroviruses.

A

Cell Line	H9	MDM	REF	DF1/DFJ8
PS	13.5 ± 1.3	11.0 ± 0.6	11.3 ± 0.3	7.2 ± 1.7
PI	8.8 ± 1.0	6.3 ± 0.4	13.4 ± 1.9	8.3 ± 1.1
PIP	1.3 ± 0.4	1.2 ± 0.3	0.5 ± 0.2	2.4 ± 0.4
PIP_2	1.6 ± 0.3	0.9 ± 0.3	0.9 ± 0.4	0.4 ± 0.2
PE	8.7 ± 1.7	6.1 ± 0.6	5.9 ± 0.5	7.7 ± 1.0
pPE	14.9 ± 1.8	15.2 ± 0.3	15.8 ± 0.6	9.6 ± 1.2
PC	16.9 ± 1.7	19.4 ± 0.8	20.5 ± 1.7	29.8 ± 3.9
ePC	4.9 ± 0.5	4.6 ± 0.2	6.0 ± 0.8	7.8 ± 0.9
SM	16.4 ± 1.0	21.6 ± 0.5	18.1 ± 1.1	22.3 ± 2.2
dhSM	4.4 ± 0.1	10.0 ± 0.2	3.7 ± 0.6	3.0 ± 0.1
Cer	1.6 ± 0.3	0.6 ± 0.1	0.8 ± 0.2	0.3 ± 0.1
GluCer	7.1 ± 0.7	3.1 ± 0.3	3.2 ± 1.0	1.2 ± 0.5
Chol	0.05 ± 0.00	0.09 ± 0.02	0.06 ± 0.01	0.03 ± 0.00
GM3	0.06 ± 0.01	0.01 ± 0.00	0.15 ± 0.01	0.001 ± 0.0

B

Virus	HIV	HIV	MLV	MLV	CD45 MV
Cell Line	**H9**	**MDM**	**REF**	**DFJ8**	**MDM**
PS	-1.0	-0.9	1.3*	2.1**	-0.8
PI	-0.3**	-0.5*	-0.1***	-0.3***	-0.4**
PIP	1.6	2.6**	4.7**	1.3	-0.6
PIP2	1.6*	4.2**	10.4***	2.0**	-0.7
PE	-0.9	-0.9	1.1	-0.9	-0.6*
pPE	-0.9	-0.8	-0.9	1.4**	-0.9
PC	1.3	-0.9	-0.7	-0.7	1.1
ePC	1.1	1.0	-0.4*	-0.7	1.6**
SM	1.3	1.2*	1.3*	1.2	1.3**
dhSM	-0.7***	-0.8**	1.8*	1.3**	-0.7***
Cer	-0.9	2.8**	2.2	1.0	3.9***
GluCer	-0.6*	1.2	-0.7	-0.3*	-0.7
GM3	1.4*	11.6**	2.9*	12	5.0***
Chol	2.7*	1.4	2.0**	3.0*	4.2***

Table 6. Comparative lipid analysis of retroviruses versus plasma membrane.
(A) Lipid composition of plasma membrane derived from host cells used in this study. Values for all lipid classes except cholesterol (Chol) and GM3 are expressed as molar percentages of a given lipid to total lipids measured for the sample. Chol and GM3 are expressed as ratios of its signal intensity to total PC level and total SM level respectively. The data represents the average and standard deviation of at least three independent samples, n≥3. (B) Ratio of retroviral lipid composition to plasma membrane lipid composition. Lipids which are significantly enriched (>1.5 fold) or excluded (<1.5 fold) in viral envelopes are highlighted in red and green, respectively. The data represents the average of at least three independent samples, i.e. n≥3. Statistical significance was calculated using unpaired student's T test, where *, ** and *** denotes $p < 0.05$, $p < 0.01$ and $p < 0.001$ respectively.

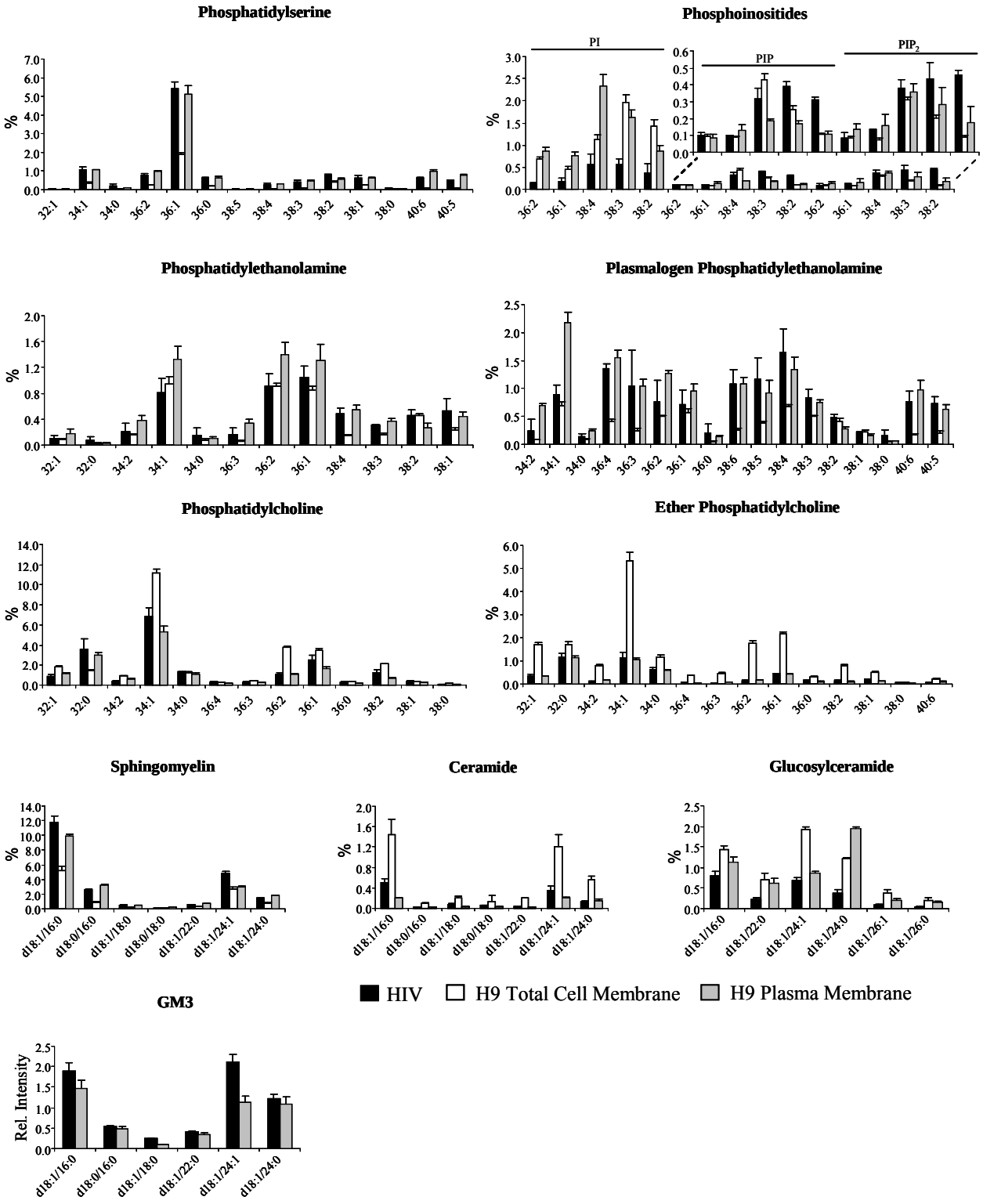

Figure 15. Glycerophospholipids and sphingolipids distribution of HIV and H9 host cells.
Abundance is represented as the molar percentages (y-axis) of a given lipid (x-axis), to total lipid measured except GM3 which was normalized to the total SM levels. Lipids were extracted from purified virus (black bars), total cell membrane (open bars), plasma membrane fractions (grey bars) and quantified via mass spectrometry using multiple reaction monitoring. Mole percentages were calculated with relevant internal standards. GM3 quantification is represented in relative levels due to the lack of suitable internal standards. Sphingolipids are presented as sphingoid base residue/fatty acyl residue. The standard deviation was derived from independent samples (at least n=3).

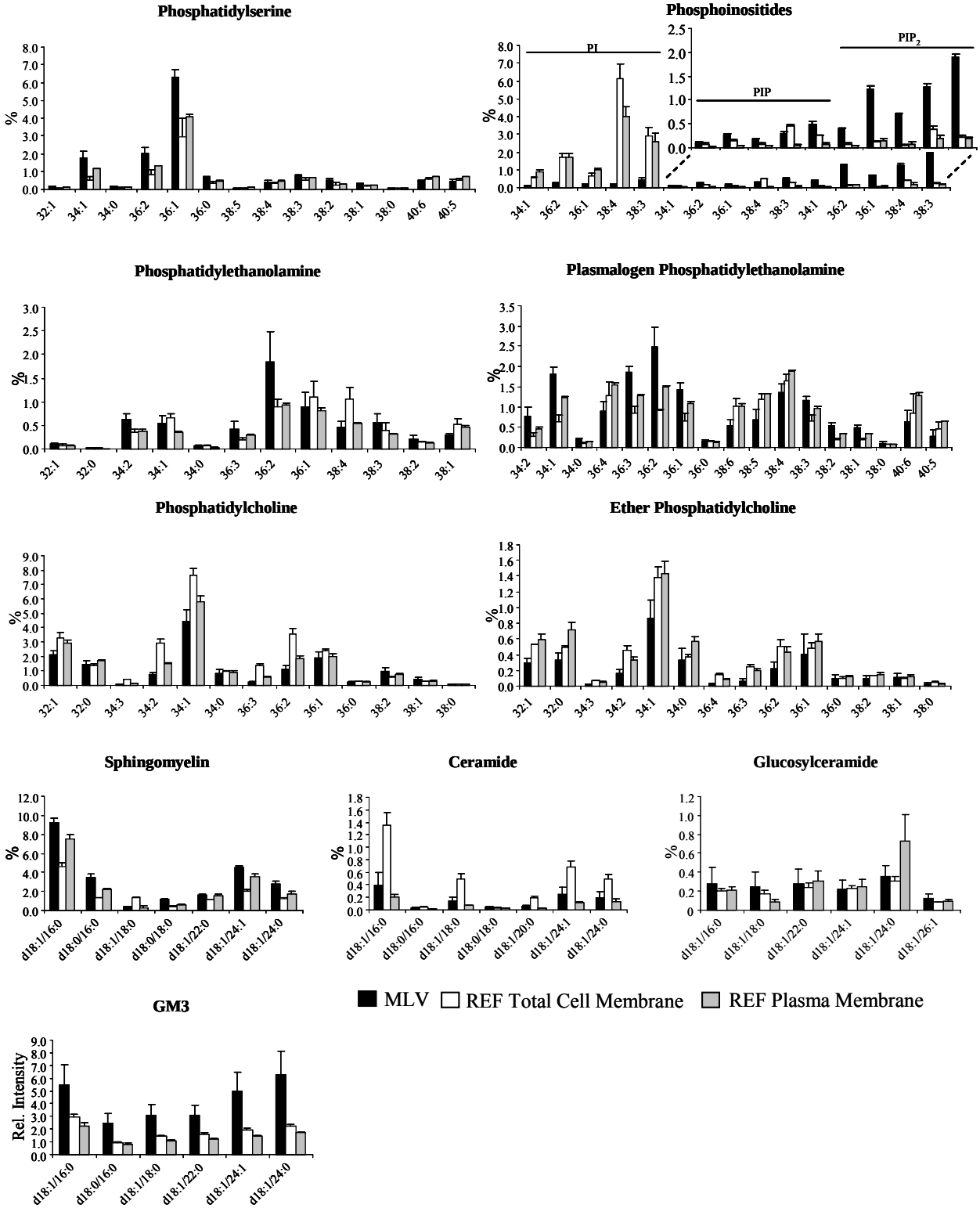

Figure 16. Glycerophospholipids and sphingolipids distribution of MLV and REF host cells.
Abundance is represented as the molar percentages (y-axis) of a given lipid (x-axis), to total lipid measured except GM3 which was normalized to the total SM levels. Lipids were extracted from purified virus (black bars), total cell membrane (open bars), plasma membrane fractions (grey bars) and quantified via mass spectrometry using multiple reaction monitoring. Mole percentages were calculated with relevant internal standards. GM3 quantification is represented in relative levels due to the lack of suitable internal standards. Sphingolipids are presented as sphingoid base residue/fatty acyl residue. The standard deviation was derived from independent samples (at least n=3).

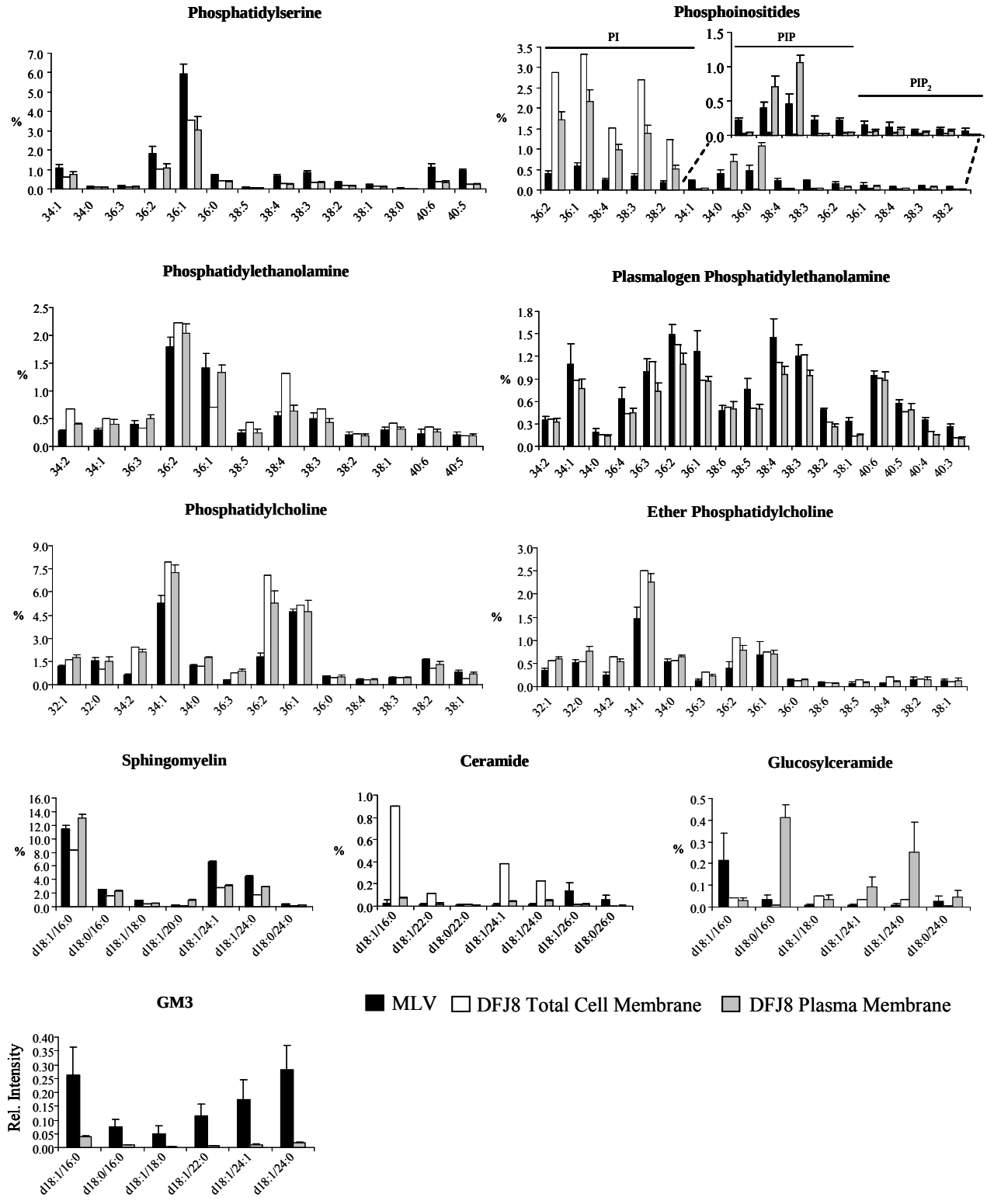

Figure 17. Glycerophospholipids and sphingolipids distribution of MLV and DFJ8 host cells.
Abundance is represented as the molar percentages (y-axis) of a given lipid (x-axis), to total lipid measured except GM3 which was normalized to the total SM levels. Lipids were extracted from purified virus (black bars), total cell membrane (open bars), plasma membrane fractions (grey bars) and quantified via mass spectrometry using multiple reaction monitoring. Mole percentages were calculated with relevant internal standards. GM3 quantification is represented in relative levels due to the lack of suitable internal standards. Sphingolipids are presented as sphingoid base residue/fatty acyl residue. The standard deviation was derived from independent samples (at least n=3 except DFJ8 total cell membrane where n=1).

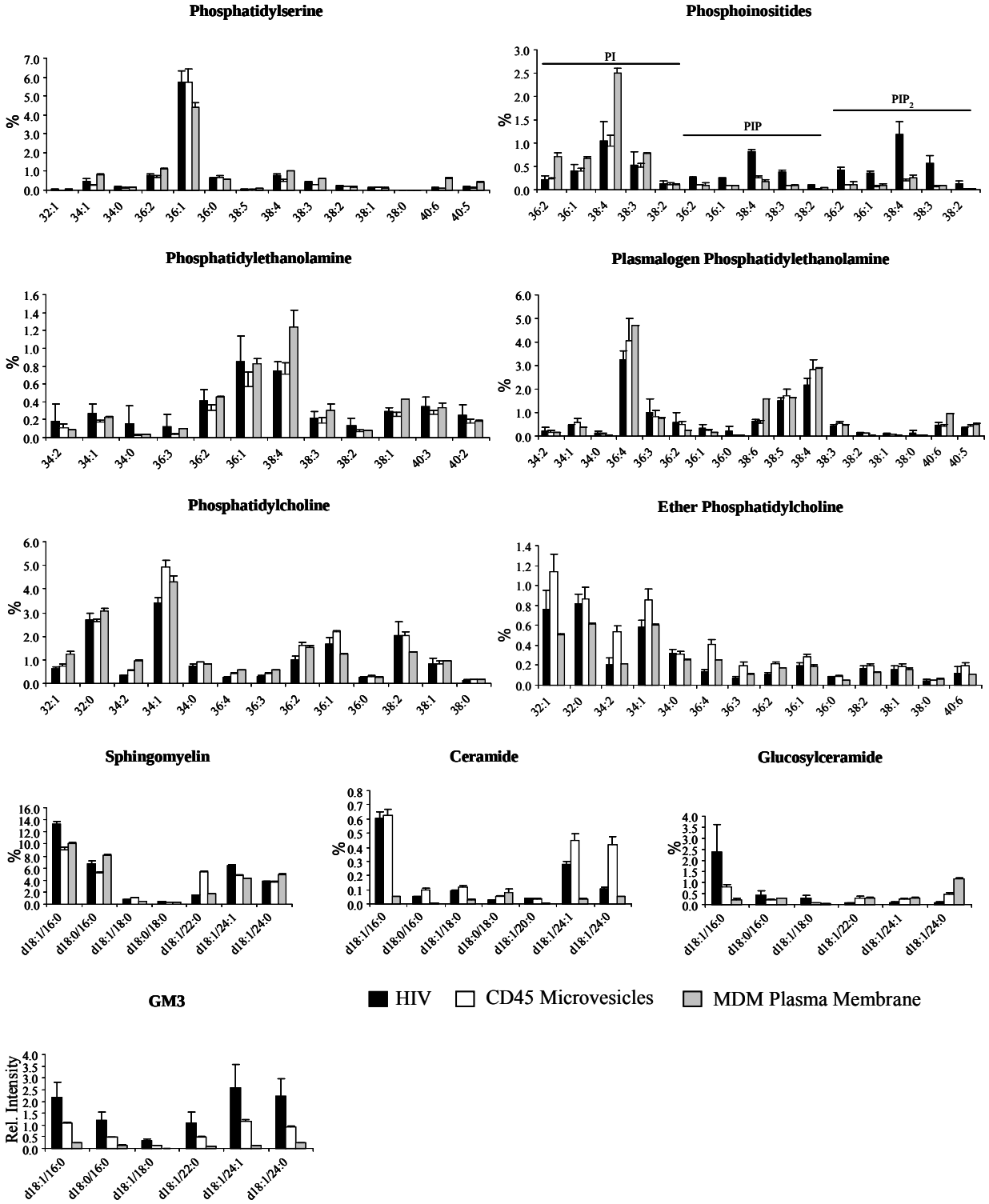

Figure 18. Glycerophospholipids and sphingolipids distribution of HIV, CD45-enriched microvesicles and monocyte derived macrophages (MDM) host cells.

Abundance is represented as the molar percentages (y-axis) of a given lipid (x-axis), to total lipid measured except GM3 which was normalized to the total SM levels. Lipids were extracted from purified virus (black bars), microvesicles (open bars), MDM plasma membrane fractions (grey bars) and quantified via mass spectrometry using multiple reaction monitoring. Mole percentages were calculated with relevant internal standards. GM3 quantification is represented in relative levels due to the lack of suitable internal standards. Sphingolipids are presented as sphingoid base residue/fatty acyl residue. The standard deviation was derived from independent samples (at least n=3).

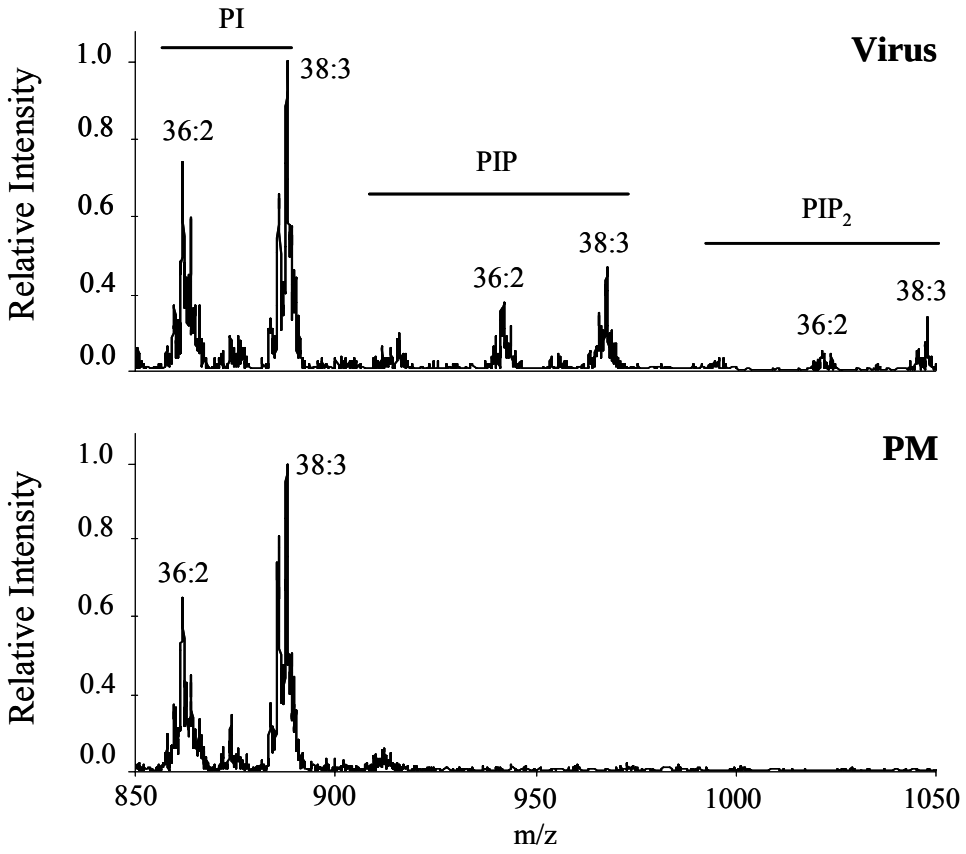

Figure 19. Profiling of phosphoinositides in retroviral envelopes.
Precursor ion scanning for m/z 241 (dehydrated inositol fragment) was used to detect PI and phosphoinositides in MLV (top) and plasma membrane (PM) (bottom).

2.3.6 Methodology for neutral lipid analysis

In earlier works on lipid analyses of HIV envelope, the authors measured only the free cholesterol levels in the envelope but neglected neutral lipids like TG, DG and cholesterol ester (CE) in their analysis (Aloia et al., 1993; Brugger et al., 2006). The analysis of neutral lipids by ESI-MS is not trivial because these lipids do not ionize efficiently. The addition of ammonium acetate (NH_4OAC) in the chromatography solvent mixture provides ammonium counter ions that charges the neutral lipid and facilitates ionization during the electrospray process, thereby increasing the sensitivity of neutral lipid detection (Hutchins et al., 2008; Krank et al., 2007; Murphy et al., 2007; Sommer et al., 2006). This prompted us to

investigate the presence of neutral lipids via a HPLC-ESI-MS method combining reverse phase C18 column separation using Chol:MeOH:2% 0.1M NH_4OAC as a solvent[5]. Using this methodology, we were able to analyze both phospholipids and neutral lipids including free Chol, CE, DG and TG, sampling from both the positive and negative ion mode simultaneously.

The elution times for the different lipid classes were previously established through the use of lipid standards (data not shown) and it is clear that HPLC separation is successful in separating the different classes of neutral lipids from phospholipids (Figure 20A). Therefore, while the polarity and m/z value of some of these lipids overlapped, we were still able to differentiate them based on the different elution time from the column. For example, cholesterol and cholesterol ester both produced 369.3 m/z species but were eluted at 7-7.5min and 12-20min respectively (Figure 20B). Although DG has the same elution time as Chol and PL (Figure 20C), their unique m/z value means that their identity will not be mistaken. In another example, the elution time of PL and TG occurs between 7-12min and 12-26min respectively (Figure 20D and E), so molecules such as TG 50:4 and PC 40:1a which have 844.8m/z will not overlap. We note that the neutral lipids are detected only in the positive modes, probably due to the positive charge originating from the ammonium counter ion.

We quantified the neutral lipid abundance using the Q3 scan mode. In the Q3 mode, the instrument is programmed to detect specific m/z species at fixed collision energy throughout the duration of the analysis. Therefore, we can follow the specific ions of interest and normalization procedures were made simpler. It should be noted that we normalized the individual lipid signal intensity to the total lipid signal intensity produced by the sample due to the lack of proper internal standards for the neutral lipid classes. Hence, the data presented is a relative value to total amount of lipids in the sample.

[5] This method was developed in-house by Dr Shui Guanghou (unpublished work).

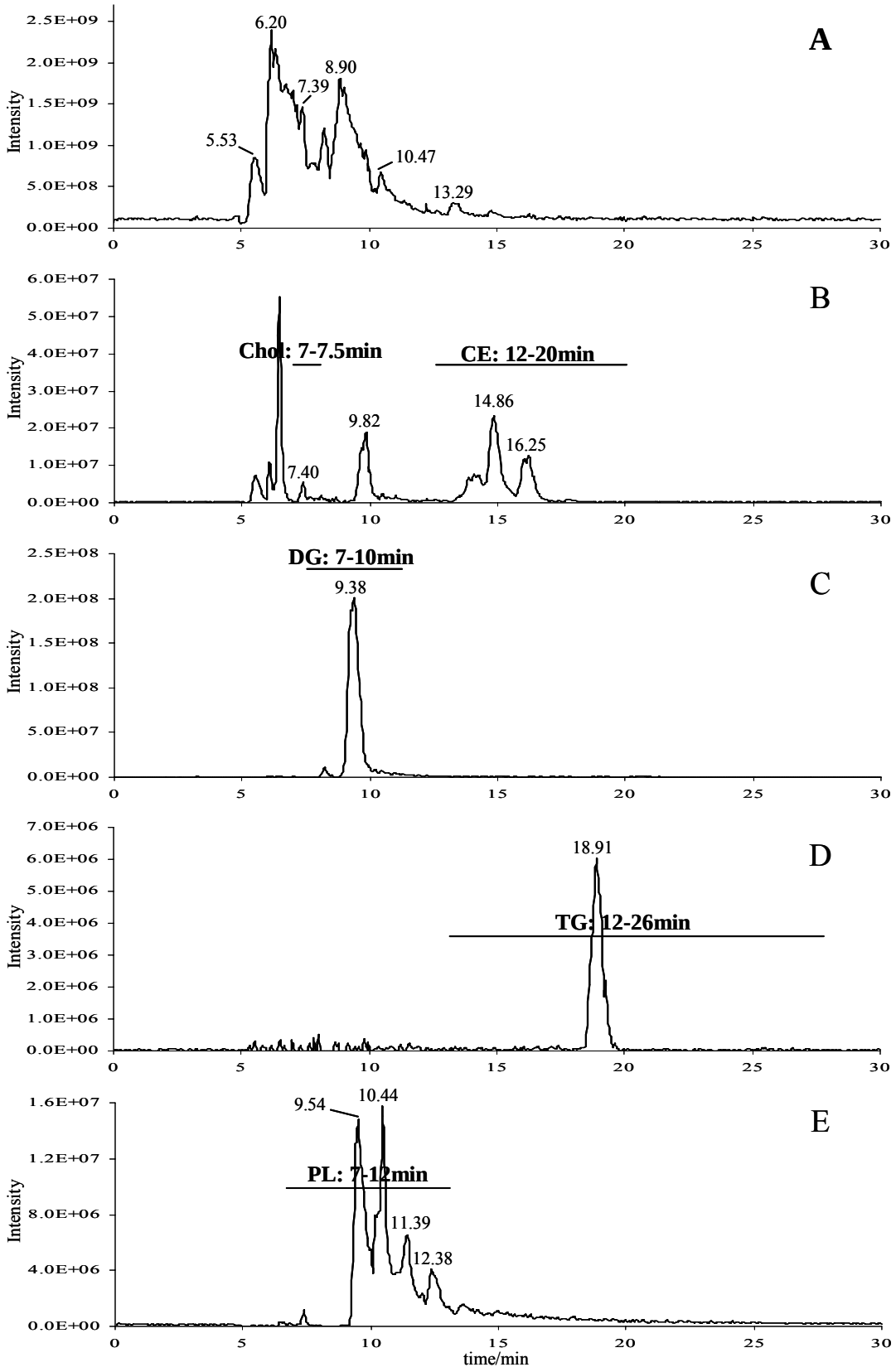

Figure 20 . HPLC chromatogram profile of MLV lipid extract.
Chromatogram of total lipid sample (A), chromatogram of Chol and CE 369.2-369.7 m/z (B), chromatogram of DG 36:0 607.5-608.0 m/z (C), chromatogram of TG 52:0 880.7-881.2 m/z (D), chromatogram of PS 36:1 788.5-790.0 m/z (E). The elution times of various lipids classes are indicated using the horizontal bars.

2.3.7 Neutral lipid composition of retroviruses envelopes

Our results show that retroviral envelope lipid contains additional neutral lipids like CE, DG and TG in addition to free Chol (Table 7). Similar analysis was carried out on the neutral lipids of total cell membrane lipids as a comparison. As expected, MLV and HIV are highly enriched in cholesterol compared to their host cell total membrane levels (Table 7). Contrary to Chol levels, the specific inclusion of CE in the retrovirus envelope is not as clear cut. One the one hand, HIV-H9 is enriched in CE compared to its producer cell total membrane while on the other hand, MLV-REF has lower levels of CE compared to their host (Table 7B). Retrovirus envelopes are also enriched in DG (Table 7B), particularly in saturated DG species such as DG 36:0 and DG 34:0 (data not shown) when compared to their host cells. The identities of these DG species were confirmed by tandem MS analysis (Figure 21A and B). Unexpectedly, TG is also found to be present in the retrovirus envelope, albeit at much lower levels compared to their host cell levels (Table 7B). It is interesting to note that the ratio saturated to unsaturated TG present in retrovirus envelopes is higher compared to the same ratio in the producer cells (Table 7A). Tandem MS analysis of an m/z value corresponding to TG 52:0 (16:0/18:0/18:0), resulted in the formation of daughter ions corresponding to saturated DG 16:0/18:0 and DG 18:0/18:0 ions, thus confirming the identity of the TG parent ion (Figure 21C). Overall, the enrichment of cholesterol and saturated DG and TG in the virus envelope compared to host cell total membrane suggests that the mechanics of lipid raft clustering may be involved during virus assembly.

A

	HIV-H9	H9 Cells TM	MLV-REF	REF TM
Chol	2.5 ± 0.2E-02	3.2 ± 0.3E-03	1.7 ± 0.1E-02	5.2 ± 0.5E-03
CE	1.5 ± 0.3E-02	1.1 ± 0.1E-02	1.4 ± 0.2E-02	3.6 ± 0.2E-02
DG	4.2 ± 0.9E-01	1.6 ± 0.5E-01	5.2 ± 0.1E-01	2.8 ± 0.5E-01
TG	1.9 ± 0.3E-01	5.5 ± 0.2E-01	5.1 ± 0.01E-02	2.6 ± 0.1E-01
DG saturated	3.5 ± 1.1E-01	1.0 ± 0.5E-01	4.2 ± 0.1E-01	1.7 ± 0.6E-01
DG mono-unsaturated	4.4 ± 1.6E-02	3.8 ± 0.5E-02	8.1 ± 0.3E-02	7.8 ± 0.2E-02
DG di-unsaturated	2.3 ± 0.6E-02	2.2 ± 0.2E-02	2.4 ± 0.1E-02	3.1 ± 0.1E-02
TG saturated	6.6 ± 0.3E-02	3.5 ± 0.6E-02	1.2 ± 0.1E-02	3.5 ± 0.1E-02
TG mono-unsaturated	1.4 ± 0.1E-02	9.1 ± 0.4E-02	7.0 ± 0.3E-03	6.0 ± 0.1E-02
TG poly-unsaturated	1.1 ± 0.1E-01	4.3 ± 0.2E-01	3.2 ± 0.1E-02	1.7 ± 0.1E-01

B

	HIV-H9	MLV-REF
Chol	7.8***	3.3***
CE	1.4	-0.4***
DG	2.6*	1.9**
TG	-0.3***	-0.2***
DG saturated	3.5*	2.5**
DG mono-unsaturated	1.2	1.0
DG di-unsaturated	1.0	-0.8**
TG saturated	1.9**	-0.3***
TG mono-unsaturated	-0.2***	-0.1**
TG poly-unsaturated	-0.3***	-0.2***

Table 7. Comparative neutral lipid analysis of retrovirus envelopes and their producer cells.
(A) LC/ESI-MS analysis was used to analyze the neutral lipids of HIV produced from H9 cells and MLV produced from REF cells and their respective producer cell total membrane (TM). The data presented show relative amounts of each lipid classes normalized to the total ion count detected from their extract. The data represents the average and standard deviation of three independent samples, n=3. (B) Ratio of retroviral neutral lipids to total membrane neutral lipid composition of host cells. Lipids which are significantly enriched (>1.5 fold) or excluded (<1.5 fold) in viral envelopes are highlighted in red and green, respectively. The data represents the average of at least three independent samples, i.e. n≥3. Statistical significance was calculated using unpaired student's T test, where *, ** and *** denotes $p < 0.05$, $p < 0.01$ and $p < 0.001$ respectively.

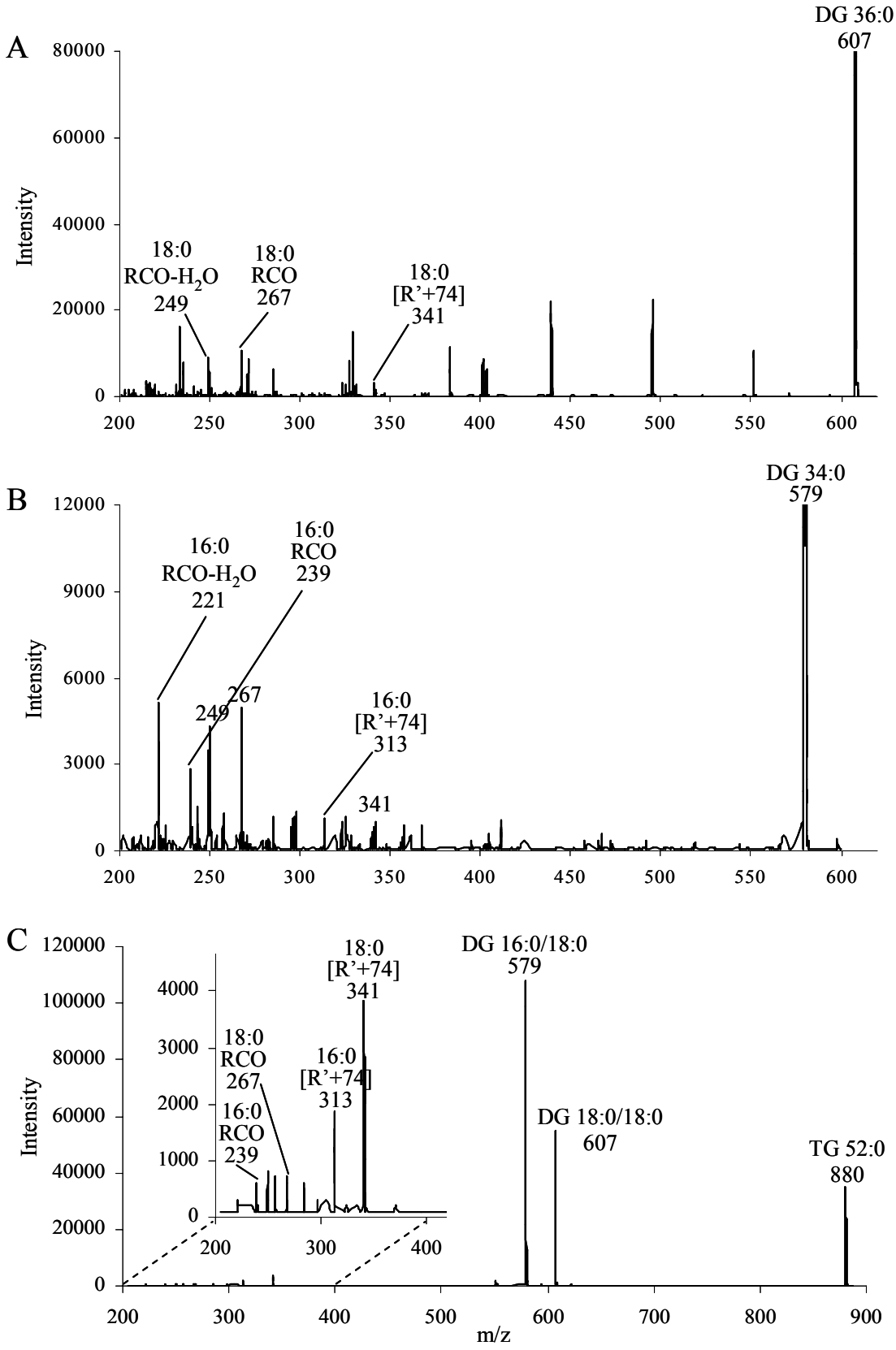

Figure 21. Tandem MS analysis of MLV neutral lipids.
MS/MS analysis was conducted using MLV lipid extracts on m/z values corresponding to DG 36:0 (A), DG34:0 (B) and TG 52:0 (C) was conducted to ascertain their identity. Acylium ions ([RCO]+), Acylium ions with loss of water ([RCO]+-H2O), and ions retaining the glycerol backbone ([R'+74]+) are present in these spectra.

Chapter 3 – Functional roles of lipids in retrovirus envelopes

3.1 Introduction

In Chapter 2, detailed lipid analysis demonstrated that the lipid compositions of retrovirus envelopes are mostly similar to the plasma membrane of their respective host cells. An interesting feature of their lipid composition is the high levels of sphingomyelin (SM), phosphatidylserine (PS) and plasmalogen phosphatidylethanolamine (pPE) that differentiate them from the total cellular membrane. Moreover, retrovirus envelopes can be further distinguished from plasma membranes by enriched levels of phosphoinositides, particularly PIP_2, and raft lipids including cholesterol (Chol), ceramide (Cer) and GM3. As we had hypothesized earlier, these enriched lipid classes will likely play important roles in the retroviral replication cycle.

We propose that the enrichment of lipids occurs because they may be crucial to the assembly and budding of retrovirus particles. Numerous lines of evidence supports the validity of lipid raft associated retrovirus assembly (Briggs et al., 2003). Therefore, retrovirus proteins are targeted to microdomains at the plasma membrane that are intrinsically enriched in rafts lipids such as cholesterol, ceramide and GM3. The targeting of retrovirus Gag also appear to be regulated electrostatically by phosphoinositide $PI(4,5)P_2$ (Ono et al., 2004; Saad et al., 2006) which would ultimately result in their enrichment in the retroviral envelope. In complex retroviruses like HIV, accessory proteins such as Nef can also regulate the inclusion of Chol and SM into the assembly site (Brugger et al., 2007; Zheng et al., 2003). Furthermore, the lipid composition of the site of retrovirus assembly must exhibit properties that enhance retrovirus budding. The result of these processes would be reflected in an enrichment of these lipids in the retrovirus envelopes as compared to the plasma membrane.

We further propose that the lipid composition of the retrovirus envelopes may have evolved to provide maximal protection to retrovirus virions when they exist outside a cell and enable it to infect a new host cell. For this purpose, the virus is required to make contact with the host through the appropriate receptors that may be protein or lipid in nature, followed by fusion of the virus envelope with the cell limiting membrane. It is clear that lipid envelope of the virus can facilitate entry in a number of ways, including (1) initial capture of the virus to the target cell surface (Ugolini et al., 1999), (2) co-receptor or alternative receptor functions (Callahan et al., 2003; Coil and Miller, 2005a; Hug et al., 2000; Puri et al., 1999) and (3) providing a micro environment that promotes membrane fusion (Haywood and Boyer, 1984; Stiasny and Heinz, 2004).

Based on the framework above, we propose to investigate the function of these enriched lipids with respect to retrovirus replication. Our paradigm suggests that if we scramble or disrupt the normal production of these lipids, specific aspects of viral replication will be disrupted. In section 2 of this chapter, we will examine the mechanism and implications of PIP_2 enrichment in retroviral envelopes through genetic manipulations. In section 3, the chemical inhibitor phenyl-2-hexadecanoylamino-3-morpholino-1-propanol (PPMP) will be used to investigate the involvement of glycolipids in MLV replication. Lastly in section 4, the topology of aminophospholipids PS, PE and pPE in the MLV envelope will be mapped via chemical modification using trinitrobenzenesulfonic acid (TNBS) followed by analysis using electrospray ionization mass spectrometry (ESI-MS)

3.2 Functional relevance of PIP_2 enrichment retrovirus envelopes

3.2.1 Introduction

In mammalian cells, a wide diversity of phosphatidylinositol polyphosphate or phosphoinositides isomers are distributed across the different membrane organelle, each performing vital functions in signaling and membrane trafficking (Rusten and Stenmark, 2006). In the plasma membrane, the majority of phosphoinositides are believed to be $PI(4,5)P_2$ while low levels of $PI(3,4)P_2$ and $PI(3,4,5)P_3$ exist and are detected upon cell stimulation (Figure 22) (Rusten and Stenmark, 2006). While we were not able to differentiate the PIP_2 isomeric components in retrovirus envelope via our MS detection methods, we are assuming, in this line of investigation, that the PIP_2 present in retrovirus envelopes are chiefly composed of $PI(4,5)P_2$. This is based on the previous and ongoing studies showing the specific interaction between Gag and $PI(4,5)P_2$ at the plasma membrane assembly site (Murray et al., 2005; Ono et al., 2004; Saad et al., 2006).

We begin our investigation by deciphering the source of PIP_2 enrichment by comparing PIP_2 levels of virus like particles (VLP) produced from wild type Gag constructs and mutant Gag constructs which lacks the polybasic residues of MA domain. This is followed by an examination of the role of $PI(4,5)P_2$ levels in the plasma membrane in supporting HIV and MLV production. We propose to enzymatically deplete $PI(4,5)P_2$ levels using well defined plasmid constructs and determine the amount of virus particles released.

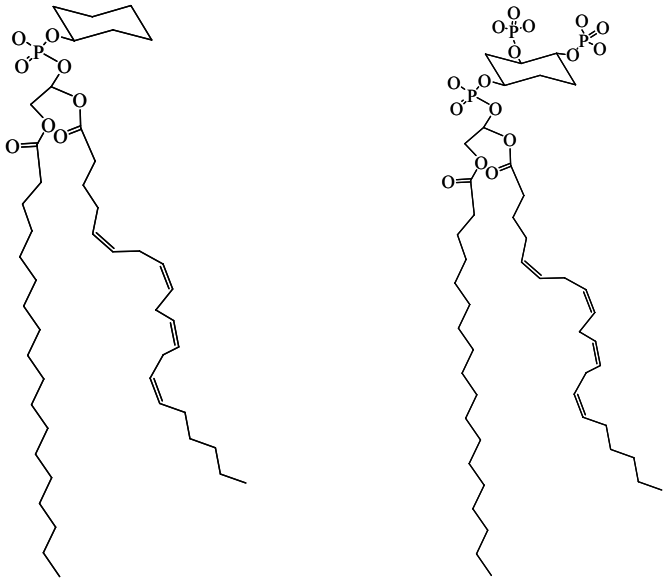

PI

PI-4,5-P_2

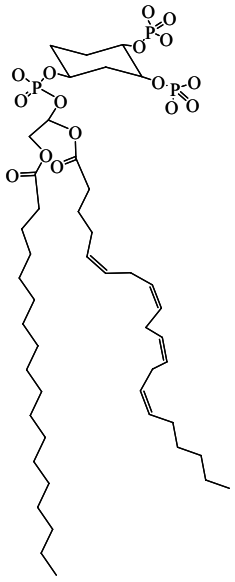

PI-3,4-P_2

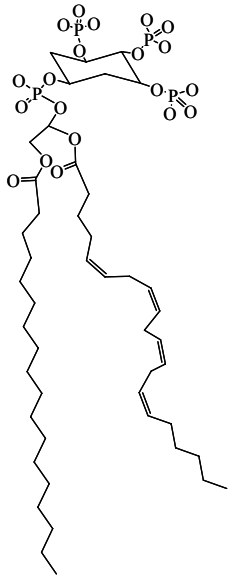

PI-3,4,5-P_3

Figure 22. Phosphoinositide species found in mammalian plasma membrane.

3.2.2 Materials and Methods

3.2.2.1 Reagents

All cell culture media and supplements were purchased from GIBCO, Invitrogen (Carsbad, CA, USA) or from the National University Medical Institute (NUMI, Singapore) supply store. All other reagents and chemicals including HPLC grade methanol, chloroform, and piperidine were purchased from Sigma Aldrich (St Louis, MO USA) unless stated otherwise.

3.2.2.2 Preparation of virus like particles[6]

Constructs expressing wild type and ΔMA HIV-Gag in the absence of Env were made based on pNL4-3/KFS (Ono et al., 2004) (a gift from Eric Freed, NCI, Frederick). Pol was deleted and a HA tag added to the C-terminus of Gag to study the release of virus-like particles (VLP) in the absence of protease. To make a ΔMA HIV-Gag expression vector, part of the globular MA head (aa 8-126) was deleted from the modified NL4-3/KFS clone. HEK293 cells were transfected with wild type and ΔMA HIV expression vector. At 48h post-transfection, the supernatants were collected and passed through a 0.45μm filter. The clarified supernatants were centrifuged at 25,000 rpm at 4^{o}C for 3h through a 15% sucrose layer to obtain purified VLPs. VLPs were lipid extracted for phosphoinositides enrichment (Bligh and Dyer, 1959) and measured using ABI 4000 Q-Trap (Applied Biosystems) as described in Chapter 2.

[6] Preparation of VLPs was carried out by our collaborator Walther Mothes' lab.

3.2.2.3 Measuring viral infectivity by flow cytometry

The level of retrovirus infectivity under different experimental conditions was assessed using flow cytometry analysis. An infectivity assay was established using purified MLV-GFP particles. These viruses were produced from REF cells that were transfected with a construct encoding Full length Friend MLV with a GFP insertion in the Env protein. As before, culture supernatant from the infected cells were collected, passed through a 0.45µm pore filter followed by ultracentrifugation through a 15% sucrose cushion at 25,000rpm at 4°C for 1.5h. The purified virus pellet was suspended in 1xPBS solution and stored at -80°C till further use. The conditions for this assay including the amount of virus to add from this stock, starting cell number and supplementation of hexadimethrine bromide or polybrene (Sigma) was initially investigated to determine the optimal conditions for subsequent experiments. For these experiments, approximately 5,000 REF cells were plated into each well of a 12 well plate and left over night to adhere to the well. The following morning, different volumes of virus stock was added to the cells in serum free media, with or without polybrene, and allowed a 2h infection period. Serum free media was used to prevent any interference between MLV particles contact to the host cell receptors. Thereafter, the unbound viruses were removed by aspiration, and fresh culture media was added to the wells. Infection was carried out for an additional 36-48h before fixing the cells in 2% paraformaldehyde for flow cytometry analysis. MLV-GFP infected cells were detected and counted by green fluorescence gating using the FACScalibur (BD Biosciences, CA USA). Chronically infected and uninfected REF cells were used as a positive and negative control respectively. The data presented are taken from the R1 gate that encompassed cells within 220-820 forward scatter (FSC) and 80-480 side scatter (SSC). In the end, we decided to use 5ul of virus from our stock without polybrene for infection of approximately 5,000 REF cells seeded per well in a 12 well plate for all subsequent experiments.

3.2.2.4 Virus budding and release assay[7]

To assess HIV release, 2.5 x 10^5 HEK293 cells in 24-wells were transfected with 150ng of replication-competent pHXB-GFP-IRES-nef construct plasmids (a gift from Premlata Shankar, Immune Disease Institute, Harvard University) together with plasmids expressing 5-phosphatase IV (5PaseIV), or catalytically inactive 5-phosphatase Δ1 (5PaseΔ1) (gifts from Eric Freed, NCI, Frederick with permission from P. Majerus, Washington University of School of Medicine, St. Louis, MO) or empty vector control. The 5PaseIV construct was obtained by cloning full-length human 5Pase IV (GenBank™ AF187891) into the *Bam*HI site of pcDNA 4/TO vector while the 5PaseΔ1 mutant lacking the phosphatase signature domain was constructed by removing a 1.1.-kb fragment between the *Nar*I and *Bst*BI restriction sites (Kisseleva et al., 2002; Ono et al., 2004). For MLV release assays, 200ng of plasmid MLV Env-GFP encoding full-length Friend 57 MLV genome with a GFP insertion into the envelope protein (Sherer et al., 2003) was co-transfected together with plasmids encoding 5PaseIV, catalytically inactive 5PaseΔ1 or vector control as above. 48h post-transfection, the released virus infectivity was measured by titering serial dilutions of the culture supernatants onto target cells TZM-bl (Derdeyn et al., 2000) and DFJ8 (Barsov et al., 2001) cell lines for HIV and MLV, respectively. TZM-bl cells are a HeLa cell line engineered to express human CD4, CCR5, and CXCR4 while DFJ8 cells express the murine ecotropic receptor MCAT-1. GFP-positive cells were enumerated after additional 36–48h using flow cytometry analysis (Bector Dickinson [BD] Biosciences, CA USA). The experiment was carried out in duplicates per trial on two separate days. The data was normalized to virus infectivity released from empty vector transfected samples and presented as fold inhibition.

[7] This work was carried out by the lab of our collaborator Dr Walther Mothes.

3.2.3 Results

3.2.3.1 Incorporation of PIP_2 into HIV is reduced in HIV lacking the MA domain.

It has been shown that the expression of retrovirus Gag alone is able to induce budding of virus like particles (VLP) (Campbell et al., 2001; Demirov and Freed, 2004). Numerous studies have argued that retrovirus Gag MA domains from different retrovirus families share a polybasic protein homology which interacts electrostatically with $PI(4,5)P_2$ at the inner leaflet of the plasma membrane during virus assembly (Chukkapalli et al., 2008; Dalton et al., 2007; Murray et al., 2005; Ono et al., 2004; Saad et al., 2006). This suggests a possible role of MA domain in the enrichment of PIP_2 in the retrovirus envelope. To test if MA is involved in PIP_2 incorporation, we produced and purified VLP from HEK293 cells expressing either wild-type HIV-Gag or mutant HIV Gag lacking the polybasic globular head of MA domain but still maintaining the N-terminal myristoylation signal (ΔMA HIV-Gag) and compared their phosphoinositide profiles (Table 8). Strikingly, PIP_2 and PIP level was reduced 2.1-fold and 1.5-fold respectively in ΔMA HIV-Gag VLP. This is close to corresponding basal levels of PIP_2 and PIP in microvesicles and plasma membrane, suggesting that the MA domain of HIV-Gag is responsible for the enrichment of these lipids in retroviral envelopes. Surprisingly, despite production from totally different cell types, the levels of PIP_2 and PIP in the HIV-Gag VLPs closely resemble those of purified HIV particles from H9 cells and monocyte derived macrophages (Table 8). This data suggest that electrostatic interaction between HIV-Gag MA with PIP_2 and PIP lipids occurs with conserved molecular specificities.

A

	WT Gag	ΔMA Gag
PI*	32.0 ± 5.7	63.2 ± 3.1
PIP	28.3 ± 5.2	18.4 ± 3.0
PIP_2*	39.8 ± 5.4	18.5 ± 6.0

B

	HIV-H9	H9-PM
PI**	36.5 ± 8.7	74.7 ± 12.3
PIP***	28.1 ± 5.3	11.5 ± 3.4
PIP_2*	35.4 ± 9.9	13.8 ± 5.2

C

	HIV-MDM	MV
PI **	31.1 ± 4.4	67.3 ± 1.4
PIP **	31.5 ± 4.1	17.6 ± 2.4
PIP_2*	37.3 ± 8.6	15.1 ± 3.6

Table 8. Contribution of polybasic MA domain to phosphoinositide incorporation into retrovirus envelope. Comparative phosphoinositide composition of WT Gag virus like particles (VLP) and ΔMA Gag VLP from HEK293 cells (A), purified HIV and plasma membrane fraction from H9 cells (B) and HIV and microvesicles (MV) produced from monocyte derived macrophages (MDM) (C). Values are expressed as molar percentages of the lipid extract and data presented represents an average of at least 3 independent experiments. Statistical significance between samples for (A) and (C) was measured using paired student's T test while the same for (B) was measured using unpaired student's T test. *, ** and *** denotes $p < 0.05$, $p < 0.01$ and $p < 0.001$ respectively.

3.2.3.2 Optimal conditions for detecting MLV infection in REF cells via flow cytometry

In order to assess the level of viral infectivity, we had to establish a flow cytometry assay to distinguish between infected and uninfected REF cells (refer to Material and Methods for full details) (Figure 23). Uninfected and chronically infected REF cells were used as a negative and positive control respectively. The background signal was arbitrarily set as being less than 5% of gated green fluorescence cells in the negative control which resulted in 79% GFP positive counts in the positive control. By plating 5,000 REF cells per well in a 12 well plate format, 24h before initiating the infection experiments, an initial well

confluency of approximately 20-25% was obtained. Such low cell density is required for these experiments because MLV replication requires cell division to take place (Goff, 2007). Based on this background, approximately 37%, 28% and 23% of cells were GFP positive 48 h post-infection when 5µl, 2µl and 1µl of virus were used respectively. When polybrene was added, infection rates increased to 48%, 35% and 31% with the same amount of virus used. Polyebrene is a cationic polymer that neutralizes the charge repulsion between virions and cell surface, thereby increasing the efficiency of infection. For the purpose of our experiments, using polybrene may be counter productive as this chemical may interfere with any alteration in net charge or cell adhesiveness that may be associated with perturbations to the virus envelope. Taking all factors into consideration, we decided to use 5µl of the virus stock without polybrene for further experiments (described from here onwards) as this amount of virus gave a good level of infection.

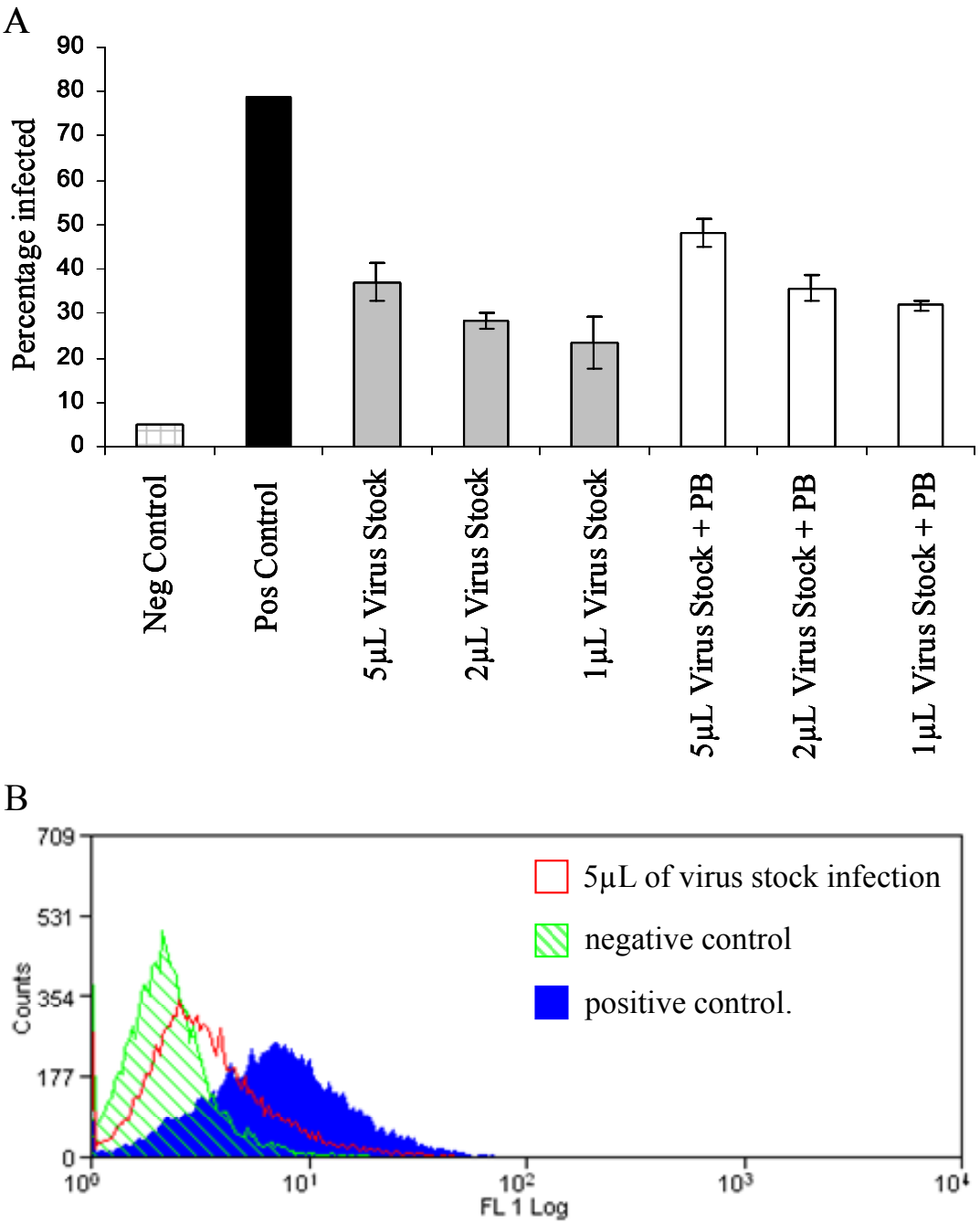

Figure 23. Optimization of conditions for measuring MLV infection using FACS analysis.
(A) A stock of MLV Env-GFP was produced and purified from REF cells, diluted in 1x PBS and stored in -80°C until further use. The volume of virus added to uninfected REF cells is indicated in the labels, with or without the cationic polymer polybrene (PB). The negative and positive controls used referred to non-infected REF and chronically infected REF cells respectively. (B) Actual FACS data showing the distribution of GFP positive cells between REF cells infected with 5µL of virus stock, negative control and positive control.

3.2.3.3 Depletion of PI(4,5)P_2 leads to reduced MLV and HIV production

While we were unable to ascertain the PIP_2 isomer identity present in retrovirus envelopes, we expected mainly PI(4,5)P_2 since it is the predominant phosphoinositide isomer present in mammalian plasma membranes. We thus decided to investigate if decreasing PI(4,5)P_2 levels in plasma membrane would have an inhibitory effect on retrovirus production (Figure 24A and B). The levels of cellular PI(4,5)P_2 were reduced by the expression of human 5PaseIV constructs which hydrolyzed the phosphate group at the D5 position of PI(4,5)P_2 (Kisseleva et al., 2002). Consistent with a role for PI(4,5)P_2 in retrovirus assembly and budding, HIV and MLV release were lowered with increasing amounts of 5PaseIV used in transfection which corresponded to decreasing cellular levels of PI(4,5)P_2. As a control experiment, we expressed the catalytically inactive form 5PaseΔ1 which lacked the phosphatase signature domain and therefore does not reduce cellular PI(4,5)P_2 levels (Ono et al., 2004). While 5PaseΔ1 did not affect virus release significantly, we observed that at high transfection levels, the inactive form of the enzyme also interfered with MLV release suggesting pleiotropic side effects under these conditions (Figure 24B).

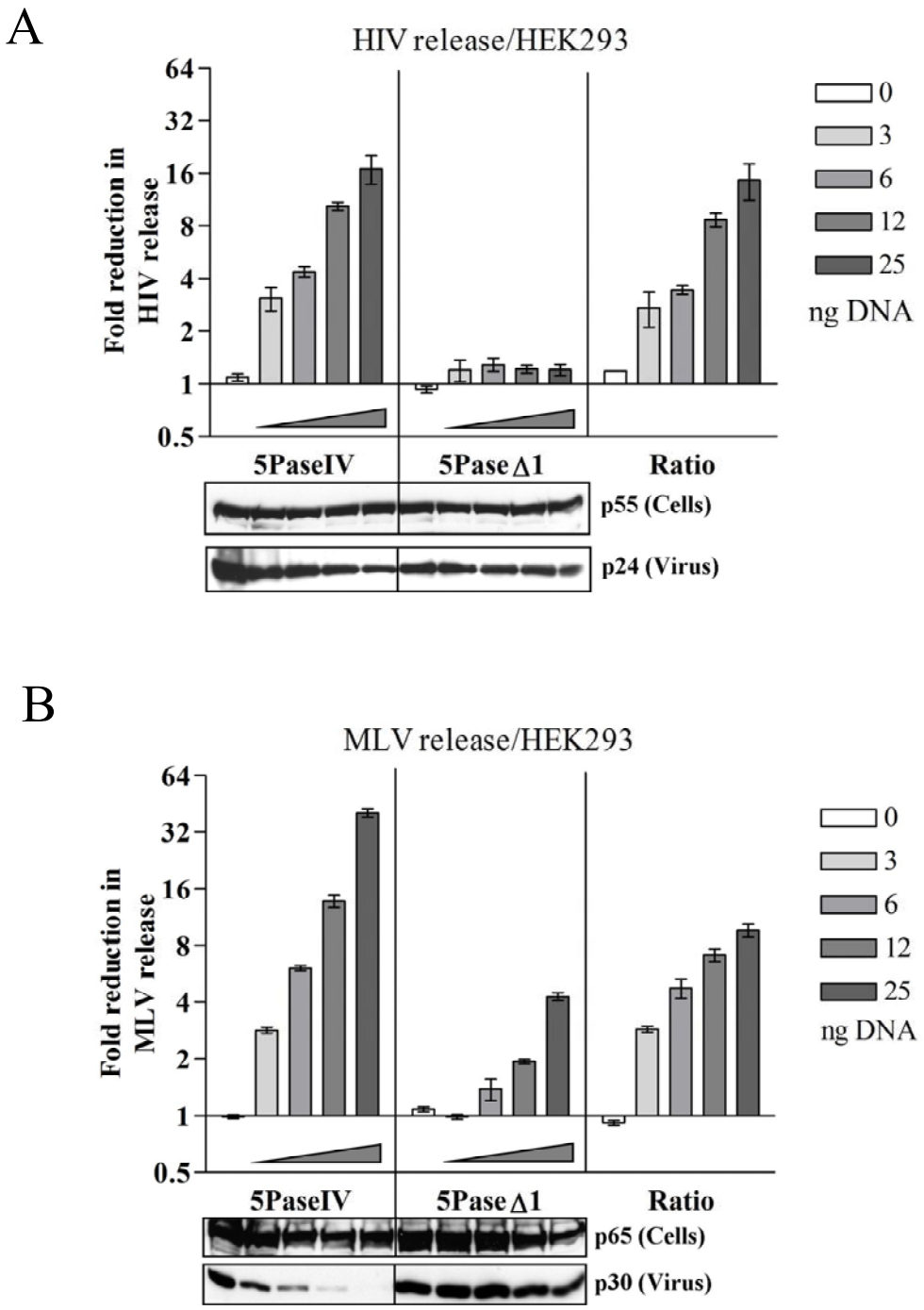

Figure 24. Effects of PI(4,5)P_2 depletion on (A) HIV and (B) MLV release from HEK293 cells.
The 5PaseIV and 5PaseΔ1 data was normalized to virus infectivity released from empty vector transfected samples and presented as fold inhibition. The ratio data was obtained by normalizing the 5PaseIV to 5PaseΔ1 data. The western blots show the levels of HIV (panel A) and MLV (panel B) Gag expression in cells and released virus detected in culture supernatants.

3.3 Glycosphingolipid depletion using PPMP

3.3.1 Introduction

Glycosphingolipids (GSLs) are ubiquitous constituents of mammalian plasma membranes that have been widely investigated for their role in viral entry (reviewed in Chapter 1). GSLs such as GluCer and GM3 are synthesized from ceramide precursors (Figure 25A), which occupy a central point in the sphingolipid biosynthetic pathway. A variety of powerful inhibitors that block enzymes specific to GSL biosynthesis or reactions steps upstream have been touted as potential anti-viral drugs (Figure 25B).

In a large body of work carried out by Blumenthal and colleagues, it was shown that pharmacological inhibition of GSL biosynthesis by phenyl-2-hexadecanoylamino-3-morpholino-1-propanol (PPMP) (Abe et al., 1992) reduces HIV-1 entry. Furthermore, entry could be restored following the addition of erythrocyte derived GSLs or purified GSLs like Gb3 and GM3 to the treated cells (Ablan et al., 2006; Finnegan and Blumenthal, 2006; Hug et al., 2000; Puri et al., 1998; Puri et al., 1999; Puri et al., 2004; Rawat et al., 2004b; Rawat et al., 2006). Other classes of sphingolipid inhibitors such as Fumonisin B1 (FB1) (Gelderblom et al., 1988) has also been used to deplete SM and GSLs from HIV producing cells, resulting in mutant HIV virions that were 5-fold weaker in infectivity compared to wild type HIV virions (Brugger et al., 2006).

While these studies show a dependence of HIV viability on the presence of GSLs in their envelope, the use of such inhibitors as antiretroviral therapeutics remains controversial. Overall lipid metabolism is co-regulated in cells and the use of chemical inhibitors can induce significant changes in glycerophospholipid and cholesterol homeostasis, membrane organization, cell growth and DNA replication (Barbour et al., 1992; Burger et al., 2007;

Glaros et al., 2005; Kovacs et al., 2000; Makino et al., 2006). Therefore, the interpretation of results obtained by using these chemicals has to be considered in correlation to overall cellular changes.

To address the issues described above, we propose to characterize the changes in lipid composition associated with the use of PPMP in MLV particles and rat embryonic fibroblast (REF) cells. We then complement this analysis by examining changes in MLV infectivity towards REF cells. Infectivity will be assessed from two perspectives: 1) comparing wild type MLV to mutant MLV produced from PPMP treated cells (Figure 26A) and 2) comparing the amount of infectivity in PPMP treated cells (Figure 26B). These experiments are important to distinguish between the effects of GSL depletion by PPMP at both virus-associated and host cell-associated levels.

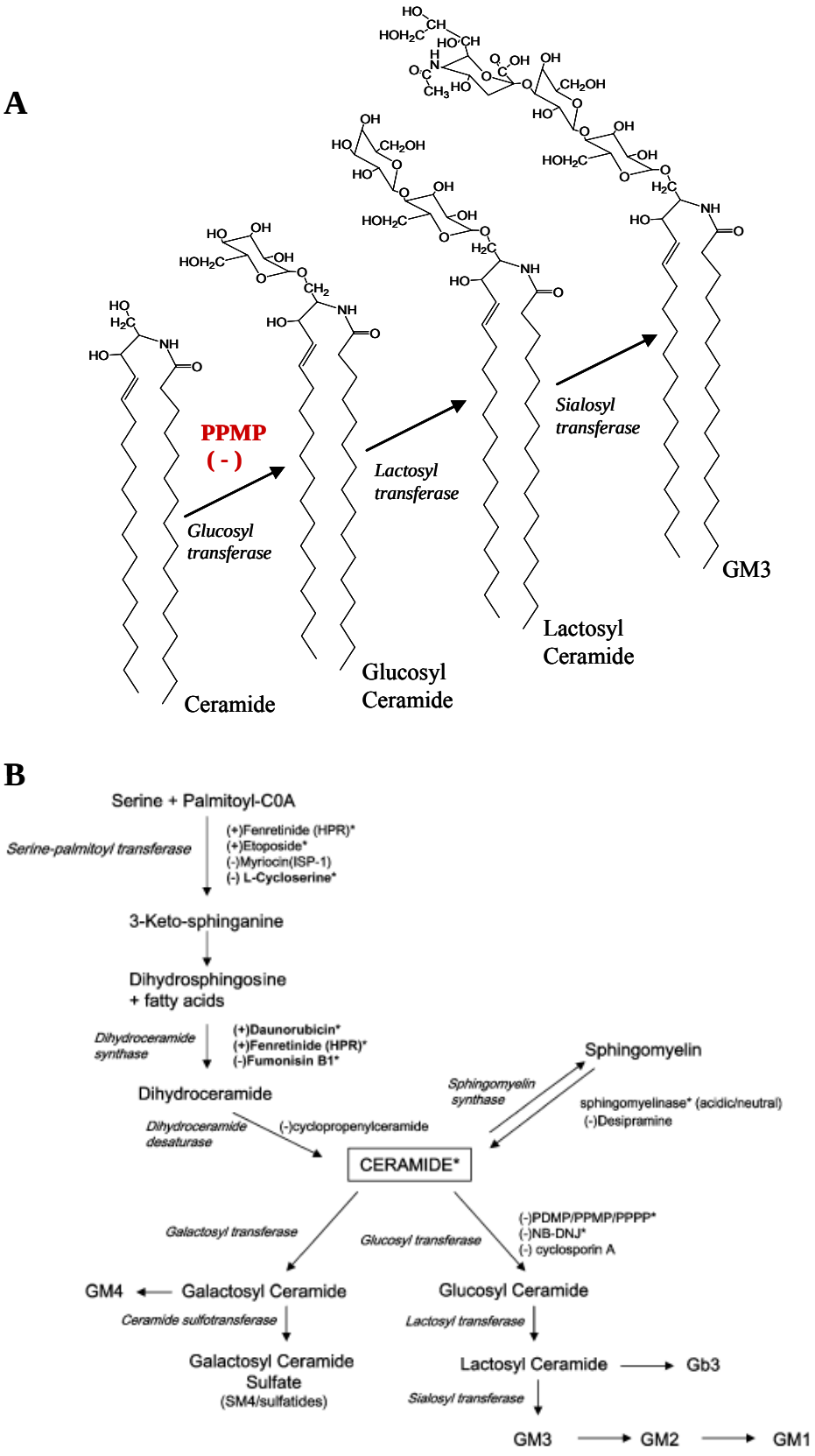

Figure 25. Formation of GM3 from sphingolipid precursors.
(A) The biosynthesis of glycosphingolipids from ceramide. Cellular enzymes responsible for the various steps in the reaction and the inhibitory action of PPMP are labeled in diagram. (B) Sphingolipid biosynthesis pathway. Cellular enzymes responsible for the various steps in the reaction and the inhibitors used to study HIV-1 entry are labeled in diagram. Taken from (Rawat et al. 2005).

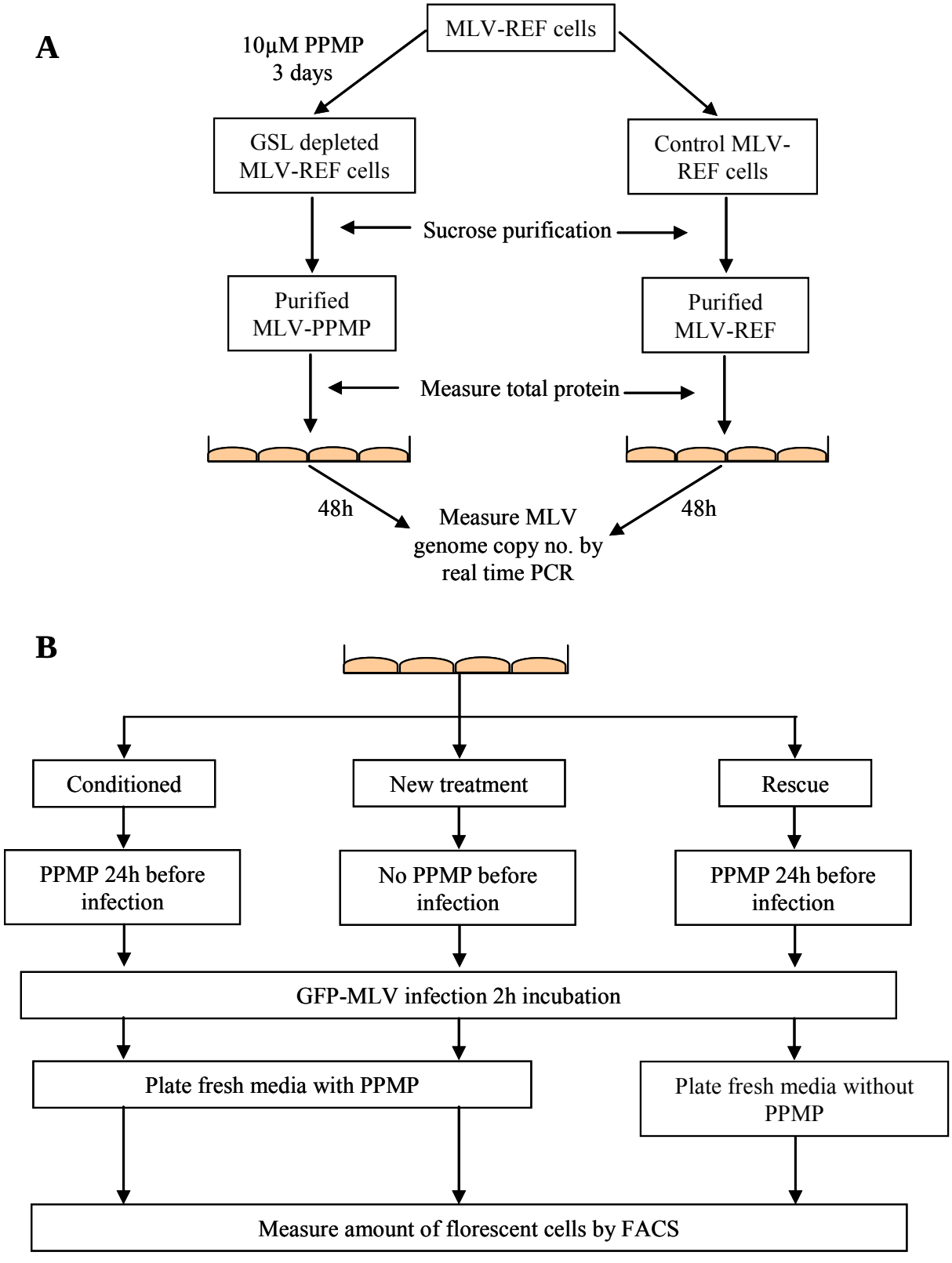

Figure 26. Schematic diagram of experimental steps to test effects of PPMP at the virus level (A) and at total cell level (B).

3.3.2 Materials and Methods

3.3.2.1 Lipid analysis of mutant MLV-PPMP envelope and PPMP treated cells

The effects of PPMP (Matreya LLC, Pleasant Gap PA) on changing lipid composition were examined in two aspects. Firstly, chronically infected REF cell lines were treated with 10μM PPMP for at least three days before MLV was purified from the culture supernatant. Previous reports have indicated the use of PPMP at concentrations of up to 10μM with complete inhibition of GSL production seen after three days (Hug et al., 2000; Puri et al., 2004). The mutant MLV-PPMP particles were then lipid extracted (Bligh and Dyer, 1959) and examined for changes in lipid profile using the ABI 4000 Q-Trap (Applied Biosystems, Foster City CA) in multiple reactions monitoring (MRM) mode and ELISA as described above. Besides lipid analysis, the structure of the mutant virus was also examined by electron microscopy[8]. All experiments were carried out in comparison to wild type MLV controls. Secondly, freshly plated REF cells were cultured in media supplemented with different media concentration of PPMP (mock, 1μM, 5μM and 10μM) for three days before harvesting and lipid extraction (Bligh and Dyer, 1959). The changes in lipid composition of PPMP-treated REF cells were examined using the MRM.

3.3.2.2 Glycosphingolipid detection by ELISA[9]

Virus particles were diluted in coating buffer to the required concentration and 100μl of diluted virus was added to the wells of a 96-wells microplate (PerkinElmer, Waltham MA, USA). The plates were sealed and incubated overnight at 4^{o}C to allow adherence of the virus.

[8] This analysis was carried out with the help of Ms Cheong Wei Fun.
[9] Refer to Appendix 1 for the recipes of reagents used under the section *"ELISA analysis"*.

The following day, the non adhering viruses were removed by aspiration and the wells were washed once with 1x PBS. Each well was then loaded with 300 µl of blocking solution, the plates sealed and incubated for 2 hours at room temperature. After this, the blocking solution was removed and the plate was washed at least five times with 1x PBS. 100µl of primary antibody, diluted to 1:250 or 1:500 using blocking solution, was then added to the wells, plate sealed and incubated overnight at 4^{o}C. The primary antibodies used were directed against gangliosides, including mouse monoclonal anti-GM3 (Seikagaku Corp, Tokyo), rabbit polyclonal anti-GM2 and rabbit polyclonal anti-GM1 (both from Matreya LLC, PA). Unbound primary antibody was then aspirated and the wells were washed with PBS at least five times. 100µl of biotinylated detection secondary antibody, diluted 1:5000 using blocking solution, was then added to the wells with a 1h incubation period. After this, unbound secondary antibody was aspirated and the wells were washed at least five times with 1x PBS. Lastly, 100µl of OptEIA TMB One-Step Substrate reagent (BD Biosciences, Franklin Lakes, NJ) solution was added to the wells and incubated for 30min for color development. The reaction was stop by adding 100µl of 1M H_3PO_4 and the final absorbance was read at 450nm.

3.3.2.3 Measuring infectivity of mutant MLV-PPMP viruses

Equal quantity of purified wild type MLV and mutant MLV-PPMP, as determined by total viral protein concentration (BioRad, Hercules CA), were used to infect untreated REF cells for 2hr (Figure 26A). After this initial incubation period, the culture media was changed to remove unbound virus. Following a further 48hr incubation period, the genomic DNA that now harbored the integrated viral genome was extracted using the DNeasy kit according to the manufacturer's protocol (Qiagen, Valencia CA). The amount of proviral integrations was analyzed using the 7300 Real Time PCR system (Applied Biosystems). IQ SYBR Green

Supermix (BioRad) was used as the reporter signal with the following PCR protocol: Cycle 1 (1X): Initialization Step 95°, 2min, Cycle2 (45X): Denaturation Step 95°, 30sec, Annealing Step 55°, 30sec, Elongation Step 72°, 1min, Cycle3 (1X): 4°, 5min. The primers used for MLV genome analysis was CTGTGTCTGTCCGATTGTCTAGTG (forward primer) and ACAGAGACAACACAGAA-CGATG (reverse primer) that amplifies the MLV LTR (Chan et al., 2008; Mothes et al., 2000a). The copies of MLV proviral genomes were normalized to the amount of cellular actin copies present. The primers used for actin analysis are ATCGCTGACAGGATGCAGAA (forward primers) and TAGAGCCACCAATCCACAC-AG (reverse primers).

3.3.2.4 Measuring infectivity of PPMP treated REF cells

Infectivity of REF cells was quantified using MLV-GFP virus as described in sections 2.2.3 and 2.3.2 of this chapter. Briefly, the infection of REF cells was initiated by incubating 5µl of MLV-GFP with REF cells in serum free media for 2hr. The serum free media with unbound virus was then aspirated and replaced with fresh media for an additional 36-48h, before the cells were harvested and fixed. Flow cytometry was used to measure the amount of infected, GFP-positive cells. To study the effect of PPMP on MLV infection of REF (Figure 26B), a number of different experimental conditions were included: 1) conditioning cells with different concentrations of PPMP 24h prior to virus infection and continuing treatment throughout the infection process, 2) treating cells with different concentration of PPMP only after the initial 2h infection period and 3) “rescuing” PPMP conditioned cells by replacing with normal cell culture media after the initial 2h infection period.

3.3.3 Results

3.3.3.1 Glycosphingolipid composition of MLV particles

In Chapter 2, it was established that the MLV envelope is enriched in GM3 over the plasma membrane fraction. GM3 with ceramide moieties d18:1/c16:0, d18:1/c24:1 and d18:1/c24:0 are the most abundant species in MLV particles (Figure 27A). The distribution of ceramide moiety closely resembles the molecular species distribution of Cer and SM of MLV (Figure 16). This is expected since the formation of glycosphingolipids like GM3 starts with a ceramide parent molecule (Figure 25A). We tried scanning for more complex gangliosides like GM1 and GM2 as well, but measurements were difficult due to lower concentrations of GM1 and GM2 and low virus titer. Moreover, due to the highly soluble nature of GM1 and GM2, these molecules normally partition to the aqueous phase during chloroform:methanol:water extraction techniques, thereby necessitating solid phase extraction. To circumvent this problem, we investigated the use of antibodies directed against GM1, GM2 and GM3 on purified MLV particles using an ELISA assay (Figure 27B). We were able to detect all three classes of GSLs on intact MLV virions but it was clear that the relative abundance is in a decreasing order where GM3>GM2>GM1.

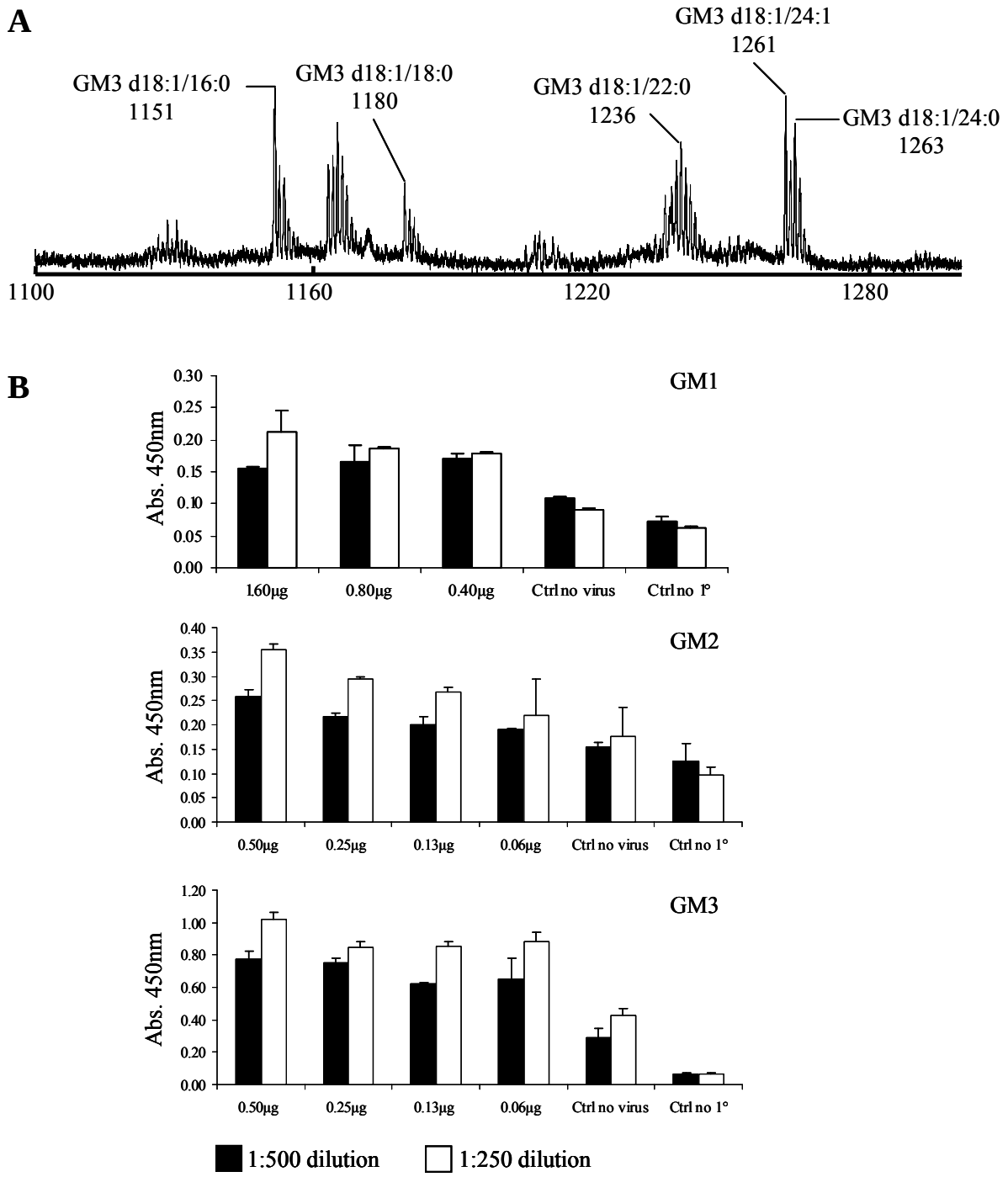

Figure 27. Complex glycosphingolipids found in MLV virus envelopes.
(A) Representative GM3 profile of purified MLV virus particles detected via ESI single stage scanning in negative ionization mode. The individual GM3 species are designated as sphingosine backbone (d18:1) to amide linked fatty acid carbon length and number of unsaturated bonds. (B) Detection of gangliosides GM1 (top), GM2 (middle) and GM3 (bottom) on purified MLV particles using ELISA. The primary (1°) antibodies were used in different dilutions as indicated in the legend. Amount of antibody binding is represented by absorbance measured at 450nm (y-axis). Experiments were carried out in a series of conditions indicated in the x-axis. The masses refer to the total MLV protein used per well. The control conditions included no virus control and no primary antibody (1°) control. Number of independent experiments for anti-GM1 is n=2, for anti-GM2 and anti-GM3 is n=3 and the error bars represent the standard deviation of the mean.

3.3.3.2 Overall lipid composition of MLV-PPMP is distinct from MLV-REF virions

PPMP is a chemical inhibitor of GSL synthesis that works by inhibiting UDP-glc glucosyltransferase activity, thereby preventing glycosylation of ceramide that leads to GluCer and other complex GSLs (Figure 25) (Abe et al., 1992). We continuously cultured MLV infected REF cells in culture media supplemented with 10μM of PPMP and collected the supernatant for virus purification, which we now refer to as MLV-PPMP. The lipid composition of these mutant viruses was compared to that of wild type MLV-REF particles.

To obtain a quantitative description of the changes in lipids composition, MLV-PPMP was compared to MLV-REF using MRM detection for phospholipids and sphingolipids (Table 9 and Figure 28). As expected, MLV-PPMP particles showed a drastic reduction in GluCer and GM3 levels compared to MLV-REF particles. The reduction of GM3 was further validated using ELISA measurements (Figure 30A). This effect caused a significant increase in Cer levels in MLV-PPMP. Significantly, the overall levels of phosphoinositides in MLV-PPMP were drastically modulated. Compared to MLV-REF, PI and PIP levels became highly elevated in MLV-PPMP envelopes while PIP_2 was drastically reduced. Another interesting observation was that MLV-PPMP envelopes became slightly enriched in long chained (C>36) PC and ePC (Figure 28). This was balanced by decreasing levels of short chained (C≤34) PC and ePC, thus resulting in minimal changes in overall PC and ePC levels (Figure 28). PE and pPE also appear to be up-regulated in MLV-PPMP envelopes although this effect is negated by large variations in signal intensity (Figure 28). No significant changes were seen in the other phospholipid classes measured.

A

	MLV-REF	MLV-PPMP
PS	4.4 ± 0.6E-02	4.8 ± 0.3E-02
PI	4.5 ± 0.0E-03	10.0 ± 1.9E-03
PIP	5.5 ± 0.8E-03	13.0 ± 2.3E-03
PIP_2	22.0 ± 1.3E-03	2.0 ± 0.9E-03
PE	1.3 ± 0.1E-03	1.7 ± 0.6E-03
pPE	3.3 ± 0.5E-03	4.1 ± 1.4E-03
PC	5.5 ± 0.1E-01	5.9 ± 0.3E-01
ePC	1.6 ± 0.0E-01	1.2 ± 0.0E-01
SM	2.0 ± 0.1E-01	2.1 ± 0.2E-01
Cer	2.1 ± 0.6E-04	4.4 ± 0.6E-04
GluCer	7.7 ± 0.9E-04	3.0 ± 0.7E-04
GM3	1.0 ± 0.2E-02	1.4 ± 0.6E-03

B

	MLV-PPMP /MLV-REF
PS	1.1
PI	2.2**
PIP	2.4**
PIP_2	-0.1***
PE	1.3
pPE	1.2
PC	1.1
ePC	-0.8
SM	1.1
Cer	2.1**
GluCer	-0.4**
GM3	-0.1***

Table 9. Effects of PPMP treatment on the overall lipid composition of MLV-REF envelope.
(A) Lipids from MLV-PPMP and MLV-REF were measured using MRM and are presented as relative values normalized to total ion counts. The data shown are averages and standard deviations of three independent samples, n=3. (B) Ratio of MLV-PPMP to MLV-REF lipid composition. Lipids which are significantly enriched (>1.5 fold) or excluded (<1.5 fold) in viral envelopes are highlighted in red and green, respectively. The data represents the average of three independent samples, n=3. Statistical significance was calculated using unpaired student's T test, where *, ** and *** denotes $p < 0.05$, $p < 0.01$ and $p < 0.001$ respectively.

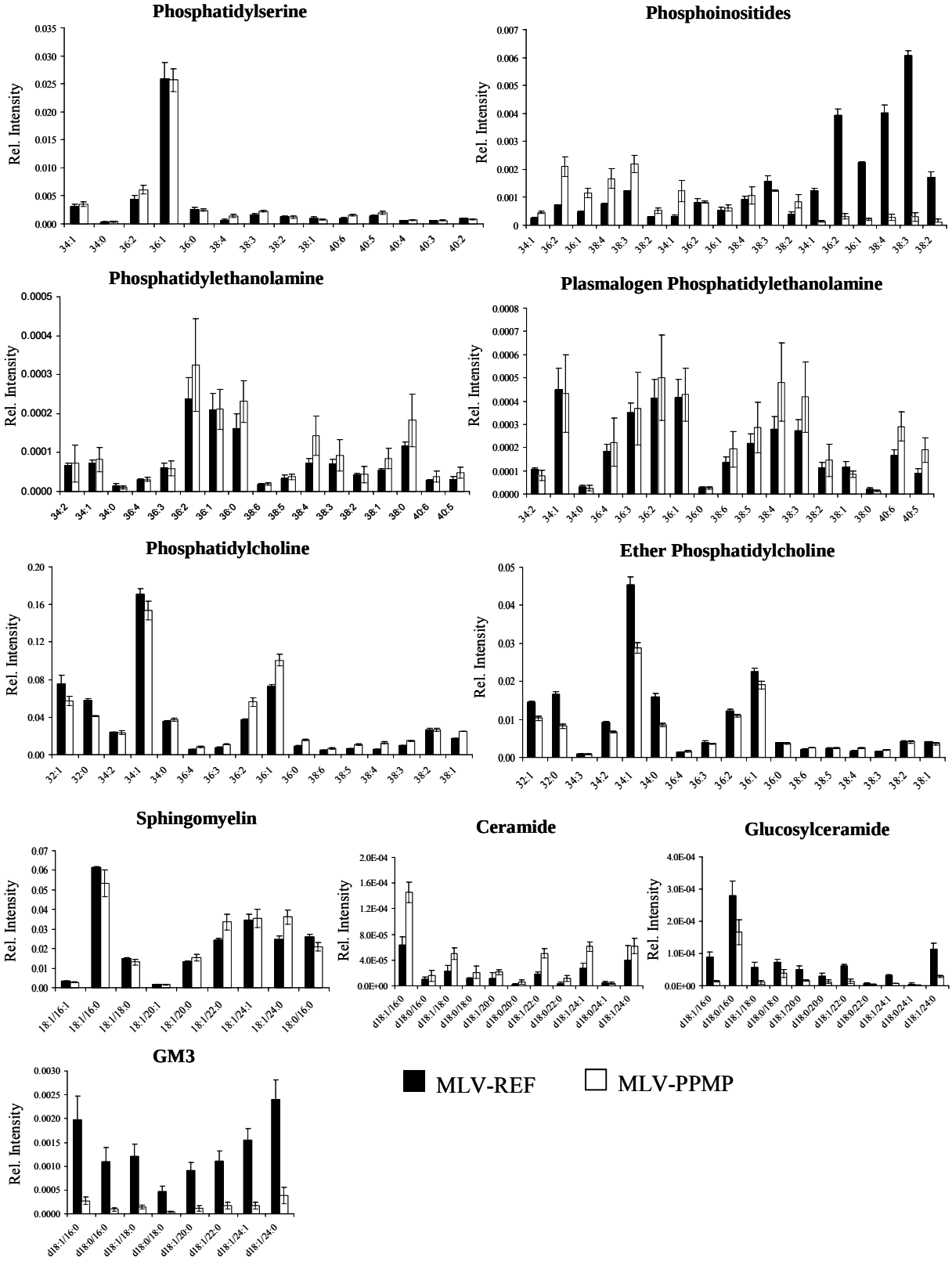

Figure 28. Glycerophospholipids and sphingolipids distribution of MLV-REF versus MLV-REF.
Abundance is represented as the relative intensity (y-axis) of a given lipid (x-axis) normalized to total lipid signal intensity in each sample. Lipids were extracted from purified MLV-REF (black bars) and MLV-PPMP (open bars), and quantified via mass spectrometry using multiple reaction monitoring. Sphingolipids are presented as sphingoid base residue/fatty acyl residue. The standard deviation was derived from a sample size of at least n=3.

3.3.3.3 MLV-PPMP virions are morphologically different from MLV-REF and show weakened infectivity

The changes in lipid composition, particularly to raft lipids like GM3 and Cer and the fatty acyl chain distribution of PC and ePC, suggested that MLV-PPMP virus may exhibit morphological differences compared to MLV-REF particles. Comparing both particles by electron microscopy, we found that MLV-PPMP particles showed abnormal membrane structure compared to MLV-REF particles (Figure 29). The membranes of MLV-PPMP virions were marked by distinct regions of increased darkening alternating with lighter areas at the edges, suggesting abnormal clustering of electron dense proteins and/or lipids in MLV-PPMP envelopes. This image is reminiscent of HIV and SIV particles that were depleted of cholesterol molecules by β-methylcyclodextrin, resulting in what was described as "a punctuate looking virus" (Graham et al., 2003). With decreased amount of GSLs exposed on its envelope surface, we predicted that MLV-PPMP virions may not be able to attach efficiently to its target cell and thus exhibit lower infectivity compared to MLV-REF. Alternatively, the changes in lipid composition and membrane structure may not provide a suitable membrane environment for the proper functioning of the MLV Env protein (Guyader et al., 2002).

We tested this hypothesis by carrying out an infectivity assay comparing purified MLV-PPMP to MLV-REF (Figure 26A). Freshly prepared MLV-PPMP and MLV-WT stocks were quantified by total protein measurements (data not shown). Since both types of particles have been purified to the same extent, total protein measurements should provide a reasonable estimation of the number of virus particles used for infection. With this new batch of virus, we also confirmed by ELISA assay that GM3 level in PPMP-MLV particles was indeed reduced compared to WT-MLV particles (Figure 30A). REF cells, plated at 20% confluence at the start of the experiment, were exposed to equal amounts of MLV-PPMP or

MLV-REF for 2h to initiate infection. Polybrene was not used in this experiment as polybrene may artificially increase the binding of the virus to the host cell surface. The cells were grown in normal cell culture media throughout the duration of the experiment. It is important to note that under such conditions, the effects of lowered GSL levels are studied only during the initial infection step since the subsequent rounds of virus particles produced would exhibit wild type morphology. In this experiment, the viruses used did not express a fluorophore, so infectivity was quantified by measuring the number of copies of proviral genome that was integrated into the host cell genome using real time PCR. The amount of viral genome detected was normalized to the cellular actin copy number to account for differences in cell number. It was found that MLV-PPMP infectivity was reduced ~5 folds compared to MLV-REF (Figure 30B).

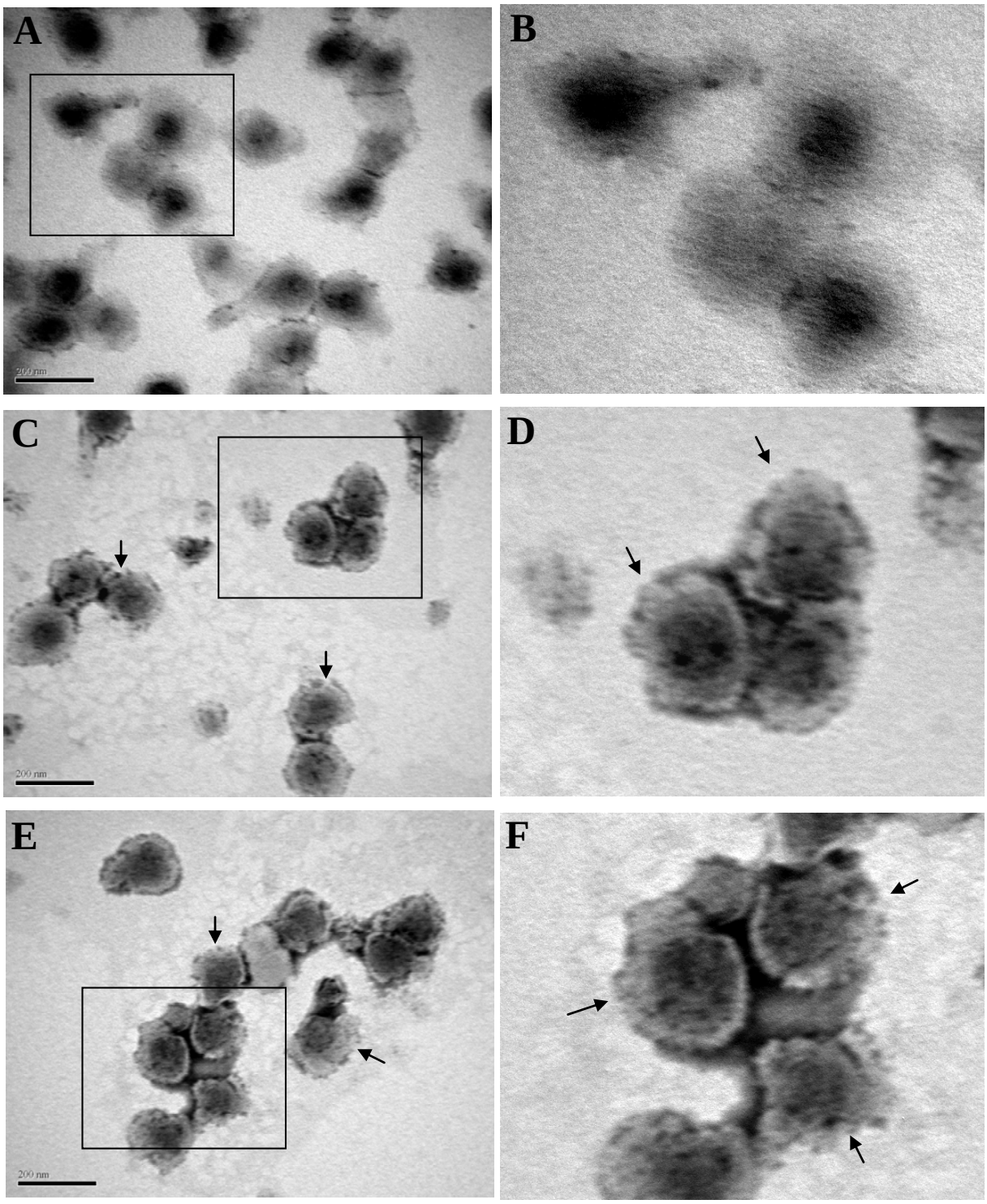

Figure 29. Changes in envelope morphology of MLV-PPMP.
Electron microscopy of wild type MLV-REF particles produced from REF cells (A and B) and MLV-PPMP particles produced from REF cells treated with 10μM PPMP (C-F). The boxed area for figures A, C and E were enlarged and presented as B, D and F respectively. The arrows point out the punctured structures.

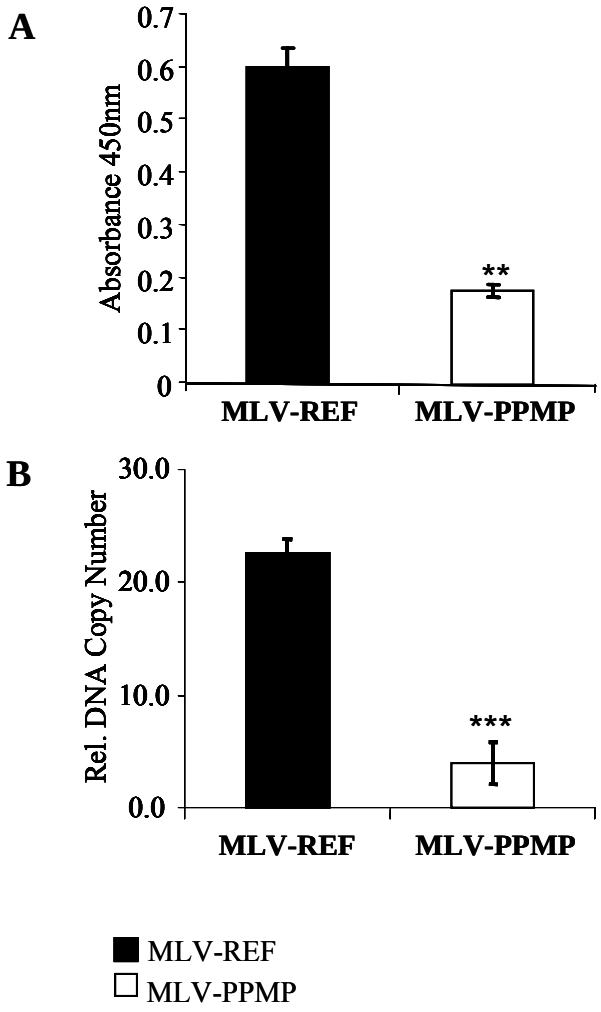

Figure 30. Differences in GM3 and infectivity levels between MLV-PPMP and MLV-REF particles.
(A) Measurement of GM3 in purified wild type MLV (■) versus MLV produced by PPMP treated REF cells (□). Detection of GM3 was via ELISA, using antibody concentration of 1:500 dilution as determined earlier. 0.5µg of virus, as determined by total viral protein, was used as the antigen. (B) Infectivity of MLV-REF versus MLV-PPMP was measured via the amount of viral genome copy number integrated into the host genome, using real time PCR analysis. The standard deviation was obtained from a sample size of n=3. Statistical significance between MLV-PPMP and MLV-REF was measured using paired student's T test. ** and *** denotes $p < 0.01$ and $p < 0.001$ respectively.

3.3.3.4 PPMP treatment of REF cells result in changes to overall lipid composition

We next examined the changes in lipid composition caused by PPMP treatment in cells. In accordance with previously reported therapeutic ranges for PPMP application (Hug et al., 2000; Puri et al., 2004), we cultured REF cells in medium supplemented with 1µM, 5µM or 10µM of PPMP for three days before harvesting and lipid extraction. We quantified

and compared the total relative sphingolipids and phospholipids composition of the cells using MRM (Table 10).

Expectedly, the level of detectable GM3 decreased with increasing concentrations of PPMP. GluCer levels also decreased with 1μM of PPMP but appeared to normalize and increase to control levels with increasing PPMP concentrations. Unlike in MLV-PPMP envelope, PPMP treated REF cells showed a reduction in Cer levels while SM levels were up-regulated compared to normally cultured REF cells. Significant changes in phopsholipid composition were detected as well. PC levels became more elevated with increasing PPMP concentrations while ePC first became elevated with low PPMP concentration then decreasing to below normal level with increasing concentrations of PPMP. In contrast, both PE and pPE levels decreased, although there seems to be a return to normal levels for long chain (C>36) and poly-unsaturated species at the highest PPMP concentration (Figure 31). In contrast to MLV-PPMP, PI levels were also decreased, specifically with their major species PI 38:3, PI 38:2 and PI 36:2 (Figure 31). Overall PS levels increased only slightly with higher PPMP concentrations, with increases in short chain (C32-34) and poly-unsaturated (PS 38:4, PS 40:5 and PS 40:4) species being balanced by decreases in long chained species (Figure 31).

A

	REF Control	REF+1uM PPMP	REF+5uM PPMP	REF+10uM PPMP
PS	3.4 ± 0.3E-01	3.3 ± 0.1E-01	3.5 ± 0.3E-01	3.9 ± 0.4E-01
PI	1.8 ± 0.2E-01	1.5 ± 0.1E-01	1.2 ± 0.1E-01	1.2 ± 0.1E-01
PE	1.6 ± 0.3E-02	9.3 ± 3.2E-03	8.8 ± 0.6E-03	1.1 ± 0.3E-02
pPE	2.2 ± 0.2E-02	9.7 ± 2.9E-03	9.1 ± 0.6E-03	1.1 ± 0.3E-02
PC	2.3 ± 0.1E-01	3.4 ± 0.2E-01	3.6 ± 0.2E-01	3.4 ± 0.3E-01
ePC	6.4 ± 0.4E-02	9.5 ± 0.5E-02	8.0 ± 0.3E-02	5.8 ± 0.3E-02
SM	4.4 ± 0.2E-02	6.1 ± 0.2E-02	6.4 ± 0.5E-02	6.3 ± 0.6E-02
Cer	4.1 ± 0.4E-04	2.5 ± 0.2E-04	2.2 ± 0.2E-04	2.5 ± 0.9E-04
GluCer	1.8 ± 0.2E-04	7.7 ± 0.6E-05	9.3 ± 1.0E-05	1.7 ± 0.1E-04
GM3	1.0 ± 0.0E-01	8.0 ± 2.4E-03	4.4 ± 0.3E-03	4.9 ± 1.3E-03

B

	REF+1uM PPMP/ REF Control	REF+5uM PPMP/ REF Control	REF+10uM PPMP/ REF Control
PS	1.0	1.0	1.1
PI	-0.8	-0.7**	-0.7**
PE	-0.6	-0.6*	-0.6
pPE	-0.4**	-0.4***	-0.5**
PC	1.5**	1.6***	1.5**
ePC	1.5**	1.3**	-0.9
SM	1.4***	1.5**	1.4**
Cer	-0.6**	-0.5**	-0.6*
GluCer	-0.4**	-0.5**	-0.9
GM3	-0.1***	-0.04***	-0.1***

Table 10. Effects of PPMP treatment on the overall lipid composition of REF total cell membrane.
(A) Lipids from control REF and PPMP treated REF cells were measured using MRM and are presented as relative values normalized to total ion counts. The data shown are averages and standard deviations of three independent samples, n=3. (B) Ratio of PPMP treated REF cells to control REF cells lipid composition. Lipids which are significantly enriched (>1.5 fold) or excluded (<1.5 fold) in viral envelopes are highlighted in red and green, respectively. The data represents the average of three independent samples, n=3. Statistical significance was calculated using unpaired student's T test, where *, ** and *** denotes $p < 0.05$, $p < 0.01$ and $p < 0.001$ respectively.

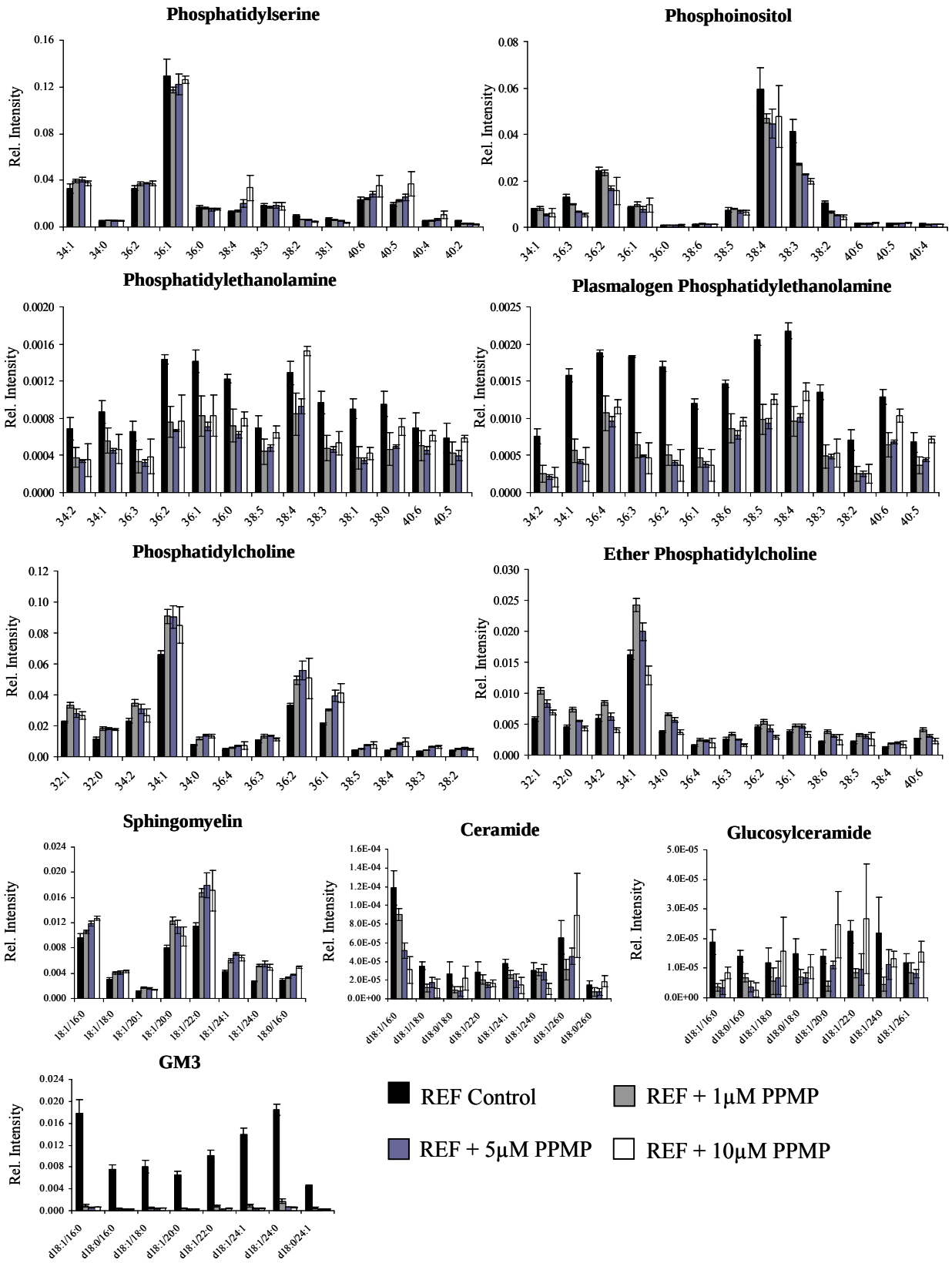

Figure 31. Glycerophospholipids and sphingolipids distribution of REF after PPMP treatment.
Abundance is represented as the relative intensity (y-axis) of a given lipid (x-axis) normalized to total lipid signal intensity in each sample. Lipids were extracted from REF Control (black bars), REF treated with 1μM (gray bars), 5μM (purple bars) and 10μM (open bars) of PPMP, and quantified via mass spectrometry using multiple reaction monitoring. Sphingolipids are presented as sphingoid base residue/fatty acyl residue. The standard deviation was derived from a sample size of at least n=3.

3.3.3.5 PPMP treated REF cells are more susceptible to MLV infection compared to untreated REF cells

We are unsure of the physiological consequences of these changes in lipid composition but it was observed that PPMP treated REF cells exhibited increasing cytoplasmic granularity (Figure 32A) and also exhibited slower growth rates in culture, particularly when 10 μM of PPMP was used (data not shown). Since MLV infection and replication requires cell division to occur, we decided to examine if treatment of REF cells with PPMP will interfere with the infectivity of the cells. In this experiment, three different conditions were investigated as illustrated in (Figure 26B). We set the threshold level of infected GFP positive cells as more than 5% GFP background signal in the negative control (Figure 32B).

Surprisingly, instead of a decrease in infection levels, it was found that cells conditioned in PPMP actually resulted in increased infection levels (Figure 33, gray bars). Infectivity peaked at 5μM PPMP concentration but decreased when 10μM PPMP concentration was used. To better determine the replication step in which PPMP treatment may enhance, we exposed the cells to the inhibitor only after the initial infection step. This also resulted in increased infectivity (Figure 33, white bars), similar in levels to conditioned cells, therefore suggesting that the enhancement of replication is likely to occur after the entry step. On the other hand, when PPMP conditioned cells were rescued, i.e. returned to normal media conditions, the level of MLV infection was reduced proportionately, although the condition with initial 10μM PPMP treatment seemed not to recover as well as those with lower PPMP concentration (Figure 33, black bars).

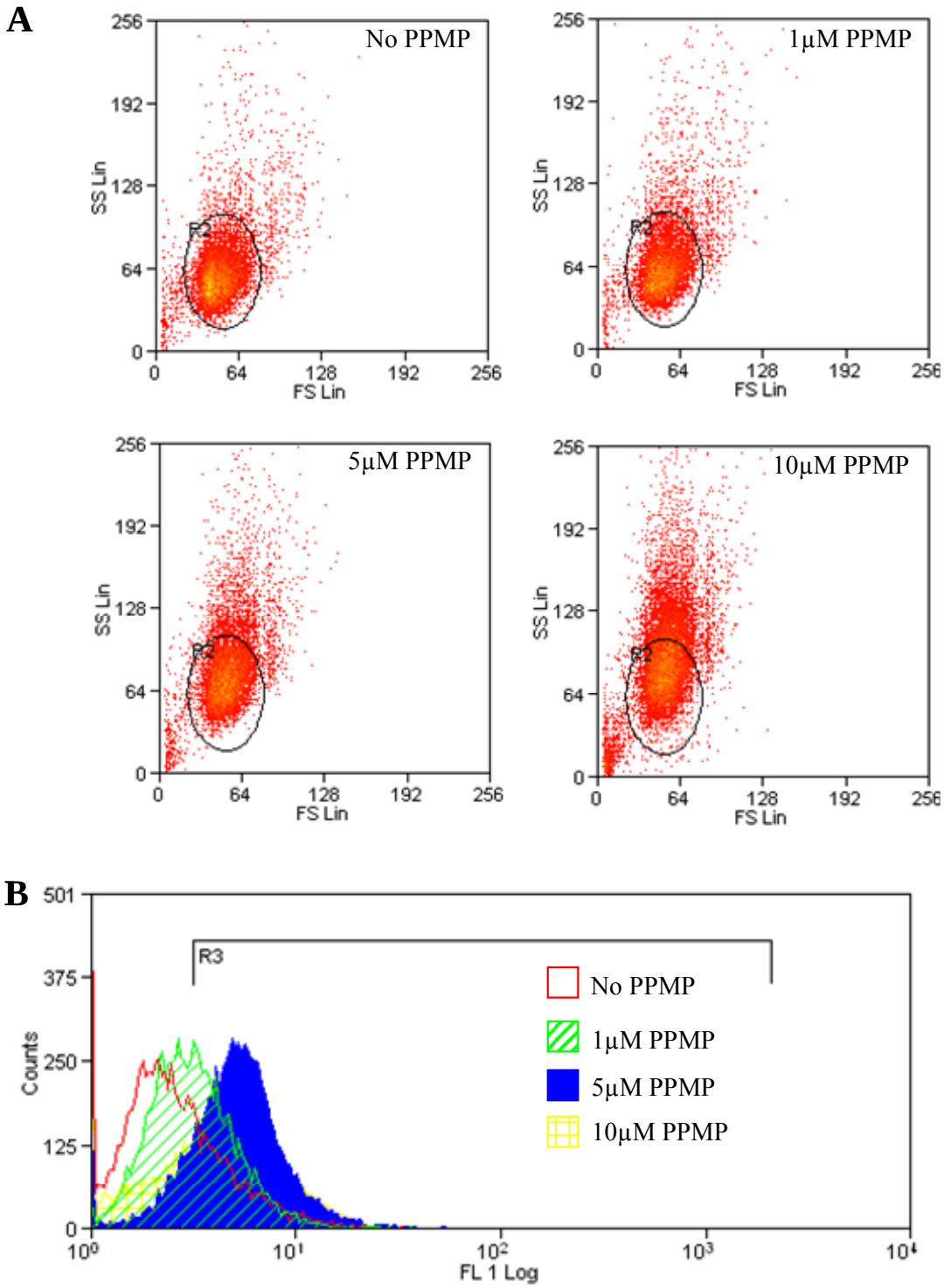

Figure 32. FACS analysis of infectivity level using MLV-GFP virus under different PPMP conditions.
(A) Scatter plot of MLV-GFP infected REF cells, cultured at the indicated PPMP concentration. The y-axis represents the side scatter of the sample, indicating the amount of granularity of the cells. The x-axis represents the forward scatted of the sample, indicating size distribution of the cells in the sample. Sample gating limits is set within oval R2, from which the FACS instrument will measured GFP positive cells. (B) Amount of infected GFP positive cells in the differently treated samples. R3 indicates the cutoff used to determine true GFP positive cells and is based on <%5 basal level of GFP positive cells in the negative control.

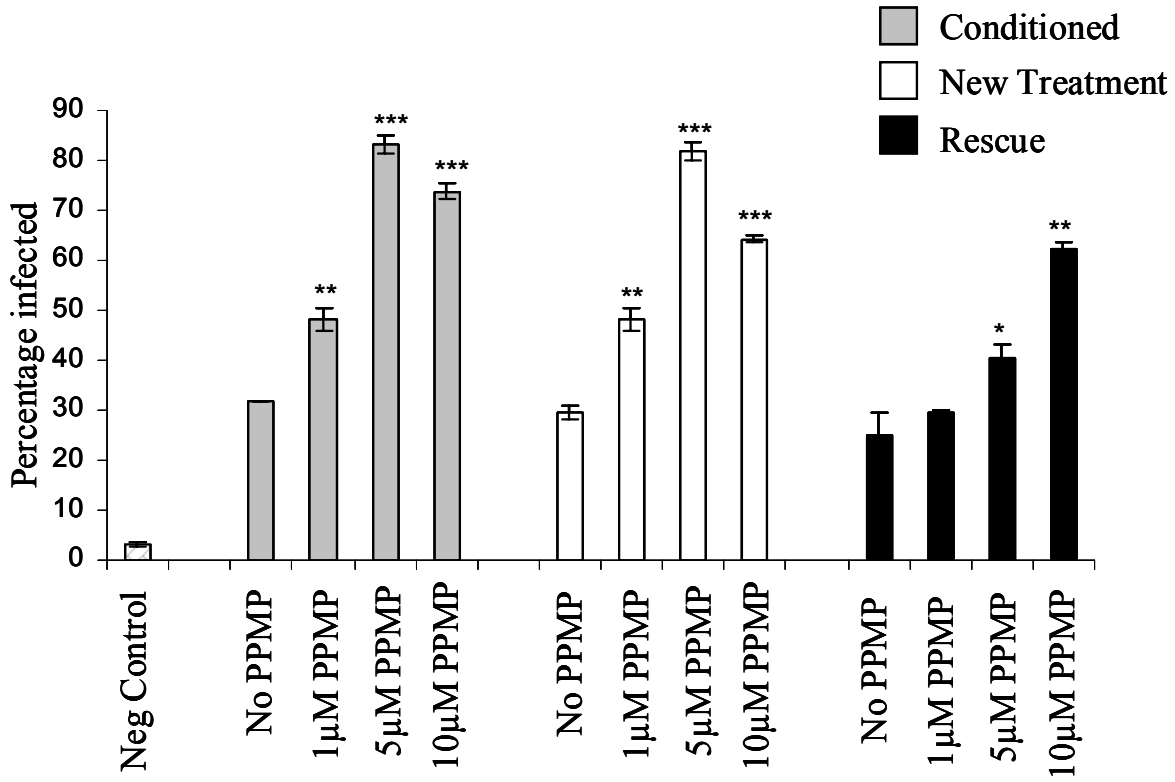

Figure 33. MLV infection of PPMP treated REF cells.
Gray bars represent experiments carried out on REF cells that were already conditioned with PPMP at the indicated concentration for at least 24h prior to infection. Cells continued to be treated with the indicated PPMP concentration for the duration of the experiment. White bars represent experiments where MLV infection was carried out on untreated REF cells first. The cells were newly treated with the indicated PPMP concentration after initial MLV infection for the duration of the experiment. Black bars show levels of infection when conditioned cells are rescued by switching to normal culture media after initial MLV infection. The infected cells were detected as percentage of GFP positive cells via flow cytometry. The results represent a sample size of n=3. Statistical significance between different PPMP treatments and their controls was measured using paired student's T test. *, ** and *** denotes $p < 0.05$, $p < 0.01$ and $p < 0.001$ respectively.

3.4 Aminophospholipids distribution in MLV envelope

3.4.1 Introduction

The aminophospholipids PS and PE represent the most abundant lipid classes in the retrovirus envelope after PC and SM. In Brugger et al., the authors reported that PS and pPE are enriched in HIV envelopes when compared to total cell membrane (Brugger et al., 2006). In this study, we recapitulated this result in all our retrovirus envelopes when using total cell membrane composition as the comparator (Table 5B). However, when we compared viral envelopes to the plasma membrane, we find that this enrichment is lost except PS in MLV (Table 6B). This is due to the fact that the plasma membrane itself is highly enriched in PS and pPE compared to the rest of the cellular organelle (van Meer, 2005).

Asymmetrical distribution of PS and PE in the plasma membrane is achieved by a number of factors including biophysical properties that restrict the ability of a lipid to cross the bilayer spontaneously and the presence of lipid binding enzymes that regulates translocation across bilayer (Holthuis and Levine, 2005). As discussed in Chapter 1, PS lipids have potential co-receptor functions in virus entry and, in some cases, is able to promote virus infections (Callahan et al., 2003; Coil and Miller, 2005a; Coil and Miller, 2005b). Another important consideration regarding, PS, PE and pPE is their contribution to membrane dynamics (McMahon and Gallop, 2005; Zimmerberg and Kozlov, 2006). Naturally, the transbilayer distribution of these lipid classes would have critical influence on their function in retroviral budding and entry.

To gain insight into the functions of aminophospholipids, we seek to investigate the topology of these lipids in MLV particles produced from REF cells. 2,4,6-trinitrobenzene sulfonic acid (TNBS) has been used to investigate the asymmetry of aminophospholipids in a

variety of biological membranes including VSV (Fong et al., 1976; Fong and Brown, 1978), exosomes (Laulagnier et al., 2004) and mammalian cells (Fontaine and Schroeder, 1979; Marinetti and Cattieu, 1982; Schwartz et al., 1987). We propose to covalently modify aminophospholipids on the external leaflet of MLV envelopes with TNBS, followed by identifying these lipids via ESI-MS. We anticipate that these results will contribute to our understanding of the roles these aminophospholipids in mediating retrovirus and/or general vesicle budding and fusion activity with the host cell.

3.4.2 Materials and Methods

3.4.2.1 Preparation of liposomes

Lipids in organic solvents were mixed in the appropriate final liposome concentration using egg yolk derived PC with suitable amounts of DMPS, DMPE or pPE 38:4 (Refer to Appendix 5). The solvent was then removed by rotary evaporation in a speed vacuum, leaving behind a thin lipid film on the side of the tube. The lipid film was rehydrated by addition of 1ml 1xPBS, incubated for 1hr at room temperature with occasional vortexing, and finally agitated in a bath sonicator for 15min. This resulted in large multilamellar vesicles (LMV) suspension. This suspension was subjected to extrusion through a polycarbonate filter with 0.45μm pore size (Millipore, MA, USA) resulting in small unilamellar vesicles (SUV).

3.4.2.2 TNBS labeling of liposomes

We used SUV to establish the non-penetrating conditions for TNBS labeling. In these experiments, TNBS labeling of SUV was carried out under different reactions conditions including temperature variation during incubation (4°C, 25°C, 37°C) and concentration of TNBS used (1mM, 2mM, 4mM). The labeling reaction was carried out for 1.5h and terminated by quenching excess TNBS with a 2% final concentration of fatty acid free BSA (Roche, IN, USA). The samples were then lipid extracted using the Bligh and Dyer method (Bligh and Dyer, 1959) and the lipid samples subjected to lipid analysis using Waters Micromass Q-TOF (Waters Corp.) and ABI 4000 Q-Trap (Applied Biosystems) mass spectrometers as described in Chapter 2. It was found that the optimal reaction condition for TNBS labeling is 4°C for 1.5h using 2mM of TNBS.

3.4.2.3 TNBS labeling of MLV particles

TNBS has been used to study asymmetry of aminophospholipids in VSV membrane bilayer (Fong et al., 1976; Fong and Brown, 1978) and we have modified the protocol accordingly for our experiments. For the labeling of MLV particles, only freshly produced MLV particles were used as it was found in that freeze thawing will affect the permeability of the virus envelope (Fong et al., 1976). Following the TNBS labeling and quenching step described above, the virus particles were layered above a 6ml volume of 15% sucrose cushion and pelleted through the cushion at 25,000rpm for 1.5h at 4°C to separate the TNBS labeled MLV particles from the reaction mixture. The labeled TNBS-MLV was then subjected to lipid extraction (Bligh and Dyer, 1959) and analysis via ESI-MS using the Waters Micromass Q-TOF (Waters Corp.) mass spectrometer using the same parameters described in Chapter 2. The results presented represents the mean of 3 replicates, i.e. n=3. Individual samples were processed by warping and presented as log10 ratio of TNBS labeled MLV to untreated MLV using a Matlab (MathWorks, Natick MA, USA) based programme that was developed in-house[10]. MRM quantification of TNBS-labeled aminophospholipid was carried out using ABI 4000 Q-Trap (Applied Biosystems). For TNBS-PS, we followed the mass transition of the parent ion to precursor ion fragment 235m/z which corresponds to charged head group TNBS+serine-H_2O. For TNBS-PE or TNBS-pPE, we followed the mass transition of the parent ion to neutral loss of 254m/z which corresponds to the TNBS+ethanolamine-H_2O head group.

[10] This programme was written by Ms Chua Gek Huey.

3.4.3 Results

3.4.3.1 ESI-MS analysis of TNBS labeled aminophospholipid standards

TNBS reacts covalently with the aminophospholipids, undergoing nucleophilic aromatic substitution with the free amino group NH_2 on the phospholipid head group, resulting in the expulsion of the SO_3^{-2} group from TNBS. This reaction would generate a mass shift from the original molecule that can be detected using ESI-MS (Figure 34). To investigate this, we made DMPS, DMPE and pPE 38:4 liposomes and treated the liposomes with TNBS. This resulted in modified aminophospholipids that we shall name as TNBS-DMPS (Figure 34A), TNBS-DMPE (Figure 34B) and TNBS-pPE 38:4 (Figure 34C) respectively. It was found that the phospholipid with a serine head group, DMPS, exhibited a mass shift of 149m/z (Figure 34A). For this to occur, we predicted that PS head group and TNBS molecule probably went through double aromatic substitution. Under increased collision energy, TNBS-DMPS produced a large characteristic precursor ion fragment with 235 m/z, predicted to be the charged head group TNBS+serine-H_2O. The fragments at m/z 363, 381 and 591 represent the neutral loss of the fatty acid chain and the TNBS-labeled head group respectively. In contrast to DMPS, DMPE and pPE 38:4 lipids exhibited a mass shift of +211 m/z, corresponding to a single nucleophilic substitution (Figure 34B and C). During MS/MS analysis, neutral loss of the TNBS-labeled head groups of both DMPE and pPE 38:4 (i.e. parent ion -254m/z), produced large peaks that correspond to PA-like fragments at 591 and 707 m/z respectively. In addition, characteristic neutral losses of the fatty acid chains resulted in lysoPA-like fragments as indicated in the figures.

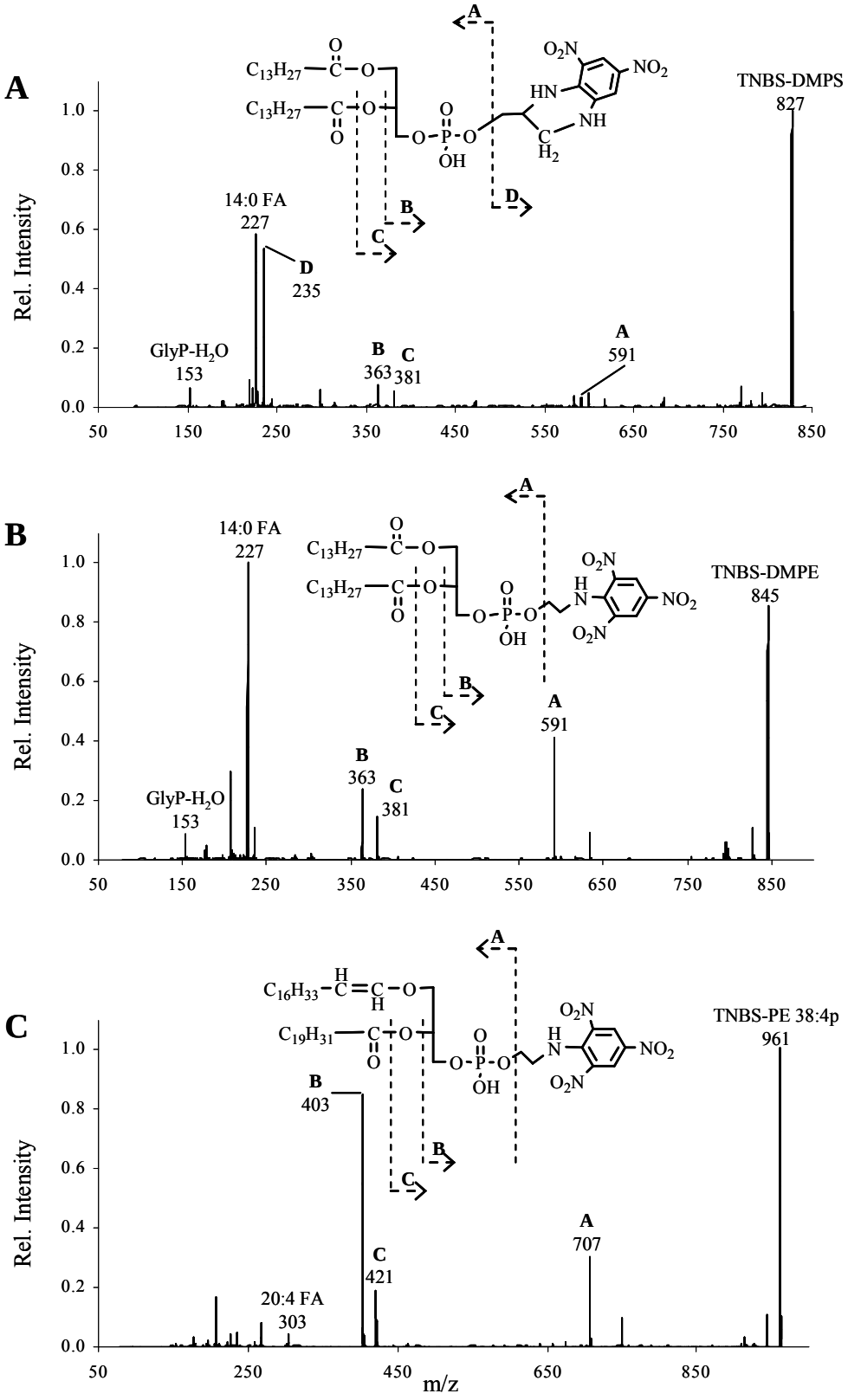

Figure 34. MS/MS of TNBS labeled phospholipids.
Proposed TNBS labeled molecular structures are presented and potential fragment daughter ions are labeled doubly in the structure and spectra. Known daughter ions such as fatty acyl (FA) and glycerphosphate – water (GlyP-H2O) are labeled in the spectra directly. Spectra are presented as relative values normalized to the highest peak in the spectra. (A) TNBS-DMPS. (B) TNBS-DMPE. (C) TNBS-PE 38:4p.

3.4.3.2 Optimization of TNBS labeling conditions

The success of these experiments would depend on the optimization of TNBS labeling conditions such that TNBS is unable to penetrate the membrane bilayer. Previous studies have suggested that the reaction temperature may be the most important factor controlling the extent of TNBS penetration (Fong et al., 1976; Fontaine and Schroeder, 1979; Williams et al., 2000). We thus investigated the loss of DMPE and gain of TNBS-DMPE after TNBS treatment on liposomes under different temperature conditions 4°C, 25°C and 37°C (Figure 35). Expectedly, higher reaction temperature resulted in increased DMPE loss and TNBS-DMPE gain. This suggests that at higher temperature, the liposome becomes more permeable to TNBS, resulting in increased labeling of both outer and inner leaflet DMPE. Because specificity is crucial in this analysis, we decided to conduct the rest of our experiments using 4°C.

Next we attempted to find the optimum concentration of TNBS based on the amount of amount of DMPE lipid molecules present (Figure 36). We had initially suspected that higher concentrations of TNBS would result in proportionally increasing loss of DMPE and gain of TNBS-DMPE. Instead, we discovered that we were unable to get a proportionate corresponding signal in DMPE after treatment while we find that the amount of TNBS-DMPS measured increased inversely compared to TNBS used. We were unable to explain why this happened except due to variance in ESI-MS signal output. Nevertheless, we decided to go with the lowest concentration of 1.0mM as that concentration seemed to give adequate labeling without causing membrane damage.

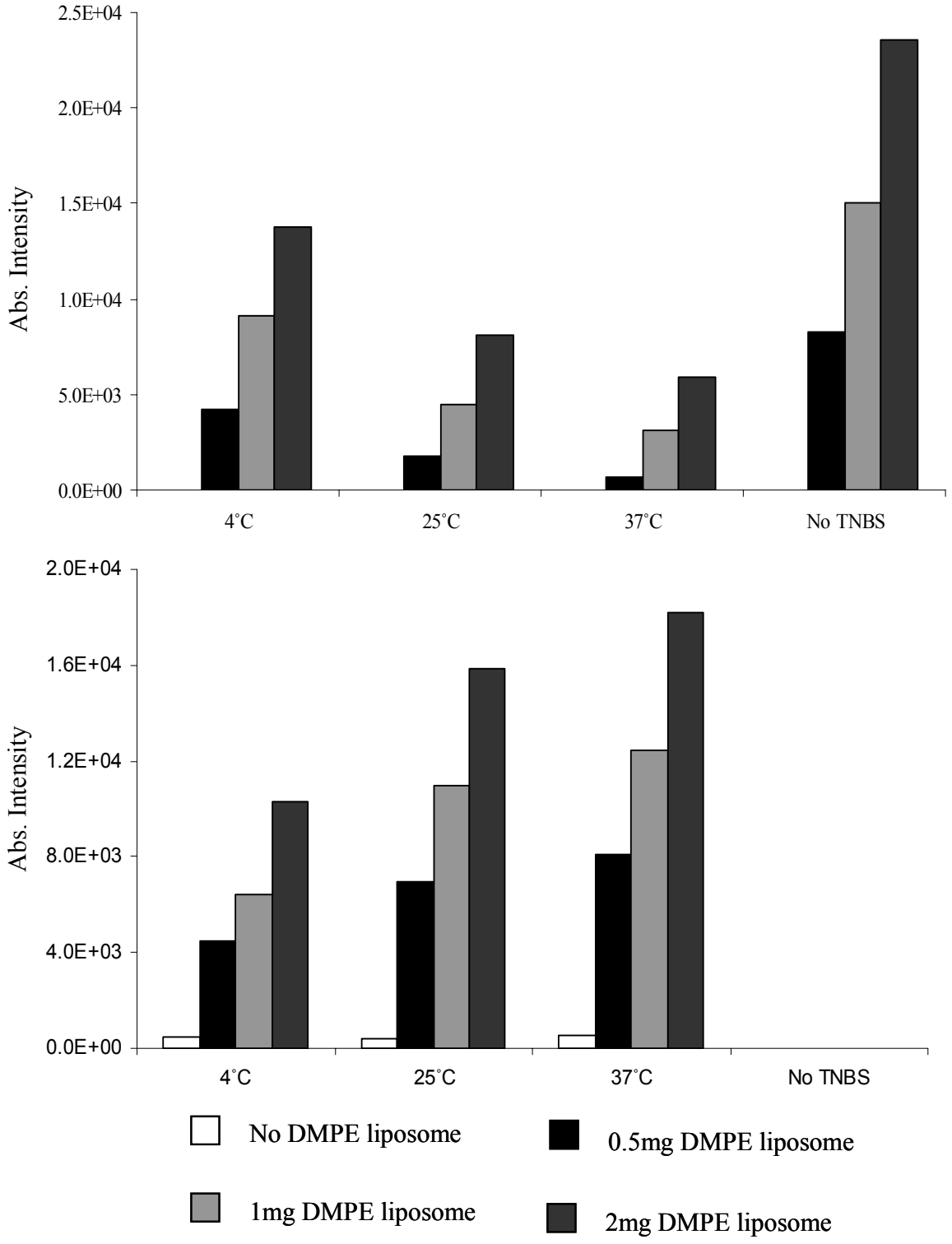

Figure 35. Effects of temperature on TNBS labeling of DMPE liposomes.
TNBS labeling of liposomes containing varying amounts of DMPE was carried out using different reaction temperatures as indicated in the x-axis. The y-axis represents the absolute signal intensity from the instrument. Top panel shows the amount of DMPE detected by MRM before and after treatment with TNBS. Bottom panel shows the corresponding signal intensity of detectable TNBS-DMPE. A single replicate was used for this initial experiment, i.e. n=1.

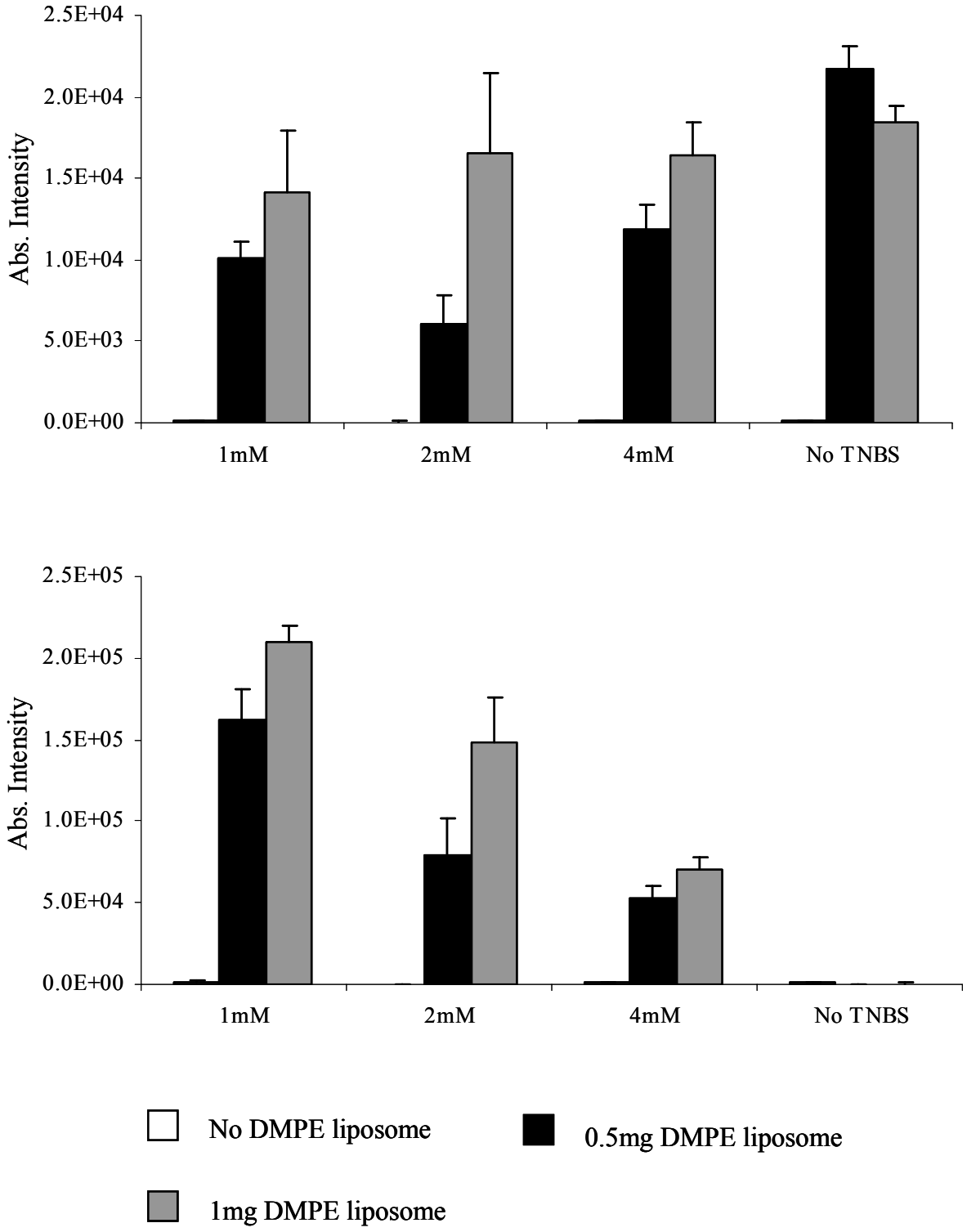

Figure 36. Effects of TNBS concentration on TNBS labeling of DMPE liposomes.
TNBS labeling of liposomes containing varying amounts of DMPE was carried out using different TNBS concentrations as indicated in the x-axis. The y-axis represents the absolute signal intensity from the instrument. Top panel shows the amount of DMPE detected by MRM before and after treatment with TNBS. Bottom panel shows the corresponding signal intensity of detectable TNBS-DMPE. The results shown represent the average of three independent replicates, n=3.

3.4.3.3 TNBS labeling of MLV particles

Freshly produced MLV particles were purified and used immediately for TNBS labeling. It was found previously that freeze thawing of VSV particles resulted in a leaky bilayer that was accessible to TNBS (Fong et al., 1976). After removal of excess TNBS and lipid extraction, the lipid samples, including mock treated samples (negative control, Figure 37A), TNBS treated MLV at 4°C (Figure 37B) and TNBS treated MLV at 37°C (positive control, Figure 37C) were subjected to ESI-MS Q-TOF analysis. Comparing the spectra of both mock treated (Figure 37A) and the 4°C TNBS labeled MLV (Figure 37B) showed that covalent modification of aminophospholipids had occurred. A slight reduction in the two most prominent PS peaks, PS 36:1 and PS 34:1, was observed along with the appearance of peaks between m/z 900 and 1000. These new peaks corresponded to the mass shift of aminophospholipids that were modified by TNBS, the most prominent of which are 937.9 (possibly TNBS-PE 36:2p and/or TNBS-PS 36:1) and 961.8 (possibly TNBS-PE 38:4p and/or TNBS-PS 38:3) (Figure 37B). At 4°C reaction temperature, TNBS cannot penetrate the MLV membrane; therefore the modified aminophospholipids must be located on the other leaflet of the MLV envelope. When temperature is increased to 37°C, TNBS is able to penetrate the MLV envelope and would label aminophospholipids on both outer and inner leaflets of the envelope. This resulted in further reduction of unlabeled PS while more TNBS labeled aminophospholipids are produced (Figure 37C).

These changes are more clearly illustrated when comparing the Log10 ratio of TNBS-MLV at 4°C (Figure 38A) and TNBS-MLV at 37°C (Figure 38B) to mock TNBS-MLV spectra. In these figures, a higher peak value in the TNBS spectra is represented in the positive y-axis while a lower peak value in the TNBS spectra is seen in negative y-axis. In this way, changes in peak intensity are based on fold changes rather than changes in absolute

abundance. One problem of identifying the new TNBS labeled lipids by mass shift alone is that there might be overlap between both classes of lipids. For instance, TNBS-PS 36:1 and TNBS-PE 36:2p both have m/z 937.9 while TNBS-PS 40:1 and TNBS-PE 40:2p both have m/z 994.0 (Table 11). It is clear that when a particular TNBS-aminophospholipid species is formed, the level of the corresponding unlabeled aminophospholipids must decrease. Thus, by identifying this reciprocal change in lipid levels, it was found that newly formed TNBS lipids in the 4°C reaction were mostly composed of TNBS-pPE (Table 11). Additionally, TNBS-PS molecules were also found to be prominent while TNBS-PE molecules were less abundant in the reaction. As a confirmation of our data, the same trend is also observed when the reaction temperature is increased to 37°C (Table 12). This indicates that pPE are mostly located on the external bilayer leaflet of the MLV envelope while PS and PE molecules are sequestered in the internal bilayer leaflet respectively.

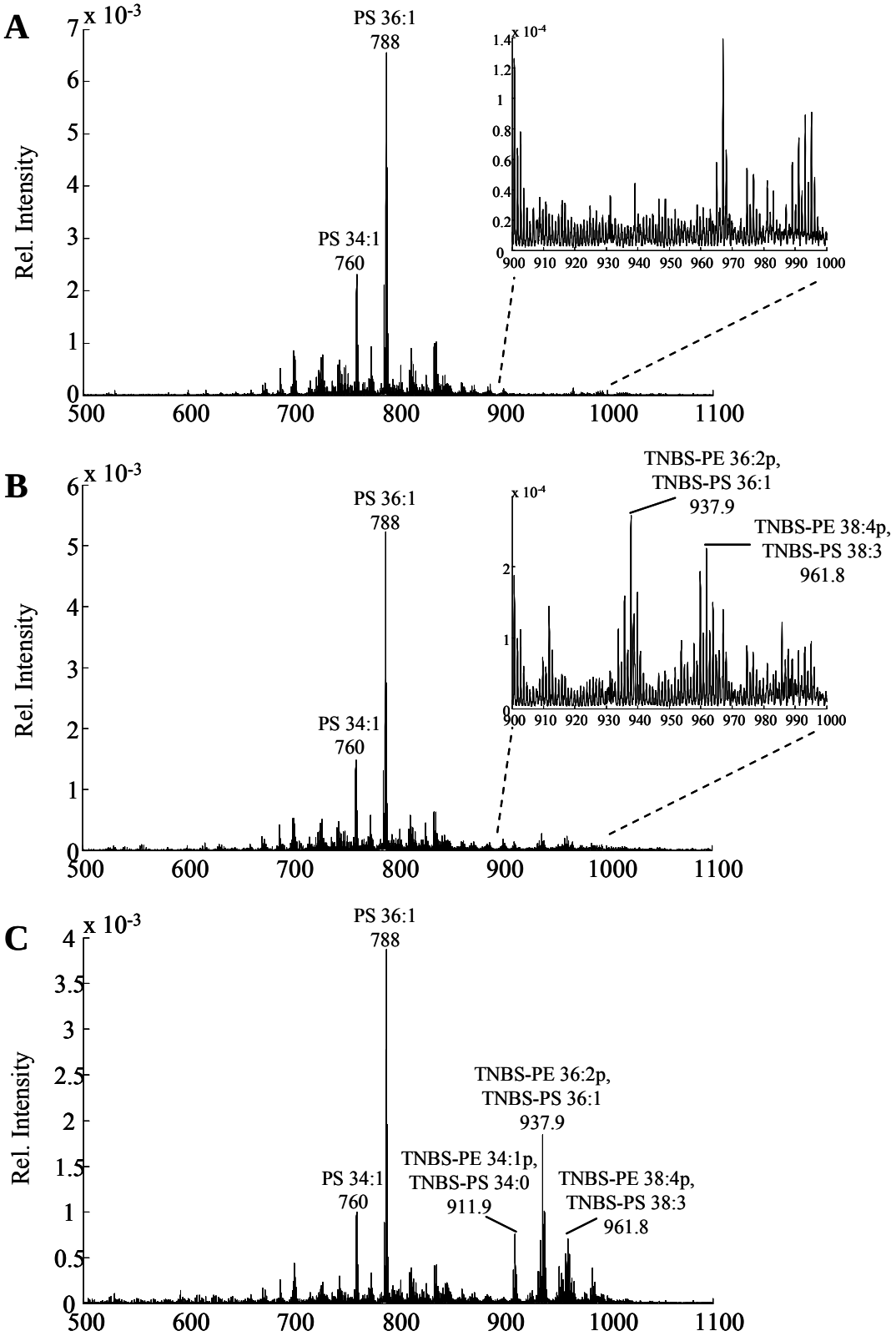

Figure 37. Qualitative lipid analysis of TNBS labeled MLV particles.
Purified MLV particles were (A) mock treated, (B) incubated with 2mM TNBS at 4°C or (C) incubated with 2mM TNBS at 37°C. These MLV particles were lipid extracted and analyzed via ESI-MS single stage scanning in negative mode. Each graph is normalized to the total signal intensity of the sample and shown as relative intensity on the y-axis and the x-axis represents the m/z range. Prominent peaks are labeled. The inserts in (A) and (B) are magnifications of the 900-1000m/z range for comparative purpose. These graphs are the average of three independent experiments, n=3.

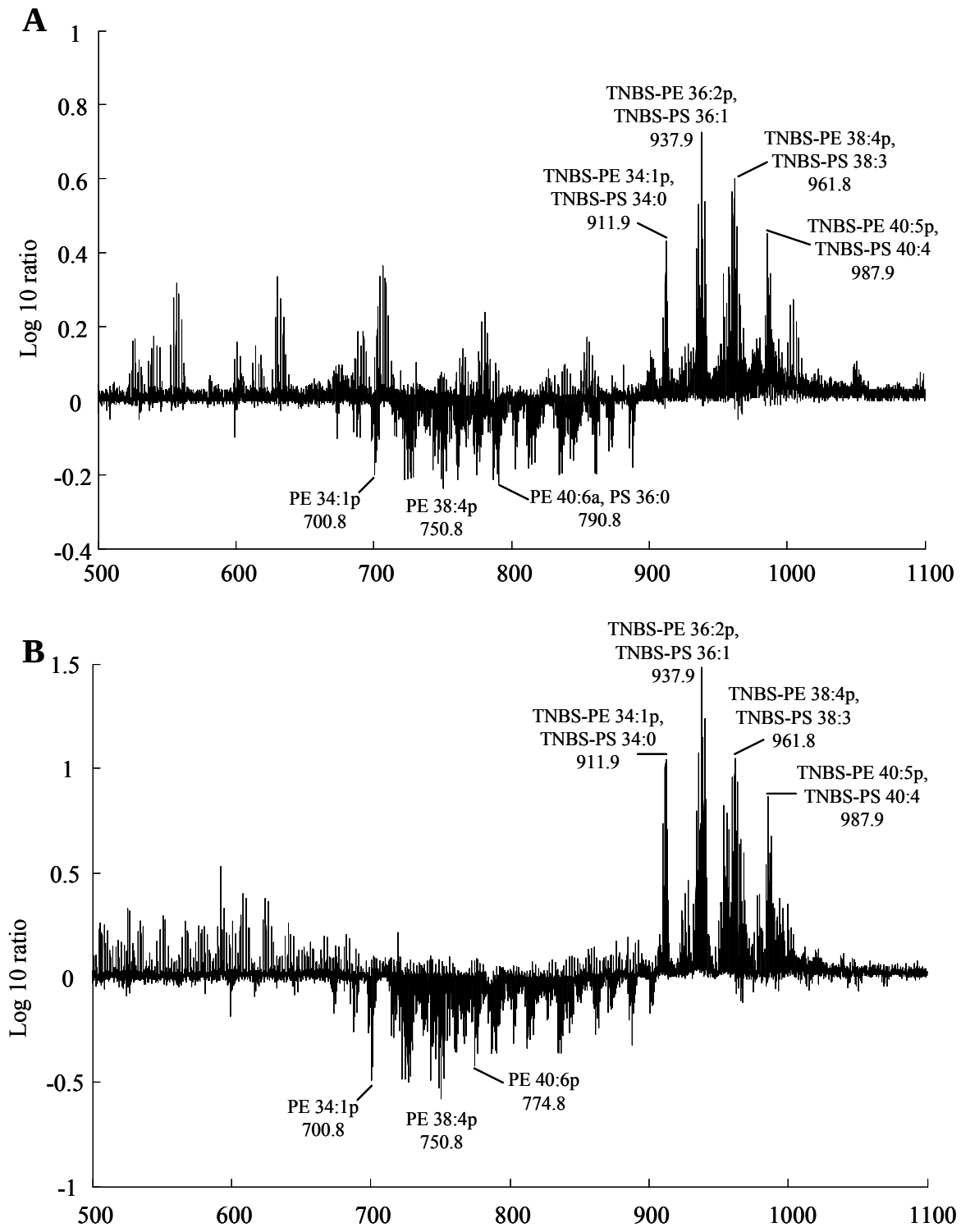

Figure 38. Changes in lipid profiles due to TNBS treatment.
The mass spectra of TNBS labeled MLV is compared to mock treated MLV and presented as log 10 ratio (y-axis) against the m/z range measured (x-axis). Positive log 10 ratio refers to an enrichment of lipids in TNBS labeled MLV while negative log 10 ratio refers to an enrichment of lipids in mock treated MLV. Log 10 ratio of MLV incubated with 2mM of TNBS at 4°C to untreated MLV particles (A). Log 10 ratio of MLV incubated with 2mM of TNBS at 37°C to untreated MLV particles (B). These graphs are the average of three independent experiments, n=3.

Up-regulated lipids				Down-regulated lipids			
m/z	**TNBS-PS**	**TNBS-PE**	**log10ratio**	**m/z**	**PS**	**PE**	**log10ratio**
937.9	TNBS-PS 36:1	TNBS-PE 36:2p	0.725	750.8		PE 38:4p	-0.238
961.8	TNBS-PS 38:3	TNBS-PE 38:4p	0.600	790.8	PS 36:0	PE 40:6a	-0.224
959.9	TNBS-PS 38:4	TNBS-PE 38:5p	0.563	722.8		PE 36:4p	-0.213
939.9	TNBS-PS 36:0	TNBS-PE 36:1p	0.539	786.8	PS 36:2	PE 40:0p	-0.213
935.9	TNBS-PS 36:2	TNBS-PE 36:3p	0.529	760.8	PS 34:1		-0.213
963.9	TNBS-PS 38:2	TNBS-PE 38:3p	0.471	748.8		PE 38:5p	-0.212
911.9	TNBS-PS 34:0	TNBS-PE 34:1p	0.432	724.7		PE 36:3p	-0.210
933.9	TNBS-PS 36:3	TNBS-PE 36:4p	0.410	726.8		PE 36:2p	-0.208
957.9	TNBS-PS 38:5	TNBS-PE 38:6p	0.361	728.7		PE 36:1p	-0.206
987.9	TNBS-PS 40:4	TNBS-PE 40:5p	0.343	700.8		PE 34:1p	-0.202
953.9		TNBS-PE 36:2a	0.342	774.8		PE 40:6p	-0.201
955.9		TNBS-PE 36:1a	0.263	834.8	PS 40:6		-0.200
965.8	TNBS-PS 38:1	TNBS-PE 38:2p	0.258	836.8	PS 40:5		-0.195
983.9	TNBS-PS 40:6	TNBS-PE 38:1a	0.228	752.8		PE 38:3p	-0.190
909.9	TNBS-PS 34:1	TNBS-PE 34:2p	0.223	742.7		PE 36:2a	-0.189
967.9	TNBS-PS 38:0	TNBS-PE 38:1p	0.195	802.8		PE 40:0a	-0.186
941.8		TNBS-PE 36:0p	0.174	812.8	PS 38:3		-0.184
979.9		TNBS-PE 38:3a	0.168	814.8	PS 38:2		-0.172
993.8	TNBS-PS 40:1	TNBS-PE 40:2p	0.167	746.7		PE 38:6p	-0.171
977.8		TNBS-PE 38:4a	0.167	816.8	PS 38:1		-0.167
927.8		TNBS-PE 34:1a	0.154	776.8		PE 40:5p	-0.165
951.9		TNBS-PE 36:3a	0.153	844.9	PS 40:1		-0.162
690.6		PE 32:0a	0.149	744.8		PE 36:1a	-0.148
925.9		TNBS-PE 34:2a	0.145	772.8		PE 38:1a	-0.144
931.8	TNBS-PS 36:4	TNBS-PE 36:5p	0.144	788.7	PS 36:1		-0.130
991.9	TNBS-PS 40:2	TNBS-PE 40:3p	0.132	766.8		PE 38:4a	-0.127
995.8	TNBS-PS 40:0	TNBS-PE 40:1p	0.129	762.8	PS 34:0	PE 38:6a	-0.121
975.6		TNBS-PE 38:5a	0.125	810.8	PS 38:4		-0.121
949.8		TNBS-PE 36:4a	0.122	846.9	PS 40:0		-0.114
901.7		TNBS-PE 32:0a	0.116	754.8		PE 38:2p	-0.113
969.9		TNBS-PE 38:0p	0.114	698.7		PE 34:2p	-0.109
973.8		TNBS-PE 38:6a	0.099	843.8	PS 40:2		-0.104
1003.9		TNBS-PE 40:5a	0.094	730.8		PE 36:0p	-0.103
981.9		TNBS-PE 38:2a	0.094	756.8		PE 38:1p	-0.103
1001.9		TNBS-PE 40:6a	0.093	768.8		PE 38:3a	-0.103
719.4		TNBS-PE 20:0a	0.081	838.8	PS 40:4		-0.098

Table 11. List of up- and down-regulated aminophospholipids in TNBS labeled MLV at 4˚C.
The list species shown here are obtained from the log 10 ratio of mass spectra of TNBS labeled MLV at 4˚C compared to mock treated MLV, where n=3 (refer to Figure 34). Newly formed TNBS aminophospholipids are arranged in descending values of log 10 ratios, which is indicative of their relative abundance in TNBS labeled MLV compared to mock treated MLV. Unlabeled aminophospholipids are arranged in ascending values of negative log 10 ratios, which is indicative of the amount of unlabeled aminophospholipids remaining in TNBS labeled MLV compared to mock treated MLV.

Up-regulated lipids				Down-regulated lipids			
m/z	**TNBS-PS**	**TNBS-PE**	**log10ratio**	**m/z**	**PS**	**PE**	**log10ratio**
937.9	TNBS-PS 36:1	TNBS-PE 36:2p	1.484	750.8		PE 38:4p	-0.578
939.9	TNBS-PS 36:0	TNBS-PE 36:1p	1.239	748.8		PE 38:5p	-0.528
935.9	TNBS-PS 36:2	TNBS-PE 36:3p	1.077	726.8		PE 36:2p	-0.501
961.7	TNBS-PS 38:3	TNBS-PE 38:4p	1.047	700.7		PE 34:1p	-0.493
911.9	TNBS-PS 34:0	TNBS-PE 34:1p	1.044	742.8		PE 36:2a	-0.492
959.9	TNBS-PS 38:4	TNBS-PE 38:5p	0.960	724.7		PE 36:3p	-0.489
963.8	TNBS-PS 38:2	TNBS-PE 38:3p	0.934	722.7		PE 36:4p	-0.488
953.9		TNBS-PE 36:2a	0.826	752.8		PE 38:3p	-0.480
933.9	TNBS-PS 36:3	TNBS-PE 36:4p	0.798	728.8		PE 36:1p	-0.472
955.9		TNBS-PE 36:1a	0.787	774.8		PE 40:6p	-0.423
909.9	TNBS-PS 34:1	TNBS-PE 34:2p	0.737	746.8		PE 38:6p	-0.388
957.7	TNBS-PS 38:5	TNBS-PE 38:6p	0.708	790.8	PS 36:0	PE 40:6a	-0.363
987.9	TNBS-PS 40:4	TNBS-PE 40:5p	0.676	786.8	PS 36:2	PE 40:0p	-0.362
965.9	TNBS-PS 38:1	TNBS-PE 38:2p	0.660	836.8	PS 40:5		-0.362
968.0	TNBS-PS 38:0	TNBS-PE 38:1p	0.596	776.8		PE 40:5p	-0.360
983.9	TNBS-PS 40:6	TNBS-PE 38:1a	0.539	834.8	PS 40:6		-0.360
941.8		TNBS-PE 36:0p	0.474	760.8	PS 34:1		-0.358
927.9		TNBS-PE 34:1a	0.466	812.8	PS 38:3		-0.337
925.9		TNBS-PE 34:2a	0.400	744.8		PE 36:1a	-0.328
979.7		TNBS-PE 38:3a	0.396	766.8		PE 38:4a	-0.314
977.8		TNBS-PE 38:4a	0.394	802.8		PE 40:0a	-0.313
994.0	TNBS-PS 40:1	TNBS-PE 40:2p	0.377	754.8		PE 38:2p	-0.299
913.8		TNBS-PE 34:0p	0.370	814.8	PS 38:2		-0.298
951.9		TNBS-PE 36:3a	0.359	716.8		PE 34:1a	-0.285
931.9	TNBS-PS 36:4	TNBS-PE 36:5p	0.348	714.7		PE 34:2a	-0.279
990.0	TNBS-PS 40:3	TNBS-PE 40:4p	0.334	768.8		PE 38:3a	-0.277
996.0	TNBS-PS 40:0	TNBS-PE 40:1p	0.330	756.8		PE 38:1p	-0.277
992.0	TNBS-PS 40:2	TNBS-PE 40:3p	0.289	816.8	PS 38:1		-0.272
949.9		TNBS-PE 36:4a	0.271	762.8	PS 34:0	PE 38:6a	-0.270
970.0		TNBS-PE 38:0p	0.250	698.7		PE 34:2p	-0.266
1001.9		TNBS-PE 40:6a	0.238	842.9	PS 40:2		-0.263
548.7	PS 20:2		0.231	740.8		PE 36:3a	-0.260
981.9		TNBS-PE 38:2a	0.222	788.8	PS 36:1		-0.257
719.4		TNBS-PE 20:0a	0.214	738.8		PE 36:4a	-0.251
975.8		TNBS-PE 38:5a	0.213	792.8		PE 40:5a	-0.222
907.7	TNBS-PS 34:2		0.207	844.9	PS 40:1		-0.220

Table 12. List of up- and down-regulated aminophospholipids in TNBS labeled MLV at 37˚C.
The list species shown here are obtained from the log 10 ratio of mass spectra of TNBS labeled MLV at 37˚C compared to mock treated MLV, where n=3 (refer to Figure 34). Newly formed TNBS aminophospholipids are arranged in descending values of log 10 ratios, which is indicative of their relative abundance in TNBS labeled MLV compared to mock treated MLV. Unlabeled aminophospholipids are arranged in ascending values of negative log 10 ratios, which is indicative of the amount of unlabeled aminophospholipids remaining in TNBS labeled MLV compared to mock treated MLV.

Chapter 4 – Discussion

4.1 Detailed lipidomics analysis of retroviruses

With this work, we present an extensive analysis of the lipidome of HIV produced from both T cells and monocyte-derived-macrophages (MDM) along with corresponding lipid contents of the plasma membrane from which the virus buds. Additionally, we analyzed the oncoretrovirus MLV to provide a more unbiased assessment of retroviral envelopes. This study greatly expands the coverage of lipid classes previously analyzed in HIV envelopes (Aloia et al., 1993; Brugger et al., 2006), including the bioactive phospholipids PIP and PIP_2, sphingolipids GM3 and neutral lipids CE, DG and TG. Moreover, to avoid biased interpretation based on cell specific differences, we produced retroviruses from different cell types for analysis. We report that retroviruses HIV and MLV share a similar lipid composition despite being produced from different cell types (Table 4).

Importantly, when retroviral lipids were compared to plasma membrane (Table 6B), it is clear that the lipid profile of retroviruses largely resembled that of plasma membrane. We demonstrated that we were able to recapitulate the results of Brugger et al. when total cell membrane was used as a reference for retroviral lipids (Table 5B). However, total cell membrane includes lipids from organelles and other membrane structures that are unlikely to support retroviral budding. In contrast, the comparison between viral envelopes and plasma membranes is more biologically relevant given the current data that support HIV budding from the plasma membrane (Booth et al., 2006; Deneka et al., 2007; Finzi et al., 2007; Jouvenet et al., 2006; Welsch et al., 2007).

4.1.1 Procedure for preparing pure retrovirus particles

The purification of MLV from cell culture supernatant was carried out with relative ease using standard methods. This involved initial filtration of the infected culture supernatant, followed by centrifugation through a 15% sucrose cushion (Figure 9A). This resulted in highly purified MLV preparations that were ready for lipid analysis (Figure 10A). The purification of HIV particles required an additional step to remove contaminating microvesicles by anti-CD45 immunodepletion (Esser et al., 2001; Trubey et al., 2003). Mircrovesicles have been shown to be a contaminating fraction when attempting to purify HIV particles from T cells and MDM (Bess, Jr. et al., 1997; Gluschankof et al., 1997). The role of this vesiculation in normal cell function is undefined but may involve the elimination of excess membrane or membrane associated proteins, or a novel mechanism of antigen presentation, or a process for membrane repair (Miyake and McNeil, 1995). Additionally, the release of exosomes may present another source of contamination in our preparation of HIV virions. Exosomes are known to form through budding into multivesicular bodies (MVBs) in immunological cells such as T-cells, B-Cells and mast cells, and are released from the cell by the fusion of the MVBs with the plasma membrane of the cells (Subra et al., 2007). While their function is controversial, they are believed to serve as intercellular communication vehicles that assist immune responses (Subra et al., 2007). Without further biochemical analysis, we are unable to determine the exact identities of vesicles present in the HIV preparation (Figure 10B). Nevertheless, there is convincing evidence that both microvesicles and exosomes are enriched in CD45 antigens while HIV specifically exclude CD45 from their envelope (Coren et al., 2008; Esser et al., 2001; Trubey et al., 2003; Wubbolts et al., 2003). Therefore, both contaminating vesicles can be removed from our HIV preparation by anti-CD45 immunodepletion (Figure 10B).

4.1.2 Considerations for preparing plasma membrane fractions

The plasma membrane preparations are crucially important as references used for comparison with retroviral lipids. We isolated plasma membrane from cells by using cationic silica beads that adhered electrostatically to negatively charged plasma membrane surface (Harila et al., 2006; Mason and Jacobson, 1985; Stolz and Jacobson, 1992). One major concern is the contamination of the plasma membrane preparations with lipids from cellular organelles which have different lipid compositions (van Meer, 2005). We ensured plasma membrane purity by testing for the presence of plasma membrane markers such as transferrin receptor (TrF) and the exclusion of cytoplasmic and endosomal markers such as actin and Rab5 (Figure 13A). In addition to purity, we were also concern that cationic silica interaction with the plasma membrane surface may artificially induce surface artifacts such as lipid rafts (Figure 13A and C). We monitored the conditions used for cationic silica binding to eliminate this possibility, finally using a low bead concentration for purification (Figure 13A and B). Our methodology was reaffirmed by purifying plasma membrane using an alternate method, continuous Optiprep gradient centrifugation, which produced similar mass spectra profile in the fraction believed to contain plasma membrane (Figure 14).

4.2 Differences between retrovirus and plasma membrane lipids

Despite the similarity between plasma membrane and viral envelopes, retroviral lipids were still distinct from plasma membrane, specifically showing enriched levels of phosphoinositides (PIP and PIP_2) and raft lipids like cholesterol, Cer (except HIV produced from H9 cells) and GM3. These data suggest that these lipid classes are specifically enriched

in the retrovirus envelope and therefore must play a role at some stage of the retrovirus replication process. We carried out additional experiments to address the possible functions of these enrichment and our observations are discussed below.

4.3 Retrovirus envelopes are enriched in phosphoinositides

The first distinction drawn from our lipid comparison is that retroviruses lack PI while PIP and PIP_2 are highly enriched compared to plasma membrane levels. We note that it is possible that cellular phosphatase activity may have reduced the native levels of PIP_2 in the plasma membrane samples during isolation and resulted in a corresponding increase in PI levels. Nevertheless, the key feature that distinguishes retroviruses and microvesicles is the level of phosphoinositides, particularly PIP_2. Microvesicles would likely reflect the PIP_2 levels in the native plasma membrane, thereby providing indirect proof of PIP_2 enrichment in retrovirus envelopes. Unfortunately, it is not possible to discriminate stereoisomers of PIPn by mass spectrometry, but we expect that the virus associated PIP_2 to consist mainly of $PI(4,5)P_2$ since this is the major PIP_2 isomer found at the plasma membrane in resting mammalian cells (Rusten and Stenmark, 2006).

4.3.1 Gag MA basic domain is the source of PIP_2 enrichment

During the late phase of HIV-1 replication, newly synthesized retroviral Gag precursor proteins are targeted to the plasma membrane where they colocalize at lipid rafts and assemble into immature virions. Before the start of this study, it had been known for some time that the membrane targeting and binding capacity of the HIV-1 Gag involve: 1) a MA domain N-terminal myristate which partitions stably into the plasma membrane bilayer

hydrocarbon environment (Schultz et al., 1988), 2) a cluster of basic residues in the MA domain that becomes exposed as a positively charged surface patch in native Gag structures, which is proposed to interact electrostatically with acidic phospholipid headgroups (Yuan et al., 1993; Zhou et al., 1994) , and 3) oligomerization of Gag that may increase membrane partitioning of Gag by producing a larger composite basic surface which favour the exposure of the myristate (Zhou and Resh, 1996). In this scenario, what is the plasma membrane component that directs the membrane binding of HIV-1 Gag oligomers?

The strong enrichment of multivalent acidic lipids PIP and PIP_2 in retrovirus envelopes (Table 6B) suggests that phosphoinositides are the plasma membrane components involved in the targeting of Gag, through electrostatic interaction with the MA domain. We investigated the cause of this enrichment by comparing the phosphoinositide profile of virus like particles (VLP) made from wild type HIV-Gag and ΔMA HIV-Gag (Table 8A). These data determined that the presence of polybasic residues found in MA domain is indeed responsible for the enrichment of PIP_2 found in the final envelope composition in wild type VLP. This conclusion is further strengthened by the observation that the wild type VLP bears similar phosphoinositide profiles as HIV particles while the mutant ΔMA VLP matches that of plasma membrane and microvesicles (Table 8B and C). Since the basic MA domain is conserved amongst all known retrovirus Gag (Murray et al., 2005; Riffel et al., 2002), it would be safe to assume that other retroviruses, as it was shown with MLV (Table 4), would also be enriched in phosphoinositide in their membrane envelope.

4.3.2 Phosphoinositides target Gag to the plasma membrane

From a functional perspective, the presence of $PI(4,5)P_2$ is clearly important for the efficient assembly and budding of a retrovirus. We proved this by showing that the depletion

of $PI(4,5)P_2$ by overexpression of 5PaseIV activity in HEK293 cells results in a decrease in HIV and MLV release (Figure 24). Our findings are consistent with the idea that $PI(4,5)P_2$ acts in the targeting of the HIV-1 Gag protein, via an interaction with the MA domain of Gag, to the plasma membrane (Ono et al., 2004). In that study, Ono et al. showed that when $PI(4,5)P_2$ was similarly depleted in HeLa cells, Gag localization was directed away from the plasma membrane to the late endosomes (Ono et al., 2004). In this manner, the retrovirus Gag targeting mechanism appears to have copied the way proteins with polybasic clusters are targeted through $PI(3,4,5)P_3$ and $PI(4,5,)P_2$ to the plasma membrane. (Heo et al., 2006).

A complementary insight to our data is provided by recent structural analysis of HIV-1 Gag and its interaction with $PI(4,5)P_2$ (Saad et al., 2006). The electrostatic interaction between the positively charged pocket of Gag MA domain and negatively charged head group of $PI(4,5)P_2$ results in the exposure of the Gag myristic acid into the budding membrane and the equivalent flipping out of the polyunsaturated 2'-fatty acid of $PI(4,5)P_2$ resulting in the formation of an extended lipid conformation. From a free energy standpoint, electrostatic interaction (ΔG ~-9/-8 kcal/mol depending on whether Gag exists as trimer or dimer) and hydrophobic interaction of the myristate (ΔG ~-12 kcal/mol) contribute a total membrane binding free energy of ΔG ~-21 kcal/mol (Murray et al., 2005). When the loss of $PI(4,5)P_2$ at the plasma membrane occurs, membrane binding free energy is decreased by almost half, thus leading to poorer association of Gag with the plasma membrane.

4.3.3 Considerations for future experiments on phosphoinositide functions in retrovirus replication

An important point to note is that the current set of data do not provide a clear picture regarding the cellular source of $PI(4,5)P_2$. Are PIP kinases activated during virus infection to

up-regulate the levels of $PI(4,5)P_2$ in the plasma membrane? Such a mechanism would increase plasma membrane concentration of $PI(4,5)P_2$ and its net negative charge, thereby increasing electrostatic attraction between Gag and the plasma membrane. Alternatively, we can look to current theories of how $PI(4,5)P_2$ is spatially regulated in the plasma membrane to provide some clues. It is believed that there are two separate pool of $PI(4,5)P_2$ in the plasma membrane (Gambhir et al., 2004). About two-thirds is believed to be electrostatically sequestered by protein buffers with clusters of basic residue such as myristylated alanine-rich C Kinase substrate (MARCKS), only to be released in response to specific stimuli such as an increase in local calcium ion concentration. The remainder of $PI(4,5)P_2$ is unbound and free to diffuse in the plasma membrane milieu. If this free pool of $PI(4,5)P_2$ is not enough to support retrovirus assembly and budding, can retrovirus replication manipulate the host cell to release the sequestered pool of $PI(4,5)P_2$? Such a mechanism would appear to "beneficial" for the host cell since it does not require the activation of PIP kinases for the production of extraneous $PI(4,5)P_2$ and would therefore use less energy.

Besides initiating retrovirus assembly through Gag, further roles for $PI(4,5)P_2$ remain a distinct possibility. Intriguingly, $PI(4,5)P_2$ is intimately involved in the inward and outward bending of plasma membrane in other biological systems. During endocytosis, BAR domain proteins bind to $PI(4,5)P_2$ rich membranes to form inward invaginations (Itoh and De Camilli, 2006; Zimmerberg and Kozlov, 2006). Conversely, during the formation of filopodia, MIM and IRSp53, proteins which contain BAR-like domains, can lead to the formation of outward bending of $PI(4,5)P_2$ rich membranes (Mattila et al., 2007). Considering the strong enrichment of PIP_2 lipids in the viral envelope, we hypothesize that binding of retroviral Gag proteins to $PI(4,5)P_2$ may contribute to the induction of membrane curvature during virus assembly and budding.

4.4 Raft lipids cholesterol, ceramide and GM3 are enriched in retrovirus envelopes

In addition to phosphoinositides, retrovirus envelopes are highly enriched in raft lipids like cholesterol, Cer (except HIV produced from H9 cells) and GM3. The enrichment of cholesterol and GM3 comes without surprise because it has been well established that HIV bud selectively from cholesterol (Ono et al., 2007) and glycolipid (Nguyen and Hildreth, 2000) enriched membrane rafts. Moreover, HIV has been shown to specifically control the enrichment of both these lipids through its accessory Nef protein (Mujawar et al., 2006; Zheng et al., 2001). However, the enrichment of Cer rather than SM or dhSM (as previously reported by Brugger et al.) signifies a fundamental difference in the type of lipid raft that forms during retroviral assembly.

4.4.1 Possible functions of ceramide in retrovirus replication

Cer molecules can dramatically change the biophysical properties of rafts. *In vivo*, the accumulation of Cer at the plasma membrane occurs as a result of activation and surface translocation of acid sphingomyelinase (SMase) (Grassme et al., 2001). Not only is Cer a strong promoter of lipid raft formation, Cer-rich rafts appear to spontaneously coalesce to form larger macrodomains or platforms through fusion (Bollinger et al., 2005). Cer further exerts its effects by selectively displacing cholesterol in the rafts and interfering with the association of cholesterol binding/interacting proteins with these platforms (Megha and London, 2004; Yu et al., 2005). Thus, Cer-enriched membrane platforms appear to function as a tool that re-organizes receptor and signaling molecules in and at the cell membrane to facilitate and amplify signaling processes.

It was recently demonstrated that Cer-enriched exosomes bud into multivesicular bodies, triggered by localized accumulation of Cer through sphingomyelinase action (Trajkovic et al., 2008). Earlier works also show that Cer plays a strong role in membrane destabilization and fusion in model membrane systems (Veiga et al., 1999). Both reports are consistent with the enrichment of Cer shown in our own data for both microvesicles and retroviruses if the budding mechanisms follow similar principles. However, it appears that the level of Cer has to be carefully regulated in order to ensure continued re-infection. Interestingly, increasing Cer levels in cells by pharmacological or enzymatic means inhibits HIV infectivity (Finnegan et al., 2004), supposedly by inducing CD4 clustering and preventing sequential co-receptor engagement and viral entry (Finnegan et al., 2007). It is intriguing to consider how the supposed formation of Cer-enriched macrodomains would fit into a dynamic model for the formation of microvesicles and retrovirus particles yet remain within the range to support infection.

An association with tetraspanins represents another parallel phenomenon seen between retroviruses, microvesicles and/or exosomes. For exosomes, the enrichment of tetraspanins, including CD37, CD 63, CD81, CD82 and CD86, has been well established (Escola et al., 1998; Wubbolts et al., 2003). Likewise, it was shown that HIV Gag and Env co-localizes with distinct tetraspanin enriched microdomains (TEM) containing CD9, CD53, CD63, CD81 and CD82 during particle assembly at the plasma membrane (Deneka et al., 2007; Jolly and Sattentau, 2007; Nydegger et al., 2006). At the same time, components of the cellular budding machinery including TSG101and VSP28 are also recruited to TEM to facilitate viral budding (Morita and Sundquist, 2004; Nydegger et al., 2006). In this context, it is possible that the precise regulation of plasma membrane cholesterol and Cer level helps control the dimensions of TEM structures, so as to accommodate all these membrane associated protein structures during the retrovirus assembly and budding process.

4.4.2 Functions of GM3 and other glycosphingolipids in retrovirus replication

Glycosphingolipids (GSLs), including GluCer and GM3, have been widely studied for their role in HIV entry, either as an alternative receptor (Fantini et al., 1993; Harouse et al., 1989) or by regulating viral receptor clustering (Hug et al., 2000; Puri et al., 2004; Rawat et al., 2004a; Rawat et al., 2006; Viard et al., 2004). Most of these studies usually involve loss of function experiments using antibodies against GSLs or pharmacological inhibitors of GSL biosynthesis like phenyl-2-hexadecanoylamino-3-morpholino-1-propanol (PPMP) and Fumonisin B1. PPMP, a cationic ceramide analogue, is a direct inhibitor of glucosyltransferase (Abe et al., 1992). While these experiments show that loss of GSLs is inhibitory to effective HIV infection, they fail to adequately address the effects of changes in overall lipid homeostasis and cell physiology, including cell growth, DNA replication and membrane organization (Barbour et al., 1992; Burger et al., 2007; Glaros et al., 2005; Kovacs et al., 2000; Makino et al., 2006). These associated phenomena suggest that the loss of GSLs alone cannot be exclusively responsible for defects in HIV infection.

4.4.2.1 MLV-PPMP virions exhibit different lipid profile and morphology compared to MLV-REF virions

We analyzed the lipids of mutant MLV-PPMP and wild type MLV-REF particles and found that their overall lipid composition was significantly different from each other (Table 9 and Figure 28). While MLV-PPMP showed the expected decrease in GM3 and MHCer levels, it was Cer, and not SM, that was up-regulated. The overall phospholipids composition (except phosphoinositides) appeared to remain constant between both conditions, but closer examination showed that MLV-PPMP was enriched in long chained (C>36) and poly-

unsaturated species of PC, ePC, PE and pPE while being depleted in short chained and saturated species of the same classes of lipids. In contrast, PI and PIP were highly up-regulated while PIP_2 was down-regulated in MLV-PPMP. Because the lipid composition of MLV-PPMP envelopes is distinctly different from MLV-REF envelopes, it is expected that the MLV-PPMP membrane morphology would be different compared to wild type virions. This was shown to be the case when we compared the structure of MLV-PPMP to MLV-REF via electron microscopy (Figure 29), revealing membrane defects reminiscent of Chol depleted HIV particles (Graham et al., 2003).

4.4.2.2 MLV-PPMP is weaker in infectivity compared to MLV-REF

We compared the infectivity of MLV-PPMP against MLV-REF particles (Figure 26A), and found that the mutant virus exhibited a much lowered infectivity (Figure 30B). One of the caveats in using purified virus particles for the above experiment is that we do not have a way of quantifying the true infectivity of the virus stock, which may have been diminished unequally during the purification process. However, one has to assume that since both virus conditions were processed in the same way, such handling errors would be negligible.

Based on the experimental design, reduced infectivity can be potentially attributed to defects in primary virus attachment and/or viral fusion. The first possibility is suggested by the loss of GM3 and other glycolipids from the surface of the virus envelope (Figure 28 and 30A). Due to their large head group moiety, GSLs are highly immunogenic (Misasi et al., 1993; Misasi et al., 2000) and have been shown to be an effective ligand for tethering viruses to the surface of its target host cell (Campanero-Rhodes et al., 2007b; Ferreira et al., 2004; Ugolini et al., 1999). In the case of HIV, this interaction would seem to complement the weak

binding affinity between HIV associated Env glycoprotein gp120 and its entry receptor CD4 (Ugolini et al., 1999). Like HIV, the binding affinity of MLV Env glycoprotein to its mCAT-1 receptor is considered weak at K_d 55nM (Davey et al., 1997). If membrane associated GSLs are indeed involved in virus attachment, the mutant MLV-PPMP particle would be less able to attach itself to the cell surface, thus lowering infectivity. Additionally, based on evidence that MLV Env is co-localized to lipid rafts (Beer et al., 2005), MLV Env targeting to the budding site may be defective since raft lipid metabolism is affected due to PPMP treatment. This may result in lower copies of the fusion Env glycoprotein in the MLV-PPMP envelope, thus effectively lowering the potential of MLV-PPMP attaching to a host cell. The second possibility for reduced infectivity is due to a defective virus-cell fusion step. The drastic changes seen in the envelope of PPMP-MLV viruses may result in altered membrane architecture (Figure 29) that may not be optimized for the proper functioning of the MLV Env glycoprotein or membrane fusion kinetics (McMahon and Gallop, 2005; Stiasny and Heinz, 2004).

4.4.2.3 PPMP treatment alters cellular lipid metabolism and physiology

In addition, we examined the effects of PPMP treatment on the overall lipid metabolism of REF cells. We discovered that PPMP treatment resulted not only in depletion of GSLs but also striking changes in the overall lipid composition of total cellular membrane in REF cells (Table 10 and Figure 31). As expected, the lipids upstream of GSLs were changed, whereby Cer levels decreased and SM level increased. Interestingly, the level of GluCer was up-regulated with increasing concentration of PPMP, suggesting that the cells may have compensatory mechanisms to cope with the inhibition of glucosyltransferase, as is the case with GM3 synthase knockout fibroblast cells (Shevchuk et al., 2007). The

phospholipid composition of treated cell also showed prominent changes in composition, with increasing levels of PC and ePC and decreasing levels of PE, pPE , PS and PI (Table 10). Intriguingly, level long chained (C>34) and poly-unsaturated lipids appear to be specifically up-regulated in PC, ePC and PS while the same were down regulated in PE and pPE (Figure 31). Docosahexanoate (C22:6) containing species of PE and PC have been shown to influence the overall lipid content and physical properties of plasma membrane in murine leukemia cells (Williams et al., 1998; Williams et al., 1999). Moreover, it has been shown that while PC 18:0/22:6 is highly cytotoxic, PE 18:0/22:6 is not (Zerouga et al., 1996). Taken together with the observation of increasing cell granularity (Figure 32A), it is clear that these lipid changes are associated with defects in normal cellular function in PPMP treated cells.

4.4.2.4 PPMP treated REF cells become susceptible to MLV infection

We investigated the inhibitory effects of PPMP treatment at the cellular level (Figure 26B). Unexpectedly, PPMP conditioned REF cells showed increased infectivity by MLV (Figure 33, gray bars). Temporally, this enhancement by PPMP treatment is likely to occur at a step after initial virus entry since cell newly treated with PPMP after initial exposure to MLV showed similar enhancements to conditioned cells (Figure 33, white bars). Additionally, we observe that infectivity is returned to normal by culturing the cells in culture media without PPMP (Figure 33, black bars), thus confirming the positive effects of PPMP treatment on MLV infection of REF cells. This result is intriguing because we had already shown that PPMP treated cells exhibit altered overall lipid metabolism (Table 13 and Figure 33) and cellular physiology (Figure 38A). It appears that this new cellular state enhances MLV infectivity.

A number of possible scenarios could have resulted in the higher infectivity observed. Firstly, the number of virus particle produced per cell may have increased, thereby compensating for the reduction of infectivity in the mutant virus. This is less likely given that an increase in MLV-PPMP production would add significant stress to the host cell metabolic system that is already under siege by the effects of the PPMP treatment. Moreover, the reduction of PIP_2 coupled with enrichment of PI and PIP in the MLV-PPMP envelope (Figure 29), suggests that the budding mechanism of MLV-PPMP may not be functioning optimally.

A second possibility is that with the changes in lipid metabolism, membrane organization, trafficking and signaling associated with PPMP treated cells, cells may become more susceptible to cell-to-cell transmission of MLV infection. Cell-to-cell transmission of HIV appear to be an efficient mode of productive infection *in vivo* and *in vitro*, requiring transient adhesive contact between infected and uninfected host cells (Groot et al., 2008; Ruggiero et al., 2008). In such a scenario, the viability of the MLV particle may not play such an important role in propagating infection. While the exact mechanism involved in increasing infection remains to be determined, these results highlight the possible danger of using inhibitor compounds such as PPMP as a clinical treatment against HIV infection.

4.5 Aminophospholipid composition of retroviruses

Aminophospholipids including PS, PE and pPE make up 28.1-39% of the total lipid composition in retrovirus envelopes (Table 4). While these lipids are not enriched when compared to plasma membrane levels (Table 6B), they make up a large percentage of the retroviral envelope and therefore may be functionally relevant in the retrovirus replication cycle, particularly as a mediator of membrane curvature (McMahon and Gallop, 2005; Zimmerberg and Kozlov, 2006) and PS as a cofactor for retrovirus entry (Callahan et al.,

2003; Coil and Miller, 2005a; Coil and Miller, 2005b). Ultimately, their function would depend on their distribution between the bilayer leaflets of the retrovirus envelope.

4.5.1 Analyzing aminophophoslipid asymmetry using TNBS

We attempted to map the asymmetry of aminophospholipids by making use of TNBS which is able to react covalently with free amino groups on the head group of PS, PE and pPE. A nucleophilic substitution reaction takes place between the aromatic TNBS molecule and the free amino group, thus resulting in a mass shift that can be detected by ESI-MS. Because this is the first reported analysis[11] of TNBS labeled aminophophoslipid using ESI-MS, an effort was put into deciphering the fragmentation pattern of the new lipids so as to find diagnostic ions for its identification. It was shown that the PS and PE/pPE lipids exhibited a mass shift of m/z 149 and 211 respectively (Figure 34). Unfortunately, we were unable to identify any unique diagnostic ions between the two classes of lipids.

For this experiment, it was important to ensure that the TNBS reaction was taking place under non-membrane penetrating conditions. We tested a number of different parameters including temperature and TNBS concentration using liposomes consisting of DMPE. Of these two parameters, it is clear that temperature was the more important factor. By carrying out the labeling reaction at three different temperatures, 4°C, 25°C and 37°C, we found increasing levels of TNBS-DMPE produced (Figure 35). This indicates either increased TNBS penetration through the bilayer and/or higher reactivity rates between TNBS and DMPE due to the increase in temperature. In previous reports of TNBS labeling experiments carried out on purified VSV particles, 25°C was used as the non-penetrating

[11] A study published by Laurinavicius et al., reported the use of TNBS labeling of PE coupled with ESI-MS. However, this study only measured decrease in PE levels after treatment, without making reference to measurements of TNBS-PE.

temperature (Fong et al., 1976; Fong and Brown, 1978). However, we decided to be more stringent with our labeling temperature, so decided to use 4°C for the rest of the reaction experiments. We also tested for the concentration effect but could not find a good correlation between labeling efficiency and TNBS concentration (Figure 36). Finally, we used a lower concentration of TNBS to prevent potential membrane disruption.

4.5.2 Plasmalogen PE are enriched in the outer leaflet of the retrovirus envelope

To ensure that the MLV membrane was intact and not leaky, the TNBS reactions were only carried out using freshly produced MLV particles. Our data revealed that the majority of the lipids available for TNBS labeling are pPE molecules while PE is mostly confined in the inner leaflet of the envelope (Figure 37 and 38, Table 11 and 12). It was found that a small amount of PS lipids were also labeled by TNBS to produce TNBS-PS molecules. There appears to be no specific enrichment involved with PS (Table 11 and 12), thereby suggesting that PS molecules are mostly confined in the inner leaflet of the envelope. Moreover, attempts to block externalized PS in MLV envelope using Annexin V did not significantly affect MLV infection of REF cells (Figure 45).

How could this asymmetry arise? As we have already shown, MLV envelopes originate from the plasma membrane of its host cell, thereby inheriting the signature properties of the host cell plasma membrane. Since membrane translocation of phospholipids in mature MLV virions is probably slow due to energetic barriers in flip across the middle hydrophobic region of a bilayer, the lipid asymmetry observed in the MLV envelope must exist at least temporarily in the plasma membrane budding site. Therefore, the origin of the asymmetry in the MLV envelope can be resolved by explaining the origin of asymmetry in the host cell plasma membrane. One possibility is that asymmetry could be generated at the

budding site of the virus, for example by the interaction of host cell phospholipids with MLV specific proteins like Gag or Env. Another possibility is that asymmetry may be a usual and normal feature of the uninfected host cell membrane, so a budding MLV virion would simply acquire a representative feature of the host cell plasma membrane. Either way, the specific localization of pPE and PE in the external and internal leaflets respectively would indicate that this feature may play a role in virus budding.

4.5.3 Possible functions of plasmalogen PE in the outer leaflet of retrovirus envelope

Plasmalogens are glycerophospholipids characterized by an alk-1′-enylether bond in position *sn*-1 and an acyl bond in position *sn*-2. The *sn*-2 acyl chain of plasmalogen lipids is oriented in a perpendicular direction to the membrane surface. This extended conformation results in an effectively longer hydrocarbon portion in plasmalogen than in the diacyl analog (Lohner, 1996). Moreover, the lack of the carbonyl oxygen in position *sn*-1 affects the hydrophilicity of the headgroup and weakens intermolecular hydrogen-bonding between the headgroups of pPE and other phospholipids in the membrane leaftlet. Therefore, pPE tend to favor the formation of non-lamellar structures which destabilizes the membrane that they are contained in (Lohner, 1996). This feature of pPE may be useful in the budding and fusion activity of the retrovirus envelope.

In support of this hypothesis, Glaser and Gross previously identified glyceraldehyde-3-phosphate dehydrogenase (GAPDH), in rat brain cytosol, as a protein that appears capable of facilitating fusion of pPE-containing vesicles (Glaser and Gross, 1995). Specifically, the ideal fusion vesicles found in this study contains approximately 40% Cholesterol, 27% PC, 27% pPE and 6% PS, which approximates the measured level of these lipids in found retrovirus envelopes (Table 4). Coincidentally, the identification of GAPDH as a host protein

that is found in the envelope of HIV particles also suggests an involvement of such fusion mechanisms in retrovirus infection (Ott et al., 2000). Concurrently, having PE concentrated on the inside of the membrane, would allow it to promote negative membrane curvature and energy favorability to the hemi-fusion stalk-like state (Haque et al., 2001; Kasson and Pande, 2007; Siegel and Epand, 1997) during both the end and start stage of budding and fusion events respectively. It would be interesting to decipher how the arrangement of pPE and PE may play synergistic roles together with other curvature inducing lipids such as phosphoinositides, PA and lysoPA, and also cellular cytoskeleton and protein activities (McMahon and Gallop, 2005) in a way unique to retrovirus membrane dynamics.

4.6 Neutral lipid composition of retroviruses

For the first time, we report the total analysis of neutral lipids from purified retrovirus envelopes, identifying not only Chol, but CE, DG and TG as well. We noted that the level of enrichment of Chol and CE is much greater in HIV compared to MLV, where CE levels appear to be lower compared to its host cell total (Table 7). The structural difference between Chol and CE is the presence of an esterified fatty acyl chain at the hydroxyl group of cholesterol. While cholesterol is predominantly present at the plasma membrane of mammalian cells, CE pools are typically found in the cytosol of the cells as part of lipid droplets (Simons and Ikonen, 2000). Alternatively, cholesterol and CE may be also be exchanged directly between circulating lipopropteins from serum and the plasma membrane (Simons and Ikonen, 2000). Recent evidence showed that the HIV-1 replication machinery harbors several mechanisms to increase cholesterol transport to the budding site of the virus. In T-cells, the Nef protein appears to not only increase the biosynthesis of cholesterol but also the uptake of cholesterol from extracellular LDL (van 't Wout et al., 2005a; Zheng et al.,

2003). In macrophages, the virus does this by impairing the ATP-binding cassette transporter A1 (ABCA1)-dependent cholesterol efflux, also mediated by Nef (Mujawar et al., 2006). Therefore, the action of Nef may have resulted in significant enrichment of Chol and CE levels in the HIV envelope. In contrast, MLV is simple retrovirus without similar accessory proteins, and therefore may not be able to control cholesterol trafficking to the same extent as HIV.

4.6.1 Saturated species of DG and TG can be found in retrovirus envelopes

The DG profile of the HIV and MLV envelopes consist a high ratio of saturated species compared to their respective host cell total membrane (Table 7). Its been shown that mono/saturated DG species are derived predominantly from PC, through an intermediate dephosphorylation step of PLD-generated PA (Hodgkin et al., 1998). In a similar manner to Cer, the presence of mono/saturated DG alone can add significant structural plasticity to the plasma membrane (Armstrong et al., 2002; Veiga et al., 1999). This will be useful not only in the trafficking of material in and out of a cell, but it may also support viral budding and fusion reactions. Unexpectedly, we also detected TG in our analysis of the purified retrovirus envelope. Similar to DG, the TG profile of both HIV and MLV envelope consist a high ratio of saturated species when compared to the total membrane. This ratio may be reflective of the plasma membrane TG profile that is reported to be rich in mono/saturated species (Mackinnon et al., 1992; May et al., 1997). It is also not difficult to conclude that these saturated DG and TG lipids would fit nicely into a lipid raft model for retrovirus assembly.

4.7 Conclusion

Taking a broader view, the lipidomics approach should be equally useful in the study of other medically important enveloped viruses. As mentioned in Chapter 1, viruses such as Vesicular Stomatis Virus, Influenza Virus and Respiratory Syncytial Virus possess structural proteins analogous to retrovirus Gag and also use the plasma membrane as an assembly and budding site. Thus, it would be interesting to examine the commonalities and differences in lipid inventory of these viruses as a means to dissect the protein-lipid interaction involved in the assembly of these viruses. In addition, it would be important to also apply lipidomics in the study of viruses that are formed in intracellular organelles such Dengue Virus and Hepatitis C Virus. Because intracellular organelles have very different lipid characteristics compared to the plasma membrane, these viruses are likely to have developed unique modes of lipid-protein interactions compared to plasma membrane budding viruses. Detailed lipid analysis of these purified viruses would therefore elucidate important lipid classes involved in the replication of these viruses.

In conclusion, we have demonstrated that detailed lipid profiling of retrovirus envelopes helped identify enriched lipids such as PIP_2 and raft lipids that are important to retrovirus replication. However, beyond analyzing the obvious enrichment of these lipids, it must be noted that other lipids that occur in high abundance but are less enriched, such as PS, pPE, SM and even PC, are nonetheless important in the formation of the native retroviral envelope and deserve further investigation as well.

Reference List

Abe A., Inokuchi J., Jimbo M., Shimeno H., Nagamatsu A., Shayman J. A., Shukla G. S., and Radin N. S. 1992. Improved inhibitors of glucosylceramide synthase. J.Biochem. 111: 191-196.

Ablan S., Rawat S. S., Viard M., Wang J. M., Puri A., and Blumenthal R. 2006. The role of cholesterol and sphingolipids in chemokine receptor function and HIV-1 envelope glycoprotein-mediated fusion. Virol.J. 3: 104-

Ahola T., Lampio A., Auvinen P., and Kaariainen L. 1999. Semliki Forest virus mRNA capping enzyme requires association with anionic membrane phospholipids for activity. EMBO J. 18: 3164-3172.

Alfsen A. and Bomsel M. 2002. HIV-1 gp41 envelope residues 650-685 exposed on native virus act as a lectin to bind epithelial cell galactosyl ceramide. J.Biol.Chem. 277: 25649-25659.

Aloia R. C., Jensen F. C., Curtain C. C., Mobley P. W., and Gordon L. M. 1988. Lipid composition and fluidity of the human immunodeficiency virus. Proc.Natl.Acad.Sci.U.S.A. 85: 900-904.

Aloia R. C., Tian H., and Jensen F. C. 1993. Lipid composition and fluidity of the human immunodeficiency virus envelope and host cell plasma membranes. Proc.Natl.Acad.Sci.U.S.A. 90: 5181-5185.

Ambrose Z., Compton L., Piatak M., Jr., Lu D., Alvord W. G., Lubomirski M. S., Hildreth J. E., Lifson J. D., Miller C. J., and KewalRamani V. N. 2008. Incomplete protection against simian immunodeficiency virus vaginal transmission in rhesus macaques by a topical antiviral agent revealed by repeat challenges. J.Virol. 82: 6591-6599.

Armstrong D. L., Borchardt D. B., and Zidovetzki R. 2002. Synergistic perturbation of phosphatidylcholine/sphingomyelin bilayers by diacylglycerol and cholesterol. Biochem.Biophys.Res.Commun. 296: 806-812.

Baek S. H., Kwak J. Y., Lee S. H., Lee T., Ryu S. H., Uhlinger D. J., and Lambeth J. D. 1997. Lipase activities of p37, the major envelope protein of vaccinia virus. J.Biol.Chem. 272: 32042-32049.

Barbour S., Edidin M., Felding-Habermann B., Taylor-Norton J., Radin N. S., and Fenderson B. A. 1992. Glycolipid depletion using a ceramide analogue (PDMP) alters growth, adhesion, and membrane lipid organization in human A431 cells. J.Cell Physiol. 150: 610-619.

Barsov E. V., Payne W. S., and Hughes S. H. 2001. Adaptation of chimeric retroviruses in vitro and in vivo: isolation of avian retroviral vectors with extended host range. J.Virol. 75: 4973-4983.

Beer C., Buhr P., Hahn H., Laubner D., and Wirth M. 2003. Gene expression analysis of murine cells producing amphotropic mouse leukaemia virus at a cultivation temperature of 32 and 37 degrees C. J.Gen.Virol. 84: 1677-1686.

Beer C., Pedersen L., and Wirth M. 2005. Amphotropic murine leukaemia virus envelope protein is associated with cholesterol-rich microdomains. Virol.J. 2: 36-

Bess J. W., Jr., Gorelick R. J., Bosche W. J., Henderson L. E., and Arthur L. O. 1997. Microvesicles are a source of contaminating cellular proteins found in purified HIV-1 preparations. Virology. 230: 134-144.

Bhattacharya J., Peters P. J., and Clapham P. R. 2004. Human immunodeficiency virus type 1 envelope glycoproteins that lack cytoplasmic domain cysteines: impact on association with membrane lipid rafts and incorporation onto budding virus particles. J.Virol. 78: 5500-5506.

Bhattacharya J., Repik A., and Clapham P. R. 2006. Gag regulates association of human immunodeficiency virus type 1 envelope with detergent-resistant membranes. J.Virol. 80: 5292-5300.

Bligh E. G. and Dyer W. J. 1959. A rapid method of total lipid extraction and purification. Can.J.Biochem.Physiol. 37: 911-917.

Bollinger C. R., Teichgraber V., and Gulbins E. 2005. Ceramide-enriched membrane domains. Biochim.Biophys.Acta. 1746: 284-294.

Booth A. M., Fang Y., Fallon J. K., Yang J. M., Hildreth J. E., and Gould S. J. 2006. Exosomes and HIV Gag bud from endosome-like domains of the T cell plasma membrane. J.Cell Biol. 172: 923-935.

Briggs J. A., Wilk T., and Fuller S. D. 2003. Do lipid rafts mediate virus assembly and pseudotyping? J.Gen.Virol. 84: 757-768.

Brown D. A. 2006. Lipid rafts, detergent-resistant membranes, and raft targeting signals. Physiology.(Bethesda.). 21: 430-439.

Brugger B., Erben G., Sandhoff R., Wieland F. T., and Lehmann W. D. 1997. Quantitative analysis of biological membrane lipids at the low picomole level by nano-electrospray ionization tandem mass spectrometry. Proc.Natl.Acad.Sci.U.S.A. 94: 2339-2344.

Brugger B., Glass B., Haberkant P., Leibrecht I., Wieland F. T., and Krausslich H. G. 2006. The HIV lipidome: a raft with an unusual composition. Proc.Natl.Acad.Sci.U.S.A. 103: 2641-2646.

Brugger B., Krautkramer E., Tibroni N., Munte C. E., Rauch S., Leibrecht I., Glass B., Breuer S., Geyer M., Krausslich H. G., Kalbitzer H. R., Wieland F. T., and Fackler O. T. 2007. Human Immunodeficiency Virus Type 1 Nef protein modulates the lipid composition of virions and host cell membrane microdomains. Retrovirology. 4: 70-

Bryant M. and Ratner L. 1990. Myristoylation-dependent replication and assembly of human immunodeficiency virus 1. Proc.Natl.Acad.Sci.U.S.A. 87: 523-527.

Burger H. M., Abel S., Snijman P. W., Swanevelder S., and Gelderblom W. C. 2007. Altered lipid parameters in hepatic subcellular membrane fractions induced by fumonisin B1. Lipids. 42: 249-261.

Callahan M. K., Popernack P. M., Tsutsui S., Truong L., Schlegel R. A., and Henderson A. J. 2003. Phosphatidylserine on HIV envelope is a cofactor for infection of monocytic cells. J.Immunol. 170: 4840-4845.

Camera E., Picardo M., Presutti C., Catarcini P., and Fanali S. 2004. Separation and characterisation of sphingoceramides by high-performance liquid chromatography-electrospray ionisation mass spectrometry. J.Sep.Sci. 27: 971-976.

Campanero-Rhodes M. A., Smith A., Chai W., Sonnino S., Mauri L., Childs R. A., Zhang Y., Ewers H., Helenius A., Imberty A., and Feizi T. 2007a. N-glycolyl GM1 ganglioside as a receptor for simian virus 40. J.Virol. 81: 12846-12858.

Campanero-Rhodes M. A., Smith A., Chai W., Sonnino S., Mauri L., Childs R. A., Zhang Y., Ewers H., Helenius A., Imberty A., and Feizi T. 2007b. N-glycolyl GM1 ganglioside as a receptor for simian virus 40. J.Virol. 81: 12846-12858.

Campbell S., Fisher R. J., Towler E. M., Fox S., Issaq H. J., Wolfe T., Phillips L. R., and Rein A. 2001. Modulation of HIV-like particle assembly in vitro by inositol phosphates. Proc.Natl.Acad.Sci.U.S.A. 98: 10875-10879.

Campbell S. M., Crowe S. M., and Mak J. 2002. Virion-associated cholesterol is critical for the maintenance of HIV-1 structure and infectivity. AIDS. 16: 2253-2261.

Chan W. T., Sherer N. M., Uchil P. D., Novak E. K., Swank R. T., and Mothes W. 2008. Murine leukemia virus spreading in mice impaired in the biogenesis of secretory lysosomes and Ca2+-regulated exocytosis. PLoS.ONE. 3: e2713-

Chernomordik L. V., Frolov V. A., Leikina E., Bronk P., and Zimmerberg J. 1998. The pathway of membrane fusion catalyzed by influenza hemagglutinin: restriction of lipids, hemifusion, and lipidic fusion pore formation. J.Cell Biol. 140: 1369-1382.

Chernomordik L. V., Vogel S. S., Sokoloff A., Onaran H. O., Leikina E. A., and Zimmerberg J. 1993. Lysolipids reversibly inhibit Ca(2+)-, GTP- and pH-dependent fusion of biological membranes. FEBS Lett. 318: 71-76.

Chukkapalli V., Hogue I. B., Boyko V., Hu W. S., and Ono A. 2008. Interaction between the human immunodeficiency virus type 1 Gag matrix domain and phosphatidylinositol-(4,5)-bisphosphate is essential for efficient gag membrane binding. J.Virol. 82: 2405-2417.

Coil D. A. and Miller A. D. 2005a. Enhancement of enveloped virus entry by phosphatidylserine. J.Virol. 79: 11496-11500.

Coil D. A. and Miller A. D. 2005b. Phosphatidylserine treatment relieves the block to retrovirus infection of cells expressing glycosylated virus receptors. Retrovirology. 2: 49-

Conte M. R. and Matthews S. 1998. Retroviral matrix proteins: a structural perspective. Virology. 246: 191-198.

Coren L. V., Shatzer T., and Ott D. E. 2008. CD45 immunoaffinity depletion of vesicles from Jurkat T cells demonstrates that exosomes contain CD45: no evidence for a distinct exosome/HIV-1 budding pathway. Retrovirology. 5: 64-

Dalton A. K., ko-Adjei D., Murray P. S., Murray D., and Vogt V. M. 2007. Electrostatic interactions drive membrane association of the human immunodeficiency virus type 1 Gag MA domain. J.Virol. 81: 6434-6445.

Davey R. A., Hamson C. A., Healey J. J., and Cunningham J. M. 1997. In vitro binding of purified murine ecotropic retrovirus envelope surface protein to its receptor, MCAT-1. J.Virol. 71: 8096-8102.

Demirov D. G. and Freed E. O. 2004. Retrovirus budding. Virus Res. 106: 87-102.

Deneka M., Pelchen-Matthews A., Byland R., Ruiz-Mateos E., and Marsh M. 2007. In macrophages, HIV-1 assembles into an intracellular plasma membrane domain containing the tetraspanins CD81, CD9, and CD53. J.Cell Biol. 177: 329-341.

Derdeyn C. A., Decker J. M., Sfakianos J. N., Wu X., O'Brien W. A., Ratner L., Kappes J. C., Shaw G. M., and Hunter E. 2000. Sensitivity of human immunodeficiency virus type 1 to the fusion inhibitor T-20 is modulated by coreceptor specificity defined by the V3 loop of gp120. J.Virol. 74: 8358-8367.

Downes C. P., Gray A., and Lucocq J. M. 2005. Probing phosphoinositide functions in signaling and membrane trafficking. Trends Cell Biol. 15: 259-268.

El-Sadr W. M., Mullin C. M., Carr A., Gibert C., Rappoport C., Visnegarwala F., Grunfeld C., and Raghavan S. S. 2005. Effects of HIV disease on lipid, glucose and insulin levels: results from a large antiretroviral-naive cohort. HIV.Med. 6: 114-121.

Escaut L., Monsuez J. J., Chironi G., Merad M., Teicher E., Smadja D., Simon A., and Vittecoq D. 2003. Coronary artery disease in HIV infected patients. Intensive Care Med. 29: 969-973.

Escola J. M., Kleijmeer M. J., Stoorvogel W., Griffith J. M., Yoshie O., and Geuze H. J. 1998. Selective enrichment of tetraspan proteins on the internal vesicles of multivesicular endosomes and on exosomes secreted by human B-lymphocytes. J.Biol.Chem. 273: 20121-20127.

Esser M. T., Graham D. R., Coren L. V., Trubey C. M., Bess J. W., Jr., Arthur L. O., Ott D. E., and Lifson J. D. 2001. Differential incorporation of CD45, CD80 (B7-1), CD86 (B7-2), and major histocompatibility complex class I and II molecules into human immunodeficiency virus type 1 virions and microvesicles: implications for viral pathogenesis and immune regulation. J.Virol. 75: 6173-6182.

Fantini J., Cook D. G., Nathanson N., Spitalnik S. L., and Gonzalez-Scarano F. 1993. Infection of colonic epithelial cell lines by type 1 human immunodeficiency virus is associated with cell surface expression of galactosylceramide, a potential alternative gp120 receptor. Proc.Natl.Acad.Sci.U.S.A. 90: 2700-2704.

Farge E., Ojcius D. M., Subtil A., and utry-Varsat A. 1999. Enhancement of endocytosis due to aminophospholipid transport across the plasma membrane of living cells. Am.J.Physiol. 276: C725-C733.

Fei W., Shui G., Gaeta B., Du X., Kuerschner L., Li P., Brown A. J., Wenk M. R., Parton R. G., and Yang H. 2008. Fld1p, a functional homologue of human seipin, regulates the size of lipid droplets in yeast. J.Cell Biol. 180: 473-482.

Ferreira L., Villar E., and Munoz-Barroso I. 2004. Gangliosides and N-glycoproteins function as Newcastle disease virus receptors. Int.J.Biochem.Cell Biol. 36: 2344-2356.

Finnegan C. and Blumenthal R. 2006. Dissecting HIV fusion: identifying novel targets for entry inhibitors. Infect.Disord.Drug Targets. 6: 355-367.

Finnegan C. M., Rawat S. S., Cho E. H., Guiffre D. L., Lockett S., Merrill A. H., Jr., and Blumenthal R. 2007. Sphingomyelinase restricts the lateral diffusion of CD4 and inhibits human immunodeficiency virus fusion. J.Virol. 81: 5294-5304.

Finnegan C. M., Rawat S. S., Puri A., Wang J. M., Ruscetti F. W., and Blumenthal R. 2004. Ceramide, a target for antiretroviral therapy. Proc.Natl.Acad.Sci.U.S.A. 101: 15452-15457.

Finzi A., Orthwein A., Mercier J., and Cohen E. A. 2007. Productive human immunodeficiency virus type 1 assembly takes place at the plasma membrane. J.Virol. 81: 7476-7490.

Fong B. S. and Brown J. C. 1978. Asymmetric distribution of phosphatidylethanolamine fatty acyl chains in the membrane of vesicular stomatitis virus. Biochim.Biophys.Acta. 510: 230-241.

Fong B. S., Hunt R. C., and Brown J. C. 1976. Asymmetric distribution of phosphatidylethanolamine in the membrane of vesicular stomatitis virus. J.Virol. 20: 658-663.

Fontaine R. N. and Schroeder F. 1979. Plasma membrane aminophospholipid distribution in transformed murine fibroblasts. Biochim.Biophys.Acta. 558: 1-12.

Freed E. O. 2006. HIV-1 Gag: flipped out for PI(4,5)P(2). Proc.Natl.Acad.Sci.U.S.A. 103: 11101-11102.

Freed E. O., Englund G., and Martin M. A. 1995. Role of the basic domain of human immunodeficiency virus type 1 matrix in macrophage infection. J.Virol. 69: 3949-3954.

Gambhir A., Hangyas-Mihalyne G., Zaitseva I., Cafiso D. S., Wang J., Murray D., Pentyala S. N., Smith S. O., and McLaughlin S. 2004. Electrostatic sequestration of PIP2 on phospholipid membranes by basic/aromatic regions of proteins. Biophys.J. 86: 2188-2207.

Gelderblom W. C., Jaskiewicz K., Marasas W. F., Thiel P. G., Horak R. M., Vleggaar R., and Kriek N. P. 1988. Fumonisins--novel mycotoxins with cancer-promoting activity produced by Fusarium moniliforme. Appl.Environ.Microbiol. 54: 1806-1811.

Giri M. S., Nebozhyn M., Showe L., and Montaner L. J. 2006. Microarray data on gene modulation by HIV-1 in immune cells: 2000-2006. J.Leukoc.Biol. 80: 1031-1043.

Glaros E. N., Kim W. S., Quinn C. M., Wong J., Gelissen I., Jessup W., and Garner B. 2005. Glycosphingolipid accumulation inhibits cholesterol efflux via the ABCA1/apolipoprotein A-

I pathway: 1-phenyl-2-decanoylamino-3-morpholino-1-propanol is a novel cholesterol efflux accelerator. J.Biol.Chem. 280: 24515-24523.

Glaser P. E. and Gross R. W. 1994. Plasmenylethanolamine facilitates rapid membrane fusion: a stopped-flow kinetic investigation correlating the propensity of a major plasma membrane constituent to adopt an HII phase with its ability to promote membrane fusion. Biochemistry. 33: 5805-5812.

Glaser P. E. and Gross R. W. 1995. Rapid plasmenylethanolamine-selective fusion of membrane bilayers catalyzed by an isoform of glyceraldehyde-3-phosphate dehydrogenase: discrimination between glycolytic and fusogenic roles of individual isoforms. Biochemistry. 34: 12193-12203.

Gluschankof P., Mondor I., Gelderblom H. R., and Sattentau Q. J. 1997. Cell membrane vesicles are a major contaminant of gradient-enriched human immunodeficiency virus type-1 preparations. Virology. 230: 125-133.

Goff S. P. 2007. Host factors exploited by retroviruses. Nat.Rev.Microbiol. 5: 253-263.

Graham D. R., Chertova E., Hilburn J. M., Arthur L. O., and Hildreth J. E. 2003. Cholesterol depletion of human immunodeficiency virus type 1 and simian immunodeficiency virus with beta-cyclodextrin inactivates and permeabilizes the virions: evidence for virion-associated lipid rafts. J.Virol. 77: 8237-8248.

Grassme H., Jekle A., Riehle A., Schwarz H., Berger J., Sandhoff K., Kolesnick R., and Gulbins E. 2001. CD95 signaling via ceramide-rich membrane rafts. J.Biol.Chem. 276: 20589-20596.

Green S. A., Zimmer K. P., Griffiths G., and Mellman I. 1987. Kinetics of intracellular transport and sorting of lysosomal membrane and plasma membrane proteins. J.Cell Biol. 105: 1227-1240.

Griggi T., Bauer R., Garofalo T., Kukel S., Lenti L., Massetti A. P., Muller C., Sorice M., and Pontieri G. M. 1994. Autoantibodies against ganglioside GM3 represent a portion of anti-lymphocyte antibodies in AIDS patients. Scand.J.Immunol. 40: 77-82.

Groot F., Welsch S., and Sattentau Q. J. 2008. Efficient HIV-1 transmission from macrophages to T cells across transient virological synapses. Blood. 111: 4660-4663.

Gunther-Ausborn S. and Stegmann T. 1997. How lysophosphatidylcholine inhibits cell-cell fusion mediated by the envelope glycoprotein of human immunodeficiency virus. Virology. 235: 201-208.

Guyader M., Kiyokawa E., Abrami L., Turelli P., and Trono D. 2002. Role for human immunodeficiency virus type 1 membrane cholesterol in viral internalization. J.Virol. 76: 10356-10364.

Han X. and Gross R. W. 2005. Shotgun lipidomics: electrospray ionization mass spectrometric analysis and quantitation of cellular lipidomes directly from crude extracts of biological samples. Mass Spectrom.Rev. 24: 367-412.

Haque M. E., McIntosh T. J., and Lentz B. R. 2001. Influence of lipid composition on physical properties and peg-mediated fusion of curved and uncurved model membrane vesicles: "nature's own" fusogenic lipid bilayer. Biochemistry. 40: 4340-4348.

Harder T. and Simons K. 1997. Caveolae, DIGs, and the dynamics of sphingolipid-cholesterol microdomains. Curr.Opin.Cell Biol. 9: 534-542.

Harila K., Prior I., Sjoberg M., Salminen A., Hinkula J., and Suomalainen M. 2006. Vpu and Tsg101 regulate intracellular targeting of the human immunodeficiency virus type 1 core protein precursor Pr55gag. J.Virol. 80: 3765-3772.

Harouse J. M., Kunsch C., Hartle H. T., Laughlin M. A., Hoxie J. A., Wigdahl B., and Gonzalez-Scarano F. 1989. CD4-independent infection of human neural cells by human immunodeficiency virus type 1. J.Virol. 63: 2527-2533.

Haywood A. M. and Boyer B. P. 1984. Effect of lipid composition upon fusion of liposomes with Sendai virus membranes. Biochemistry. 23: 4161-4166.

Heo W. D., Inoue T., Park W. S., Kim M. L., Park B. O., Wandless T. J., and Meyer T. 2006. PI(3,4,5)P3 and PI(4,5)P2 lipids target proteins with polybasic clusters to the plasma membrane. Science. 314: 1458-1461.

Hodgkin M. N., Pettitt T. R., Martin A., Michell R. H., Pemberton A. J., and Wakelam M. J. 1998. Diacylglycerols and phosphatidates: which molecular species are intracellular messengers? Trends Biochem.Sci. 23: 200-204.

Holthuis J. C. and Levine T. P. 2005. Lipid traffic: floppy drives and a superhighway. Nat.Rev.Mol.Cell Biol. 6: 209-220.

Hua Z. and Graham T. R. 2003. Requirement for neo1p in retrograde transport from the Golgi complex to the endoplasmic reticulum. Mol.Biol.Cell. 14: 4971-4983.

Hug P., Lin H. M., Korte T., Xiao X., Dimitrov D. S., Wang J. M., Puri A., and Blumenthal R. 2000. Glycosphingolipids promote entry of a broad range of human immunodeficiency virus type 1 isolates into cell lines expressing CD4, CXCR4, and/or CCR5. J.Virol. 74: 6377-6385.

Hutchins P. M., Barkley R. M., and Murphy R. C. 2008. Separation of cellular nonpolar neutral lipids by normal-phase chromatography and analysis by electrospray ionization mass spectrometry. J.Lipid Res. 49: 804-813.

Isaac G., Bylund D., Mansson J. E., Markides K. E., and Bergquist J. 2003. Analysis of phosphatidylcholine and sphingomyelin molecular species from brain extracts using capillary liquid chromatography electrospray ionization mass spectrometry. J.Neurosci.Methods. 128: 111-119.

Itoh T. and De Camilli P. 2006. BAR, F-BAR (EFC) and ENTH/ANTH domains in the regulation of membrane-cytosol interfaces and membrane curvature. Biochim.Biophys.Acta. 1761: 897-912.

Ivanova P. T., Cerda B. A., Horn D. M., Cohen J. S., McLafferty F. W., and Brown H. A. 2001. Electrospray ionization mass spectrometry analysis of changes in phospholipids in

RBL-2H3 mastocytoma cells during degranulation. Proc.Natl.Acad.Sci.U.S.A. 98: 7152-7157.

Jiang X., Cheng H., Yang K., Gross R. W., and Han X. 2007. Alkaline methanolysis of lipid extracts extends shotgun lipidomics analyses to the low-abundance regime of cellular sphingolipids. Anal.Biochem. 371: 135-145.

Jolly C. and Sattentau Q. J. 2007. Human immunodeficiency virus type 1 assembly, budding, and cell-cell spread in T cells take place in tetraspanin-enriched plasma membrane domains. J.Virol. 81: 7873-7884.

Jouvenet N., Neil S. J., Bess C., Johnson M. C., Virgen C. A., Simon S. M., and Bieniasz P. D. 2006. Plasma membrane is the site of productive HIV-1 particle assembly. PLoS.Biol. 4: e435-

Kapadia S. B. and Chisari F. V. 2005. Hepatitis C virus RNA replication is regulated by host geranylgeranylation and fatty acids. Proc.Natl.Acad.Sci.U.S.A. 102: 2561-2566.

Kasson P. M. and Pande V. S. 2007. Control of membrane fusion mechanism by lipid composition: predictions from ensemble molecular dynamics. PLoS.Comput.Biol. 3: e220-

Kisseleva M. V., Cao L., and Majerus P. W. 2002. Phosphoinositide-specific inositol polyphosphate 5-phosphatase IV inhibits Akt/protein kinase B phosphorylation and leads to apoptotic cell death. J.Biol.Chem. 277: 6266-6272.

Kovacs P., Pinter M., and Csaba G. 2000. Effect of glucosphingolipid synthesis inhibitor (PPMP and PDMP) treatment on Tetrahymena pyriformis: data on the evolution of the signaling system. Cell Biochem.Funct. 18: 269-280.

Krank J., Murphy R. C., Barkley R. M., Duchoslav E., and McAnoy A. 2007. Qualitative analysis and quantitative assessment of changes in neutral glycerol lipid molecular species within cells. Methods Enzymol. 432: 1-20.

Kuge O., Akamatsu Y., and Nishijima M. 1989. Abortive infection with Sindbis virus of a Chinese hamster ovary cell mutant defective in phosphatidylserine and phosphatidylethanolamine biosynthesis. Biochim.Biophys.Acta. 986: 61-69.

Laulagnier K., Motta C., Hamdi S., Roy S., Fauvelle F., Pageaux J. F., Kobayashi T., Salles J. P., Perret B., Bonnerot C., and Record M. 2004. Mast cell- and dendritic cell-derived exosomes display a specific lipid composition and an unusual membrane organization. Biochem.J. 380: 161-171.

Le B., I, Luyet P. P., Pons V., Ferguson C., Emans N., Petiot A., Mayran N., Demaurex N., Faure J., Sadoul R., Parton R. G., and Gruenberg J. 2005. Endosome-to-cytosol transport of viral nucleocapsids. Nat.Cell Biol. 7: 653-664.

Liao Z., Cimakasky L. M., Hampton R., Nguyen D. H., and Hildreth J. E. 2001. Lipid rafts and HIV pathogenesis: host membrane cholesterol is required for infection by HIV type 1. AIDS Res.Hum.Retroviruses. 17: 1009-1019.

Liao Z., Graham D. R., and Hildreth J. E. 2003. Lipid rafts and HIV pathogenesis: virion-associated cholesterol is required for fusion and infection of susceptible cells. AIDS Res.Hum.Retroviruses. 19: 675-687.

Lindwasser O. W. and Resh M. D. 2001. Multimerization of human immunodeficiency virus type 1 Gag promotes its localization to barges, raft-like membrane microdomains. J.Virol. 75: 7913-7924.

Lindwasser O. W. and Resh M. D. 2002. Myristoylation as a target for inhibiting HIV assembly: unsaturated fatty acids block viral budding. Proc.Natl.Acad.Sci.U.S.A. 99: 13037-13042.

Lodge R., Delamarre L., Lalonde J. P., Alvarado J., Sanders D. A., Dokhelar M. C., Cohen E. A., and Lemay G. 1997a. Two distinct oncornaviruses harbor an intracytoplasmic tyrosine-based basolateral targeting signal in their viral envelope glycoprotein. J.Virol. 71: 5696-5702.

Lodge R., Lalonde J. P., Lemay G., and Cohen E. A. 1997b. The membrane-proximal intracytoplasmic tyrosine residue of HIV-1 envelope glycoprotein is critical for basolateral targeting of viral budding in MDCK cells. EMBO J. 16: 695-705.

Lohner K. 1996. Is the high propensity of ethanolamine plasmalogens to form non-lamellar lipid structures manifested in the properties of biomembranes? Chem.Phys.Lipids. 81: 167-184.

Mackinnon W. B., May G. L., and Mountford C. E. 1992. Esterified cholesterol and triglyceride are present in plasma membranes of Chinese hamster ovary cells. Eur.J.Biochem. 205: 827-839.

MacPherson J. C., Pavlovich J. G., and Jacobs R. S. 1996. Biosynthesis of arachiodonic acid metabolites in Limulus polyphemus amebocytes: analysis by liquid chromatography-electrospray ionization mass spectrometry. Biochim.Biophys.Acta. 1303: 127-136.

Makino A., Ishii K., Murate M., Hayakawa T., Suzuki Y., Suzuki M., Ito K., Fujisawa T., Matsuo H., Ishitsuka R., and Kobayashi T. 2006. D-threo-1-phenyl-2-decanoylamino-3-morpholino-1-propanol alters cellular cholesterol homeostasis by modulating the endosome lipid domains. Biochemistry. 45: 4530-4541.

Malim M. H. and Emerman M. 2008. HIV-1 accessory proteins--ensuring viral survival in a hostile environment. Cell Host.Microbe. 3: 388-398.

Marinetti G. V. and Cattieu K. 1982. Asymmetric metabolism of phosphatidylethanolamine in the human red cell membrane. J.Biol.Chem. 257: 245-248.

Martin I. and Ruysschaert J. M. 1995. Lysophosphatidylcholine inhibits vesicles fusion induced by the NH2-terminal extremity of SIV/HIV fusogenic proteins. Biochim.Biophys.Acta. 1240: 95-100.

Marty A., Meanger J., Mills J., Shields B., and Ghildyal R. 2004. Association of matrix protein of respiratory syncytial virus with the host cell membrane of infected cells. Arch.Virol. 149: 199-210.

Mason P. W. and Jacobson B. S. 1985. Isolation of the dorsal, ventral and intracellular domains of HeLa cell plasma membranes following adhesion to a gelatin substrate. Biochim.Biophys.Acta. 821: 264-276.

Mattila P. K., Pykalainen A., Saarikangas J., Paavilainen V. O., Vihinen H., Jokitalo E., and Lappalainen P. 2007. Missing-in-metastasis and IRSp53 deform PI(4,5)P2-rich membranes by an inverse BAR domain-like mechanism. J.Cell Biol. 176: 953-964.

May G. L., Wright L. C., Obbink K. G., Byleveld P. M., Garg M. L., Ahmad Z. I., and Sorrell T. C. 1997. Increased saturated triacylglycerol levels in plasma membranes of human neutrophils stimulated by lipopolysaccharide. J.Lipid Res. 38: 1562-1570.

McDonald J. G., Thompson B. M., McCrum E. C., and Russell D. W. 2007. Extraction and analysis of sterols in biological matrices by high performance liquid chromatography electrospray ionization mass spectrometry. Methods Enzymol. 432: 145-170.

McLaughlin S. and Murray D. 2005. Plasma membrane phosphoinositide organization by protein electrostatics. Nature. 438: 605-611.

McMahon H. T. and Gallop J. L. 2005. Membrane curvature and mechanisms of dynamic cell membrane remodelling. Nature. 438: 590-596.

Megha and London E. 2004. Ceramide selectively displaces cholesterol from ordered lipid domains (rafts): implications for lipid raft structure and function. J.Biol.Chem. 279: 9997-10004.

Mercer J. and Helenius A. 2008. Vaccinia virus uses macropinocytosis and apoptotic mimicry to enter host cells. Science. 320: 531-535.

Merrill A. H., Jr., Sullards M. C., Allegood J. C., Kelly S., and Wang E. 2005. Sphingolipidomics: high-throughput, structure-specific, and quantitative analysis of sphingolipids by liquid chromatography tandem mass spectrometry. Methods. 36: 207-224.

Misasi R., Sorice M., Garofalo T., Griggi T., Giammarioli A. M., D'Ettorre G., Vullo V., Pontieri G. M., Malorni W., and Pavan A. 2000. Overexpression of lymphocytic GD3 ganglioside and presence of anti-GD3 antibodies in patients with HIV infection. AIDS Res.Hum.Retroviruses. 16: 1539-1549.

Misasi R., Sorice M., Griggi T., d'Agostino F., Garofalo T., Masala C., Pontieri G. M., and Lenti L. 1993. GM3 as a target of anti-lymphocytic ganglioside antibodies in AIDS patients. Clin.Immunol.Immunopathol. 67: 216-223.

Miyake K. and McNeil P. L. 1995. Vesicle accumulation and exocytosis at sites of plasma membrane disruption. J.Cell Biol. 131: 1737-1745.

Morita E. and Sundquist W. I. 2004. Retrovirus budding. Annu.Rev.Cell Dev.Biol. 20: 395-425.

Mothes W., Boerger A. L., Narayan S., Cunningham J. M., and Young J. A. 2000a. Retroviral entry mediated by receptor priming and low pH triggering of an envelope glycoprotein. Cell. 103: 679-689.

Mothes W., Boerger A. L., Narayan S., Cunningham J. M., and Young J. A. 2000b. Retroviral entry mediated by receptor priming and low pH triggering of an envelope glycoprotein. Cell. 103: 679-689.

Mujawar Z., Rose H., Morrow M. P., Pushkarsky T., Dubrovsky L., Mukhamedova N., Fu Y., Dart A., Orenstein J. M., Bobryshev Y. V., Bukrinsky M., and Sviridov D. 2006. Human immunodeficiency virus impairs reverse cholesterol transport from macrophages. PLoS.Biol. 4: e365-

Murphy R. C., James P. F., McAnoy A. M., Krank J., Duchoslav E., and Barkley R. M. 2007. Detection of the abundance of diacylglycerol and triacylglycerol molecular species in cells using neutral loss mass spectrometry. Anal.Biochem. 366: 59-70.

Murray P. S., Li Z., Wang J., Tang C. L., Honig B., and Murray D. 2005. Retroviral matrix domains share electrostatic homology: models for membrane binding function throughout the viral life cycle. Structure. 13: 1521-1531.

Nagan N. and Zoeller R. A. 2001. Plasmalogens: biosynthesis and functions. Prog.Lipid Res. 40: 199-229.

Nayak D. P., Hui E. K., and Barman S. 2004. Assembly and budding of influenza virus. Virus Res. 106: 147-165.

Neil S. J., Eastman S. W., Jouvenet N., and Bieniasz P. D. 2006. HIV-1 Vpu promotes release and prevents endocytosis of nascent retrovirus particles from the plasma membrane. PLoS.Pathog. 2: e39-

Nguyen D. G., Booth A., Gould S. J., and Hildreth J. E. 2003. Evidence that HIV budding in primary macrophages occurs through the exosome release pathway. J.Biol.Chem. 278: 52347-52354.

Nguyen D. H., Giri B., Collins G., and Taub D. D. 2005. Dynamic reorganization of chemokine receptors, cholesterol, lipid rafts, and adhesion molecules to sites of CD4 engagement. Exp.Cell Res. 304: 559-569.

Nguyen D. H. and Hildreth J. E. 2000. Evidence for budding of human immunodeficiency virus type 1 selectively from glycolipid-enriched membrane lipid rafts. J.Virol. 74: 3264-3272.

Nguyen D. H. and Taub D. 2002. Cholesterol is essential for macrophage inflammatory protein 1 beta binding and conformational integrity of CC chemokine receptor 5. Blood. 99: 4298-4306.

Nguyen D. H. and Taub D. D. 2004. Targeting Lipids to Prevent HIV Infection. Mol.Interv. 4: 318-320.

Nydegger S., Khurana S., Krementsov D. N., Foti M., and Thali M. 2006. Mapping of tetraspanin-enriched microdomains that can function as gateways for HIV-1. J.Cell Biol. 173: 795-807.

Ono A., Ablan S. D., Lockett S. J., Nagashima K., and Freed E. O. 2004. Phosphatidylinositol (4,5) bisphosphate regulates HIV-1 Gag targeting to the plasma membrane. Proc.Natl.Acad.Sci.U.S.A. 101: 14889-14894.

Ono A. and Freed E. O. 2001. Plasma membrane rafts play a critical role in HIV-1 assembly and release. Proc.Natl.Acad.Sci.U.S.A. 98: 13925-13930.

Ono A. and Freed E. O. 2004. Cell-type-dependent targeting of human immunodeficiency virus type 1 assembly to the plasma membrane and the multivesicular body. J.Virol. 78: 1552-1563.

Ono A. and Freed E. O. 2005. Role of lipid rafts in virus replication. Adv.Virus Res. 64: 311-358.

Ono A., Waheed A. A., and Freed E. O. 2007. Depletion of cellular cholesterol inhibits membrane binding and higher-order multimerization of human immunodeficiency virus type 1 Gag. Virology. 360: 27-35.

Ostrowski S. G., Van Bell C. T., Winograd N., and Ewing A. G. 2004. Mass spectrometric imaging of highly curved membranes during Tetrahymena mating. Science. 305: 71-73.

Ott D. E., Coren L. V., Johnson D. G., Kane B. P., Sowder R. C., Kim Y. D., Fisher R. J., Zhou X. Z., Lu K. P., and Henderson L. E. 2000. Actin-binding cellular proteins inside human immunodeficiency virus type 1. Virology. 266: 42-51.

Ott D. E., Nigida S. M., Jr., Henderson L. E., and Arthur L. O. 1995. The majority of cells are superinfected in a cloned cell line that produces high levels of human immunodeficiency virus type 1 strain MN. J.Virol. 69: 2443-2450.

Pelchen-Matthews A., Kramer B., and Marsh M. 2003. Infectious HIV-1 assembles in late endosomes in primary macrophages. J.Cell Biol. 162: 443-455.

Pelkmans L., Fava E., Grabner H., Hannus M., Habermann B., Krausz E., and Zerial M. 2005. Genome-wide analysis of human kinases in clathrin- and caveolae/raft-mediated endocytosis. Nature. 436: 78-86.

Popik W., Alce T. M., and Au W. C. 2002. Human immunodeficiency virus type 1 uses lipid raft-colocalized CD4 and chemokine receptors for productive entry into CD4(+) T cells. J.Virol. 76: 4709-4722.

Puri A., Hug P., Jernigan K., Barchi J., Kim H. Y., Hamilton J., Wiels J., Murray G. J., Brady R. O., and Blumenthal R. 1998. The neutral glycosphingolipid globotriaosylceramide promotes fusion mediated by a CD4-dependent CXCR4-utilizing HIV type 1 envelope glycoprotein. Proc.Natl.Acad.Sci.U.S.A. 95: 14435-14440.

Puri A., Hug P., Jernigan K., Rose P., and Blumenthal R. 1999. Role of glycosphingolipids in HIV-1 entry: requirement of globotriosylceramide (Gb3) in CD4/CXCR4-dependent fusion. Biosci.Rep. 19: 317-325.

Puri A., Rawat S. S., Lin H. M., Finnegan C. M., Mikovits J., Ruscetti F. W., and Blumenthal R. 2004. An inhibitor of glycosphingolipid metabolism blocks HIV-1 infection of primary T-cells. AIDS. 18: 849-858.

Rajendran L. and Simons K. 2005. Lipid rafts and membrane dynamics. J.Cell Sci. 118: 1099-1102.

Ramstedt B. and Slotte J. P. 2002. Membrane properties of sphingomyelins. FEBS Lett. 531: 33-37.

Ramstedt B. and Slotte J. P. 2006. Sphingolipids and the formation of sterol-enriched ordered membrane domains. Biochim.Biophys.Acta. 1758: 1945-1956.

Rawat S. S., Eaton J., Gallo S. A., Martin T. D., Ablan S., Ratnayake S., Viard M., KewalRamani V. N., Wang J. M., Blumenthal R., and Puri A. 2004a. Functional expression of CD4, CXCR4, and CCR5 in glycosphingolipid-deficient mouse melanoma GM95 cells and susceptibility to HIV-1 envelope glycoprotein-triggered membrane fusion. Virology. 318: 55-65.

Rawat S. S., Gallo S. A., Eaton J., Martin T. D., Ablan S., KewalRamani V. N., Wang J. M., Blumenthal R., and Puri A. 2004b. Elevated expression of GM3 in receptor-bearing targets confers resistance to human immunodeficiency virus type 1 fusion. J.Virol. 78: 7360-7368.

Rawat S. S., Viard M., Gallo S. A., Blumenthal R., and Puri A. 2006. Sphingolipids, cholesterol, and HIV-1: a paradigm in viral fusion. Glycoconj.J. 23: 189-197.

Resh M. D. 1999. Fatty acylation of proteins: new insights into membrane targeting of myristoylated and palmitoylated proteins. Biochim.Biophys.Acta. 1451: 1-16.

Resh M. D. 2004. A myristoyl switch regulates membrane binding of HIV-1 Gag. Proc.Natl.Acad.Sci.U.S.A. 101: 417-418.

Riffel N., Harlos K., Iourin O., Rao Z., Kingsman A., Stuart D., and Fry E. 2002. Atomic resolution structure of Moloney murine leukemia virus matrix protein and its relationship to other retroviral matrix proteins. Structure. 10: 1627-1636.

Rousso I., Mixon M. B., Chen B. K., and Kim P. S. 2000. Palmitoylation of the HIV-1 envelope glycoprotein is critical for viral infectivity. Proc.Natl.Acad.Sci.U.S.A. 97: 13523-13525.

Rudner L., Nydegger S., Coren L. V., Nagashima K., Thali M., and Ott D. E. 2005. Dynamic fluorescent imaging of human immunodeficiency virus type 1 gag in live cells by biarsenical labeling. J.Virol. 79: 4055-4065.

Ruggiero E., Bona R., Muratori C., and Federico M. 2008. Virological consequences of early events following cell-cell contact between human immunodeficiency virus type 1-infected and uninfected CD4+ cells. J.Virol. 82: 7773-7789.

Rusten T. E. and Stenmark H. 2006. Analyzing phosphoinositides and their interacting proteins. Nat.Methods. 3: 251-258.

Saad J. S., Loeliger E., Luncsford P., Liriano M., Tai J., Kim A., Miller J., Joshi A., Freed E. O., and Summers M. F. 2007. Point mutations in the HIV-1 matrix protein turn off the myristyl switch. J.Mol.Biol. 366: 574-585.

Saad J. S., Miller J., Tai J., Kim A., Ghanam R. H., and Summers M. F. 2006. Structural basis for targeting HIV-1 Gag proteins to the plasma membrane for virus assembly. Proc.Natl.Acad.Sci.U.S.A. 103: 11364-11369.

Scheiffele P., Rietveld A., Wilk T., and Simons K. 1999. Influenza viruses select ordered lipid domains during budding from the plasma membrane. J.Biol.Chem. 274: 2038-2044.

Schultz A. M., Henderson L. E., and Oroszlan S. 1988. Fatty acylation of proteins. Annu.Rev.Cell Biol. 4: 611-647.

Schwartz R. S., Olson J. A., Raventos-Suarez C., Yee M., Heath R. H., Lubin B., and Nagel R. L. 1987. Altered plasma membrane phospholipid organization in Plasmodium falciparum-infected human erythrocytes. Blood. 69: 401-407.

Sheff D. R., Daro E. A., Hull M., and Mellman I. 1999. The receptor recycling pathway contains two distinct populations of early endosomes with different sorting functions. J.Cell Biol. 145: 123-139.

Sherer N. M., Lehmann M. J., Jimenez-Soto L. F., Ingmundson A., Horner S. M., Cicchetti G., Allen P. G., Pypaert M., Cunningham J. M., and Mothes W. 2003. Visualization of retroviral replication in living cells reveals budding into multivesicular bodies. Traffic. 4: 785-801.

Shevchuk N. A., Hathout Y., Epifano O., Su Y., Liu Y., Sutherland M., and Ladisch S. 2007. Alteration of ganglioside synthesis by GM3 synthase knockout in murine embryonic fibroblasts. Biochim.Biophys.Acta. 1771: 1226-1234.

Shkriabai N., Datta S. A., Zhao Z., Hess S., Rein A., and Kvaratskhelia M. 2006. Interactions of HIV-1 Gag with assembly cofactors. Biochemistry. 45: 4077-4083.

Shui G., Bendt A. K., Pethe K., Dick T., and Wenk M. R. 2007b. Sensitive profiling of chemically diverse bioactive lipids. J.Lipid Res. 48: 1976-1984.

Shui G., Bendt A. K., Pethe K., Dick T., and Wenk M. R. 2007a. Sensitive profiling of chemically diverse bioactive lipids. J.Lipid Res. 48: 1976-1984.

Siegel D. P. and Epand R. M. 1997. The mechanism of lamellar-to-inverted hexagonal phase transitions in phosphatidylethanolamine: implications for membrane fusion mechanisms. Biophys.J. 73: 3089-3111.

Silvestris F., Frassanito M. A., Cafforio P., Potenza D., Di L. M., Tucci M., Grizzuti M. A., Nico B., and Dammacco F. 1996. Antiphosphatidylserine antibodies in human immunodeficiency virus-1 patients with evidence of T-cell apoptosis and mediate antibody-dependent cellular cytotoxicity. Blood. 87: 5185-5195.

Simons K. and Ikonen E. 2000. How cells handle cholesterol. Science. 290: 1721-1726.

Slosberg B. N. and Montelaro R. C. 1982. A comparison of the mobilities and thermal transitions of retrovirus lipid envelopes and host cell plasma membranes by electron spin resonance spectroscopy. Biochim.Biophys.Acta. 689: 393-402.

Sommer U., Herscovitz H., Welty F. K., and Costello C. E. 2006. LC-MS-based method for the qualitative and quantitative analysis of complex lipid mixtures. J.Lipid Res. 47: 804-814.

Sorice M., Garofalo T., Misasi R., Longo A., Mattei V., Sale P., Dolo V., Gradini R., and Pavan A. 2001. Evidence for cell surface association between CXCR4 and ganglioside GM3 after gp120 binding in SupT1 lymphoblastoid cells. FEBS Lett. 506: 55-60.

Sorice M., Garofalo T., Misasi R., Longo A., Mikulak J., Dolo V., Pontieri G. M., and Pavan A. 2000. Association between GM3 and CD4-Ick complex in human peripheral blood lymphocytes. Glycoconj.J. 17: 247-252.

Spuul P., Salonen A., Merits A., Jokitalo E., Kaariainen L., and Ahola T. 2007. Role of the amphipathic peptide of Semliki forest virus replicase protein nsP1 in membrane association and virus replication. J.Virol. 81: 872-883.

Stiasny K. and Heinz F. X. 2004. Effect of membrane curvature-modifying lipids on membrane fusion by tick-borne encephalitis virus. J.Virol. 78: 8536-8542.

Stolz D. B. and Jacobson B. S. 1992. Examination of transcellular membrane protein polarity of bovine aortic endothelial cells in vitro using the cationic colloidal silica microbead membrane-isolation procedure. J.Cell Sci. 103 (Pt 1): 39-51.

Strack B., Calistri A., Craig S., Popova E., and Gottlinger H. G. 2003. AIP1/ALIX is a binding partner for HIV-1 p6 and EIAV p9 functioning in virus budding. Cell. 114: 689-699.

Su A. I., Pezacki J. P., Wodicka L., Brideau A. D., Supekova L., Thimme R., Wieland S., Bukh J., Purcell R. H., Schultz P. G., and Chisari F. V. 2002. Genomic analysis of the host response to hepatitis C virus infection. Proc.Natl.Acad.Sci.U.S.A. 99: 15669-15674.

Subra C., Laulagnier K., Perret B., and Record M. 2007. Exosome lipidomics unravels lipid sorting at the level of multivesicular bodies. Biochimie. 89: 205-212.

Swinteck B. D. and Lyles D. S. 2008. Plasma membrane microdomains containing vesicular stomatitis virus M protein are separate from microdomains containing G protein and nucleocapsids. J.Virol. 82: 5536-5547.

Tettamanti G. 2004. Ganglioside/glycosphingolipid turnover: new concepts. Glycoconj.J. 20: 301-317.

Trajkovic K., Hsu C., Chiantia S., Rajendran L., Wenzel D., Wieland F., Schwille P., Brugger B., and Simons M. 2008. Ceramide triggers budding of exosome vesicles into multivesicular endosomes. Science. 319: 1244-1247.

Trubey C. M., Chertova E., Coren L. V., Hilburn J. M., Hixson C. V., Nagashima K., Lifson J. D., and Ott D. E. 2003. Quantitation of HLA class II protein incorporated into human immunodeficiency type 1 virions purified by anti-CD45 immunoaffinity depletion of microvesicles. J.Virol. 77: 12699-12709.

Ugolini S., Mondor I., and Sattentau Q. J. 1999. HIV-1 attachment: another look. Trends Microbiol. 7: 144-149.

UNAIDS and WHO. 2007. AIDS epidemic update 2007.

van 't Wout A. B., Swain J. V., Schindler M., Rao U., Pathmajeyan M. S., Mullins J. I., and Kirchhoff F. 2005a. Nef induces multiple genes involved in cholesterol synthesis and uptake in human immunodeficiency virus type 1-infected T cells. J.Virol. 79: 10053-10058.

van 't Wout A. B., Swain J. V., Schindler M., Rao U., Pathmajeyan M. S., Mullins J. I., and Kirchhoff F. 2005b. Nef induces multiple genes involved in cholesterol synthesis and uptake in human immunodeficiency virus type 1-infected T cells. J.Virol. 79: 10053-10058.

van Genderen I., Brandimarti R., Torrisi M. R., Campadelli G., and van Meer G. 1994. The phospholipid composition of extracellular herpes simplex virions differs from that of host cell nuclei. Virology. 200: 831-836.

van Meer G. 2005. Cellular lipidomics. EMBO J. 24: 3159-3165.

Vance J. E. and Steenbergen R. 2005. Metabolism and functions of phosphatidylserine. Prog.Lipid Res. 44: 207-234.

Veiga M. P., Arrondo J. L., Goni F. M., and Alonso A. 1999. Ceramides in phospholipid membranes: effects on bilayer stability and transition to nonlamellar phases. Biophys.J. 76: 342-350.

Viard M., Parolini I., Rawat S. S., Fecchi K., Sargiacomo M., Puri A., and Blumenthal R. 2004. The role of glycosphingolipids in HIV signaling, entry and pathogenesis. Glycoconj.J. 20: 213-222.

von Schwedler U. K., Stuchell M., Muller B., Ward D. M., Chung H. Y., Morita E., Wang H. E., Davis T., He G. P., Cimbora D. M., Scott A., Krausslich H. G., Kaplan J., Morham S. G., and Sundquist W. I. 2003. The protein network of HIV budding. Cell. 114: 701-713.

Welsch S., Keppler O. T., Habermann A., Allespach I., Krijnse-Locker J., and Krausslich H. G. 2007. HIV-1 buds predominantly at the plasma membrane of primary human macrophages. PLoS.Pathog. 3: e36-

Wenk M. R. 2005. The emerging field of lipidomics. Nat.Rev.Drug Discov. 4: 594-610.

Wenk M. R. 2006. Lipidomics of host-pathogen interactions. FEBS Lett. 580: 5541-5551.

Wenk M. R., Lucast L., Di Paolo G., Romanelli A. J., Suchy S. F., Nussbaum R. L., Cline G. W., Shulman G. I., McMurray W., and De Camilli P. 2003. Phosphoinositide profiling in complex lipid mixtures using electrospray ionization mass spectrometry. Nat.Biotechnol. 21: 813-817.

Williams E. E., Cooper J. A., Stillwell W., and Jenski L. J. 2000. The curvature and cholesterol content of phospholipid bilayers alter the transbilayer distribution of specific molecular species of phosphatidylethanolamine. Mol.Membr.Biol. 17: 157-164.

Williams E. E., Jenski L. J., and Stillwell W. 1998. Docosahexaenoic acid (DHA) alters the structure and composition of membranous vesicles exfoliated from the surface of a murine leukemia cell line. Biochim.Biophys.Acta. 1371: 351-362.

Williams E. E., May B. D., Stillwell W., and Jenski L. J. 1999. Docosahexaenoic acid (DHA) alters the phospholipid molecular species composition of membranous vesicles exfoliated from the surface of a murine leukemia cell line. Biochim.Biophys.Acta. 1418: 185-196.

Wu X., Okada N., Momota H., Irie R. F., and Okada H. 1999. Complement-mediated anti-HIV-1 effect induced by human IgM monoclonal antibody against ganglioside GM2. J.Immunol. 162: 533-539.

Wubbolts R., Leckie R. S., Veenhuizen P. T., Schwarzmann G., Mobius W., Hoernschemeyer J., Slot J. W., Geuze H. J., and Stoorvogel W. 2003. Proteomic and biochemical analyses of human B cell-derived exosomes. Potential implications for their function and multivesicular body formation. J.Biol.Chem. 278: 10963-10972.

Xu X. and London E. 2000. The effect of sterol structure on membrane lipid domains reveals how cholesterol can induce lipid domain formation. Biochemistry. 39: 843-849.

Ye J., Wang C., Sumpter R., Jr., Brown M. S., Goldstein J. L., and Gale M., Jr. 2003. Disruption of hepatitis C virus RNA replication through inhibition of host protein geranylgeranylation. Proc.Natl.Acad.Sci.U.S.A. 100: 15865-15870.

Yeung T., Gilbert G. E., Shi J., Silvius J., Kapus A., and Grinstein S. 2008. Membrane phosphatidylserine regulates surface charge and protein localization. Science. 319: 210-213.

Yeung T., Terebiznik M., Yu L., Silvius J., Abidi W. M., Philips M., Levine T., Kapus A., and Grinstein S. 2006. Receptor activation alters inner surface potential during phagocytosis. Science. 313: 347-351.

Yu C., Alterman M., and Dobrowsky R. T. 2005. Ceramide displaces cholesterol from lipid rafts and decreases the association of the cholesterol binding protein caveolin-1. J.Lipid Res. 46: 1678-1691.

Yuan X., Yu X., Lee T. H., and Essex M. 1993. Mutations in the N-terminal region of human immunodeficiency virus type 1 matrix protein block intracellular transport of the Gag precursor. J.Virol. 67: 6387-6394.

Zerouga M., Stillwell W., Stone J., Powner A., and Jenski L. J. 1996. Phospholipid class as a determinant in docosahexaenoic acid's effect on tumor cell viability. Anticancer Res. 16: 2863-2868.

Zheng Y. H., Plemenitas A., Fielding C. J., and Peterlin B. M. 2003. Nef increases the synthesis of and transports cholesterol to lipid rafts and HIV-1 progeny virions. Proc.Natl.Acad.Sci.U.S.A. 100: 8460-8465.

Zheng Y. H., Plemenitas A., Linnemann T., Fackler O. T., and Peterlin B. M. 2001. Nef increases infectivity of HIV via lipid rafts. Curr.Biol. 11: 875-879.

Zhou W., Parent L. J., Wills J. W., and Resh M. D. 1994. Identification of a membrane-binding domain within the amino-terminal region of human immunodeficiency virus type 1 Gag protein which interacts with acidic phospholipids. J.Virol. 68: 2556-2569.

Zhou W. and Resh M. D. 1996. Differential membrane binding of the human immunodeficiency virus type 1 matrix protein. J.Virol. 70: 8540-8548.

Zimmerberg J. and Kozlov M. M. 2006. How proteins produce cellular membrane curvature. Nat.Rev.Mol.Cell Biol. 7: 9-19.

Appendix 1

Recipe list

Plasma membrane extraction from cells using cationic silica beads

1. Plasma membrane coating buffer (PMCB)

    20 mM MES, 0.8 M sorbitol, 150 mM NaCl
    Mix together 20ml 1M MES, 140ml 2M sorbitol and 30ml 5M NaCl
    Adjust to pH 5.5-6.0 with conc. NaOH
    Make up to 1L with ddH_2O

2. Polyacrylic acid (PAA) (Sigma) in PMCB, PAA/PMCB

    Dissolve PAA (average molecular weight 100,000Da) in PMCB (1mg/ml)
    Adjust to pH 6-6.5 with conc. NaOH
    *Check pH using pH paper because PAA may damage pH electrodes

3. Lysis buffer

    2.5 mM imidazole in ddH_2O
    Supplement with protease inhibitor tablet (Roche)

4. 70% Histodenz (Sigma)

    Make a 100% w/v Histodenz by dissolving 10g Histodenz in 5.5ml of lysis buffer.
    Dilute 100% stock solution to 70% using lysis buffer

Plasma membrane extraction from cells using optiprep

1. Optiprep diluent

    235mM KCl, 12 mM $MgCl_2$, 25 mM $CaCl_2$, 30mM EGTA, 150mM Hepes-NaOH
    Mix together 23.5ml 1M KCl, 1.2ml 1M $MgCl_2$, 2.5ml 1M $CaCl_2$, 30ml 100mM EGTA and 15ml 1M Hepes

Adjust to pH 7.0 with 1M KOH

Make up to 100ml with ddH_2O

2. Working solution (WS)

78mM KCl, 4 mM MgCl2, 8.4 mM CaCl2, 10mM EGTA, 50mM Hepes-NaOH

Mix together 7.8ml 1M KCl, 0.4ml 1M $MgCl_2$, 0.84 1M $CaCl_2$, 10ml 100mM EGTA and 5ml 1M Hepes

Adjust to pH 7.0 with 1M KOH

Make up to 100ml with ddH_2O

3. Homogenization buffer

Dissolve 8.5g sucrose in WS

Adjust to pH 7.0 with 1M KOH

Make up to 100ml with WS

Protein analysis

1. SDS-Page Resolving Gel, 10ml recipe

(ml)	10% Gel	12% Gel
ddH_2O	4	3.3
30% Acrylamide	3.3	4
1.5M Tris (pH 8.8)	2.5	2.5
10% SDS	0.1	0.1
10% APS	0.1	0.1
TEMED	0.004	0.004

2. SDS-Page Stacking Gel, 5ml recipe

(ml)	Stacking
ddH_2O	3.4
30% Acrylamide	0.83
1.0M Tris (pH 6.8)	0.63
10% SDS	0.05
10% APS	0.05
TEMED	0.005

3. Electrophoresis running buffer (10x solution)

Dissolve 144 g Glycine, 24g Tris base, 10g SDS in ddH2O
Adjust to pH 8.3 with conc. HCl
Make up to 1L with ddH_2O
*Dilute to 1x before use

4. Transfer buffer

Dissolve 3.02g Tris base, 14.41g Glycine in 200ml methanol
Make up to 1L with ddH_2O

5. Wash solution (TBST)

Dissolve 8.8g Tris base, 1.2g NaCl and 500µl in ddH_2O
Make up to 1L with ddH_2O
*Blocking solution is prepared by dissolving 5g of non-fat milk powder with 100ml of TBST

ELISA analysis

1. Coating buffer

Dissolve 3.03g Na_2CO_3 and 6.0g $NaHCO_3$ in ddH_2O
Adjust to pH 9.6 with conc. HCl
Make up to 1L with ddH_2O

2. Blocking solution

Dissolve 1g BSA in 100ml coating buffer

Appendix 2

Optimized MRM parameters for glycerophospholipids detection by liquid chromatography

ESI-	Q1	Q3	Dwell Time (ms)	Declustering Potential (V)	Collision Energy (V)	Cell Exit Potential (V)
PS						
DMPS	678.6	591.6	50	-110	-32	-16
PS 32:1	732.6	645.6	50	-120	-34	-20
PS 32:0	734.6	647.6	50	-130	-34	-18
PS 34:2	758.6	671.7	50	-115	-34	-10
PS 34:1	760.6	673.7	50	-105	-32	-16
PS 34:0	762.6	675.7	50	-120	-36	-18
PS 36:4	782.6	695.7	50	-115	-34	-18
PS 36:3	784.6	697.6	50	-140	-34	-20
PS 36:2	786.6	699.6	50	-130	-36	-22
PS 36:1	788.6	701.6	50	-140	-36	-13
PS 36:0	790.6	703.7	50	-125	-38	-10
PS 38:5	808.6	721.6	50	-145	-38	-15
PS 38:4	810.6	723.6	50	-105	-36	-10
PS 38:3	812.6	725.7	50	-130	-34	-10
PS 38:2	814.6	727.7	50	-145	-34	-10
PS 38:1	816.6	729.7	50	-110	-38	-10
PS 38:0	818.6	731.7	50	-135	-36	-14
PS 40:6	834.6	747.7	50	-125	-34	-10
PS 40:5	836.6	749.7	50	-115	-38	-26
PS 40:4	838.6	751.7	50	-145	-38	-26
PS 40:3	840.6	753.7	50	-120	-34	-12
PS 40:2	842.6	755.7	50	-145	-36	-15
PS 40:1	844.6	757.7	50	-140	-38	-20
PS 40:0	846.6	759.7	50	-125	-38	-20
PS 42:6	862.6	775.7	50	-180	-36	-20
PS 42:5	864.6	777.7	50	-185	-36	-20
PS 42:4	866.6	779.7	50	-155	-40	-22
PS 42:3	868.6	781.7	50	-130	-34	-12
PS 42:2	870.6	783.7	50	-90	-45	-15
PS 42:1	872.6	785.7	50	-150	-60	-15
PS 42:0	874.7	787.8	50	-130	-60	-6
PI						
diC8-PI	585.5	241.1	50	-130	-65	-12
PI 34:1	835.5	241.1	50	-120	-60	-18
PI 34:0	837.6	241.1	50	-90	-80	-6
PI 36:4	857.6	241.1	50	-120	-65	-18
PI 36:3	859.6	241.1	50	-130	-65	-12
PI 36:2	861.6	241.1	50	-110	-65	-6
PI 36:1	863.6	241.1	50	-120	-65	-21
PI 36:0	865.6	241.1	50	-120	-80	-15
PI 38:6	881.6	241.1	50	-90	-80	-9
PI 38:5	883.6	241.1	50	-140	-80	-27
PI 38:4	885.6	241.1	50	-150	-70	-15
PI 38:3	887.6	241.1	50	-160	-70	-15
PI 38:2	889.6	241.1	50	-90	-60	-12
PI 38:1	891.6	241.1	50	-150	-65	-15
PI 38:0	893.6	241.1	50	-110	-80	-24
PI 40:6	909.6	241.1	50	-90	-80	-24
PI 40:5	911.6	241.1	50	-100	-80	-27

PI 40:4	913.6	241.1	50	-115	-55	-5
PI 40:3	915.6	241.1	50	-115	-55	-5
PI 40:2	917.6	241.1	50	-115	-55	-5
PI 40:1	919.6	241.1	50	-115	-55	-5
PI 40:0	921.6	241.1	50	-115	-55	-5
PE & pPE						
DMPE	634.6	196.1	50	-120	-45	-9
PE 32:1a	688.6	196.1	50	-110	-45	-15
PE 32:0a	690.6	196.1	50	-140	-53	-12
PE 34:2a	714.6	196.1	50	-130	-53	-9
PE 34:1a	716.6	196.1	50	-165	-53	-12
PE 34:0a	718.6	196.1	50	-170	-60	-9
PE 36:4a	738.6	196.1	50	-140	-53	-24
PE 36:3a	740.6	196.1	50	-140	-45	-6
PE 36:2a	742.6	196.1	50	-155	-60	-25
PE 36:1a	744.6	196.1	50	-185	-50	-18
PE 38:6a	762.6	196.1	50	-170	-50	-33
PE 38:5a	764.6	196.1	50	-100	-53	-33
PE 38:4a	766.6	196.1	50	-145	-53	-33
PE 38:3a	768.6	196.1	50	-145	-55	-33
PE 38:2a	770.6	196.1	50	-160	-53	-18
PE 38:1a	772.6	196.1	50	-155	-65	-20
PE 40:6a	790.6	196.1	50	-145	-53	-33
PE 40:5a	792.6	196.1	50	-145	-53	-12
PE 40:4a	794.6	196.1	50	-140	-65	-6
PE 40:3a	796.6	196.1	50	-100	-63	-6
PE 40:2a	798.6	196.1	50	-110	-60	-9
PE 40:1a	800.6	196.1	50	-130	-63	-33
PE 40:0a	802.6	196.1	50	-100	-75	-6
PE 34:2p	698.6	196.1	50	-135	-65	-9
PE 34:1p	700.6	196.1	50	-130	-63	-6
PE 34:0p	702.6	196.1	50	-130	-65	-9
PE 36:4p	722.6	196.1	50	-145	-63	-9
PE 36:3p	724.6	196.1	50	-100	-63	-9
PE 36:2p	726.6	196.1	50	-145	-63	-9
PE 36:1p	728.6	196.1	50	-175	-60	-17
PE 36:0p	730.6	196.1	50	-175	-60	-8
PE 38:6p	746.6	196.1	50	-145	-63	-9
PE 38:5p	748.6	196.1	50	-170	-63	-6
PE 38:4p	750.6	196.1	50	-165	-63	-9
PE 38:3p	752.6	196.1	50	-165	-63	-9
PE 38:2p	754.6	196.1	50	-165	-63	-9
PE 38:1p	756.6	196.1	50	-155	-63	-13
PE 38:0p	758.6	196.1	50	-100	-53	-9
PE 40:6p	774.6	196.1	50	-135	-60	-15
PE 40:5p	776.6	196.1	50	-160	-60	-25
PE 40:4p	778.6	196.1	50	-160	-60	-33
PE 40:3p	780.6	196.1	50	-170	-62	-17
PE 40:2p	782.6	196.1	50	-145	-75	-30
PE 40:1p	784.6	196.1	50	-145	-63	-30
PE 40:0p	786.6	196.1	50	-145	-75	-30
PE 16:0p	436.3	196.1	50	-160	-40	-6
PE 18:2p	460.3	196.1	50	-100	-40	-27
PE 18:1p	462.3	196.1	50	-100	-53	-12
PE 18:0p	464.3	196.1	50	-100	-40	-12
PE 18:2a	476.3	196.1	50	-110	-40	-9
PE 18:1a	478.3	196.1	50	-120	-40	-33
PE 18:0a	480.3	196.1	50	-120	-45	-24

PE 20:4a	500.3	196.1	50	-115	-55	-5
PE 20:3a	502.3	196.1	50	-115	-55	-5
PE 20:2a	504.3	196.1	50	-115	-55	-5
PC & ePC						
DMPC	678.5	184.1	50	135	42	10
PC 32:2a	730.6	184.1	50	125	38	16
PC 32:1a	732.6	184.1	50	80	42	10
PC 32:0a	734.6	184.1	50	135	42	10
PC 34:3a	756.6	184.1	50	125	42	10
PC 34:2a	758.6	184.1	50	125	42	10
PC 34:1a	760.6	184.1	50	135	42	10
PC 34:0a	762.6	184.1	50	135	42	10
PC 36:4a	782.6	184.1	50	125	46	10
PC 36:3a	784.6	184.1	50	125	46	10
PC 36:2a	786.6	184.1	50	150	42	10
PC 36:1a	788.6	184.1	50	135	50	10
PC 36:0a	790.6	184.1	50	125	42	13
PC 38:6a	806.6	184.1	50	135	46	13
PC 38:5a	808.6	184.1	50	125	42	10
PC 38:4a	810.6	184.1	50	125	42	31
PC 38:3a	812.6	184.1	50	125	50	31
PC 38:2a	814.6	184.1	50	125	42	34
PC 38:1a	816.6	184.1	50	125	42	34
PC 38:0a	818.6	184.1	50	80	46	31
PC 40:6a	834.6	184.1	50	125	50	31
PC 40:5a	836.6	184.1	50	125	42	31
PC 40:4a	838.6	184.1	50	125	50	34
PC 40:3a	840.6	184.1	50	125	50	37
PC 40:2a	842.6	184.1	50	125	38	34
PC 40:1a	844.6	184.1	50	125	38	31
PC 40:0a	846.6	184.1	50	90	54	13
PC 32:1e	718.6	184.1	50	125	38	31
PC 32:0e	720.6	184.1	50	125	38	31
PC 34:3e	742.6	184.1	50	80	34	34
PC 34:2e	744.6	184.1	50	135	38	34
PC 34:1e	746.6	184.1	50	135	38	31
PC 34:0e	748.6	184.1	50	135	42	31
PC 36:4e	768.6	184.1	50	90	46	37
PC 36:3e	770.6	184.1	50	90	42	37
PC 36:2e	772.6	184.1	50	90	38	34
PC 36:1e	774.6	184.1	50	90	38	10
PC 36:0e	776.6	184.1	50	135	54	34
PC 38:6e	792.6	184.1	50	90	46	10
PC 38:5e	794.6	184.1	50	90	46	10
PC 38:4e	796.6	184.1	50	90	42	13
PC 38:3e	798.6	184.1	50	80	38	34
PC 38:2e	800.6	184.1	50	90	46	10
PC 38:1e	802.6	184.1	50	80	50	31
PC 38:0e	804.6	184.1	50	125	42	10
PC 40:6e	820.6	184.1	50	80	46	10
PC 40:5e	822.6	184.1	50	80	54	10
PC 40:4e	824.6	184.1	50	80	54	34
PC 40:3e	826.6	184.1	50	80	46	10
PC 40:2e	828.6	184.1	50	80	42	34
PC 40:1e	830.6	184.1	50	80	46	31
PC 40:0e	832.6	184.1	50	80	46	34

Appendix 3

Optimized MRM parameters for sphingolipids detection by liquid chromatography.

ESI-	Q1	Q3	Dwell Time (ms)	Declustering Potential (V)	Collision Energy (V)	Cell Exit Potential (V)
SM						
L-SM	647.6	184.1	50	130	50	34
SM 18:1/16:1	701.5	184.1	50	140	65	15
SM 18:1/16:0	703.5	184.1	50	140	45	36
SM 18:1/18:1	729.6	184.1	50	140	65	36
SM 18:1/18:0	731.6	184.1	50	140	60	36
SM 18:1/20:1	757.6	184.1	50	150	65	10
SM 18:1/20:0	759.6	184.1	50	130	60	36
SM 18:1/22:0	787.6	184.1	50	130	60	33
SM 18:1/24:1	813.6	184.1	50	130	60	36
SM 18:1/24:0	815.6	184.1	50	130	60	33
SM 18:0/16:0	705.8	184.1	50	120	35	27
SM 18:0/18:0	733.8	184.1	50	120	35	27
SM 18:0/20:0	761.8	184.1	50	110	40	33
SM 18:0/22:0	789.9	184.1	50	130	52.5	33
SM 18:0/24:0	817.9	184.1	50	140	52.5	30
SM 18:0/26:1	843.9	184.1	50	140	52.5	30
SM 18:0/26:0	845.9	184.1	50	140	65	30
Cer						
C17-Cer	552.7	264.4	50	100	52.5	36
Cer 18:1/16:0	538.7	264.4	50	100	52.5	36
Cer 18:0/16:0	540.7	266.4	50	100	52.5	36
Cer 18:1/18:0	566.7	264.4	50	100	55	36
Cer 18:0/18:0	568.7	266.4	50	100	40	28
Cer 18:1/20:0	594.7	264.4	50	120	52.5	44
Cer 18:0/20:0	596.7	266.4	50	80	55	16
Cer 18:1/22:0	622.8	264.4	50	120	55	36
Cer 18:0/22:0	624.8	266.4	50	80	30	32
Cer 18:1/24:1	648.9	264.4	50	120	55	32
Cer 18:0/24:1	650.9	266.4	50	120	55	32
Cer 18:1/24:0	650.9	264.4	50	120	55	32
Cer 18:0/24:0	652.9	266.4	50	80	55	32
Cer 18:1/26:1	676.9	264.4	50	120	55	32
Cer 18:0/26:1	678.9	266.4	50	70	40	24
Cer 18:1/26:0	678.9	264.4	50	80	30	12
Cer 18:0/26:0	680.9	266.4	50	50	30	12
Glu-Cer						
C8-GC	588.7	264.4	50	90	60	36
GC 18:1/16:0	700.7	264.4	50	80	60	33
GC 18:0/16:0	702.7	266.4	50	100	65	14
GC 18:1/18:0	728.7	264.4	50	80	60	27
GC 18:0/18:0	730.7	266.4	50	55	50	14
GC 18:1/20:0	756.7	264.4	50	90	60	33
GC 18:0/20:0	758.7	266.4	50	90	70	17
GC 18:1/22:0	784.8	264.4	50	80	60	33
GC 18:0/22:0	786.8	266.4	50	90	55	14
GC 18:1/24:1	810.9	264.4	50	80	60	33
GC 18:0/24:1	812.9	266.4	50	90	70	33
GC 18:1/24:0	812.9	264.4	50	80	60	30
GC 18:0/24:0	814.9	266.4	50	80	60	33
GC 18:1/26:1	838.9	264.4	50	45	70	14
GC 18:0/26:1	840.9	266.4	50	90	45	17

GC 18:1/26:0	840.9	264.4	50	80	60	30
GC 18:0/26:0	842.9	266.4	50	80	70	33
GM3						
GM3 18:1/16:1	1149.6	290.1	50	-190	-65	-15
GM3 18:1/16:0	1151.6	290.1	50	-180	-65	-20
GM3 18:0/16:0	1153.6	290.1	50	-180	-65	-15
GM3 18:1/18:1	1177.6	290.1	50	-190	-65	-15
GM3 18:1/18:0	1179.6	290.1	50	-180	-65	-15
GM3 18:0/18:0	1181.6	290.1	50	-190	-65	-20
GM3 18:1/20:1	1205.6	290.1	50	-190	-65	-15
GM3 18:1/20:0	1207.6	290.1	50	-180	-65	-15
GM3 18:0/20:0	1209.6	290.1	50	-180	-65	-15
GM3 18:1/22:1	1233.6	290.1	50	-180	-65	-15
GM3 18:1/22:0	1235.6	290.1	50	-190	-65	-15
GM3 18:0/22:0	1237.6	290.1	50	-180	-65	-15
GM3 18:1/24:1	1261.6	290.1	50	-180	-65	-15
GM3 18:1/24:0	1263.6	290.1	50	-180	-65	-15
GM3 18:0/24:1	1265.6	290.1	50	-170	-65	-15
GM3 18:1/26:1	1289.6	290.1	50	-180	-65	-15
GM3 18:1/26:0	1291.6	290.1	50	-180	-65	-15

Appendix 4

Optimized MRM parameters for phosphoinositides detection by direct infusion.

ESI-	Q1	Q3	Dwell Time (ms)	Declustering Potential (V)	Collision Energy (V)	Cell Exit Potential (V)
PI						
diC8-PI	585.6	241.1	50	-120	-40	-4
PI 32:2	805.6	241.1	50	-125	-55	-4
PI 32:1	807.6	241.1	50	-125	-55	-4
PI 32:0	809.6	241.1	50	-125	-55	-4
PI 34:2	833.6	241.1	50	-140	-60	-4
PI 34:1	835.6	241.1	50	-140	-60	-4
PI 34:0	837.6	241.1	50	-140	-60	-4
PI 36:4	857.6	241.1	50	-140	-60	-4
PI 36:3	859.6	241.1	50	-150	-60	-4
PI 36:2	861.6	241.1	50	-150	-62.5	-4
PI 36:1	863.6	241.1	50	-150	-62.5	-4
PI 36:0	865.6	241.1	50	-150	-62.5	-4
PI 38:5	883.7	241.1	50	-150	-62.5	-4
PI 38:4	885.7	241.1	50	-150	-62.5	-4
PI 38:3	887.7	241.1	50	-150	-62.5	-4
PI 38:2	889.7	241.1	50	-150	-62.5	-4
PI 38:1	891.7	241.1	50	-150	-62.5	-4
PI 38:0	893.7	241.1	50	-150	-62.5	-4
PI 40:6	909.7	241.1	50	-160	-65	-4
PI 40:5	911.7	241.1	50	-160	-65	-4
PI 40:4	913.7	241.1	50	-160	-65	-4
PIP						
diC8-PIP	665.7	321.1	50	-150	-45	-4
PIP 32:2	885.7	321.1	50	-160	-50	-4
PIP 32:1	887.7	321.1	50	-160	-50	-4
PIP 32:0	889.7	321.1	50	-165	-52.5	-4
PIP 34:2	913.7	321.1	50	-165	-52.5	-4
PIP 34:1	915.7	321.1	50	-165	-52.5	-4
PIP 34:0	917.7	321.1	50	-175	-55	-4
PIP 36:4	937.7	321.1	50	-175	-55	-4
PIP 36:3	939.7	321.1	50	-175	-55	-4
PIP 36:2	941.7	321.1	50	-175	-55	-4
PIP 36:1	943.7	321.1	50	-175	-55	-4
PIP 36:0	945.7	321.1	50	-175	-57.5	-4
PIP 38:5	963.7	321.1	50	-175	-60	-4
PIP 38:4	965.7	321.1	50	-175	-60	-4
PIP 38:3	967.7	321.1	50	-175	-60	-4
PIP 38:2	969.7	321.1	50	-175	-60	-4
PIP 38:1	971.7	321.1	50	-175	-60	-4
PIP 38:0	973.7	321.1	50	-180	-62.5	-4
PIP 40:6	989.7	321.1	50	-180	-62.5	-4
PIP 40:5	991.7	321.1	50	-180	-62.5	-4
PIP 40:4	993.7	321.1	50	-180	-63.5	-4
PIP_2						
diC8-PIP_2	745.8	401.1	50	-170	-47.5	-4
PIP_2 32:2	965.8	401.1	50	-180	-50	-4
PIP_2 32:1	967.8	401.1	50	-180	-52.5	-4
PIP_2 32:0	969.8	401.1	50	-180	-52.5	-4
PIP_2 34:2	993.8	401.1	50	-180	-52.5	-4
PIP_2 34:1	995.8	401.1	50	-180	-55	-4

PIP_2 34:0	997.8	401.1	50	-180	-55	-4
PIP_2 36:4	1017.8	401.1	50	-180	-55	-4
PIP_2 36:3	1019.8	401.1	50	-180	-55	-4
PIP_2 36:2	1021.8	401.1	50	-180	-55	-4
PIP_2 36:1	1023.8	401.1	50	-180	-57.5	-4
PIP_2 36:0	1025.8	401.1	50	-180	-57.5	-4
PIP_2 38:5	1043.8	401.1	50	-180	-57.5	-4
PIP_2 38:4	1045.8	401.1	50	-180	-57.5	-4
PIP_2 38:3	1047.8	401.1	50	-180	-57.5	-4
PIP_2 38:2	1049.8	401.1	50	-180	-57.5	-4
PIP_2 38:1	1051.8	401.1	50	-180	-60	-4
PIP_2 38:0	1053.8	401.1	50	-180	-60	-4
PIP_2 40:6	1069.8	401.1	50	-180	-60	-4
PIP_2 40:5	1071.8	401.1	50	-180	-50	-4
PIP_2 40:4	1073.8	401.1	50	-180	-55	-4

Appendix 5

Liposome composition mix.

Lipid standard concentration	Egg yolk PC 10mg/ml	DMPS 5mg/ml	DMPE 5mg/ml	pPE 38:4 1mg/ml
Liposomes for Section 4.3.1				
DMPS	9.5µl	1.0µl	-	-
DMPE	9.5µl	-	1.0µl	-
pPE 38:4	9.5µl	-	-	5.0µl
Liposome for Section 4.3.2				
No DMPE	10.0µl	-	-	-
0.5mg DMPE	9.5µl	-	1.0µl	-
1mg DMPE	9.0µl	-	2.0µl	-
2mg DMPE	8.0µl	-	4.0µl	-